Common mechanism of activated catalysis in P-loop fold nucleoside triphosphatases – united in diversity.

Maria I. Kozlova[1&], Daria N. Shalaeva[1&], Daria V. Dibrova[1], Armen Y Mulkidjanian[1,2]

[1]School of Physics and [2]Center of Cellular Nanoanalytics, Osnabrueck University, 49069, Osnabrueck, Germany.

[&]These two authors contributed equally to the study

***For correspondence**: Armen Y. Mulkidjanian, School of Physics, University of Osnabrueck, D-49069, Osnabrueck, Germany. Tel. +49-541-969-2698;
E-mail: amulkid@uni-osnabrueck.de

E-mail addresses:

Maria I. Kozlova, makozlova@uni-osnabrueck.de, ORCID: 0000-0003-0699-5064

Daria N. Shalaeva, dshalaeva@uni-osnabrueck.de, ORCID: 0000-0003-0582-2612

Daria V. Dibrova, udavdasha@gmail.com, ORCID: 0000-0002-6954-6437

Armen Y. Mulkidjanian, amulkid@uni-osnabrueck.de, ORCID: 0000-0001-5844-3064

Abstract

Though P-loop fold nucleoside triphosphatases (also known as Walker NTPases) are widespread, their catalytic mechanism remains unclear. Based on a comparative structure analysis of 3136 Mg-NTP-containing catalytic sites, we propose a common scheme of activated catalysis for P-loop NTPases. In this scheme, a hydrogen bond (H-bond) between the strictly conserved, Mg-coordinating Ser/Thr of the Walker A motif ([Ser/Thr]^{WA}) and the conserved aspartate of the Walker B motif (Asp^{WB}) plays the key role. We found that this H-bond is very short in the structures with bound transition state analogs. Given that a short hydrogen bond (also known as a low-barrier hydrogen bond) implies parity of pK values of the H-bond partners, we suggest that the proton affinities of these two residues reverse upon activation so that the proton relocates from [Ser/Thr]^{WA} to Asp^{WB}. The anionic [Ser/Thr]^{WA} alkoxide withdraws then a proton from the would-be nucleophile (either a water molecule or a sugar moiety in some P-loop kinases), and the nascent anion attacks the gamma-phosphate group. When gamma-phosphate breaks away, the trapped proton relays from Asp^{WB}, via [Ser/Thr]^{WA}, to beta-phosphate and compensates for its developing negative charge.

1. Introduction

Hydrolysis of nucleoside triphosphates (NTPs), such as ATP or GTP, by widespread P-loop fold nucleoside triphosphatases (also known as Walker NTPases) is one of the key enzymic reactions. P-loop NTPase domains (see Fig. 1 for their overview), which are coded by up to 20% gene products in a typical cell, drive the activity of rotary ATP synthases, DNA and RNA helicases, kinesins and myosins, ABC-transporters, ubiquitous translation factors, α-subunits of signaling heterotrimeric G-proteins and even oncogenic Ras-GTPases [1-19]. In the ECOD database [20], the topology-level entry "P-loop_NTPase" contains 193 protein families. In the Pfam database [21], the P-loop NTPase clan CL0023 contains 217 families. The main classes of P-loop NTPases were already present in the Last Universal Cellular Ancestor (LUCA) [9, 10, 17, 19, 22-27].

The P-loop fold domain is a 3-layer αβα sandwich, see Fig. 1 and [10, 18, 28-31]. In small P-loop NTPases (Fig. 1C), the titular *p*hosphate-binding loop (P-loop) usually connects the first β-strand (β_1-strand) with the first α-helix (α_1-helix); the P-loop together with the two first residues of the α_1-helix have the [G/A]xxxxGK[S/T] sequence, known as the Walker A motif [1]. This motif is responsible for the binding of the triphosphate chain and cofactor Mg^{2+} ion, see [1, 2, 32] and Fig. 1A-D. The Walker B motif *hhhh*D, where '*h*' denotes a hydrophobic residue, is the other shared motif of P-loop NTPases, see Fig. 1A-F and [1, 2, 32]. The aspartate residue of the Walker B motif is thought to contribute to the stabilization of the Mg^{2+} binding site. In small P-loop NTPases, this residue is at the C-terminal tip (hereafter C-cap) of the β_3-strand [9], just opposite of the α_1-helix. A few P-loop NTPases have a glutamate residue in the respective position; we explicitly address these cases below. Still, throughout the manuscript, the conserved carboxylic residue of Walker B motif is denoted as Asp^{WB} for the sake of simplicity, see Fig. 1E-F. Asp^{WB} makes a hydrogen bond (H-bond) with the conserved Ser/Thr

of the Walker A motif that follows the conserved Lys residue, see Fig. 1E and 1F where the respective residues are denoted as Thr19^{K+1} and Ser193^{K+1}, respectively.

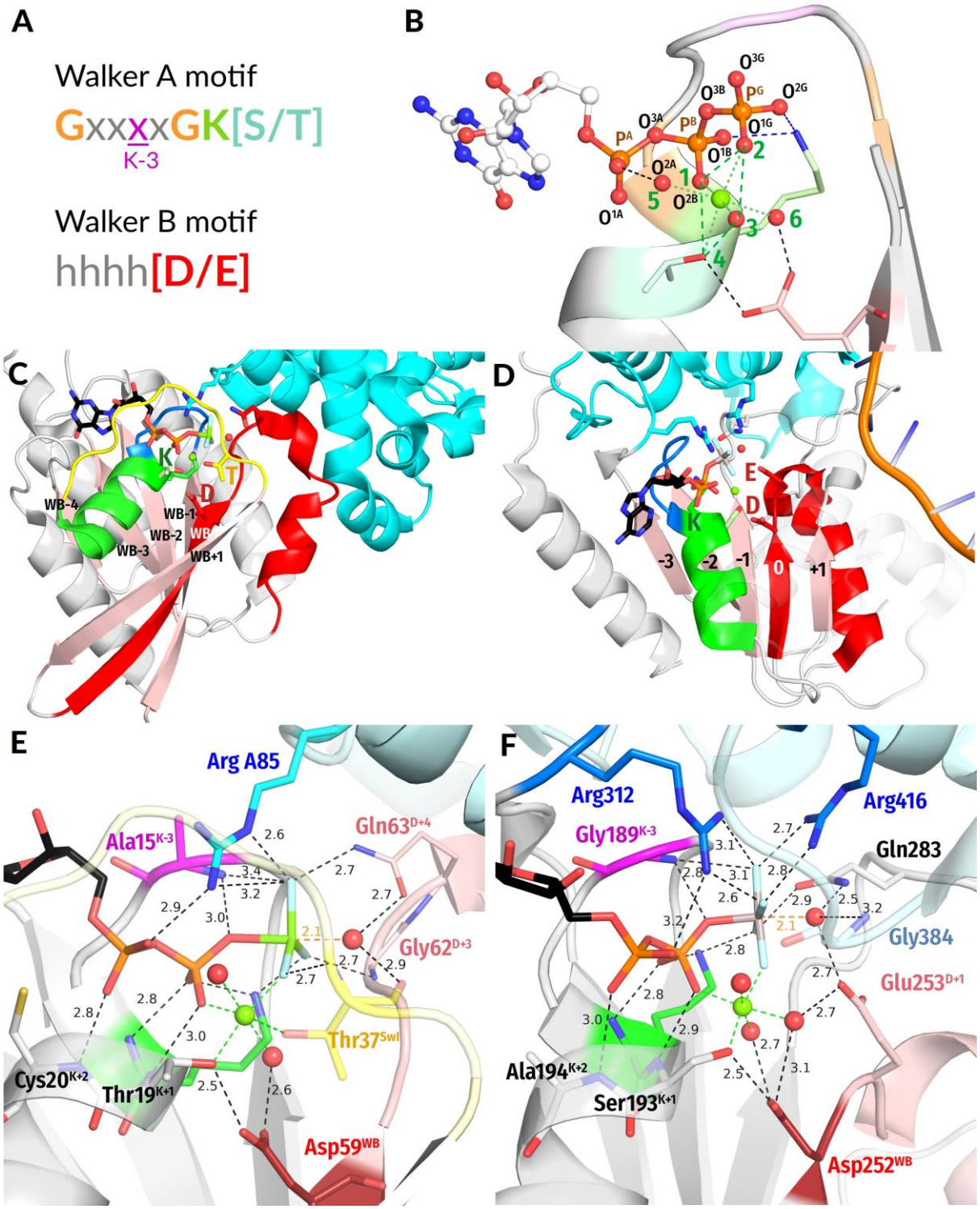

Figure 1. P-loop fold NTPases.
A, conserved Walker motifs in P-loop NTPases; **B**, naming of atoms according to IUPAC recommendations for nucleoside triphosphates [33] and typical Mg^{2+} coordination; **C, D,** Typical folds of P-loop NTPases. **C**, GTPase Rho with its activator RhoGAP, (PDB ID 1OW3

[34]); **D**, Chikungunya virus nsP2 SF1-helicase (PDB ID 6JIM [35]). **E, F**, Close-ups of structures shown in **C, D** as examples of typical catalytic sites of P-loop NTPases. **E,** GTPase Rho with its activator RhoGAP and the transition state analog GDP-MgF_3^-, (PDB ID 1OW3 [34]); **F,** Chikungunya virus nsP2 SF1 helicase complexed with transition state analog ADP-AlF_4^- (PDB ID 6JIM [35]).
Color code: Polypeptide chains are shown as gray cartoons, β-strands, pink; α_1-helix, green; P-loop, blue; Walker B motif and the following residues, red, Switch I loop, yellow, the activating partners are colored cyan. Nucleotides, their analogs, and important amino acid residues are shown as sticks, water molecules – as red spheres, Mg^{2+} ions are shown as lime spheres, sphere; the conserved Lys residue of Walker A motif is shown in green with the amino acid residue three residues before it highlighted in magenta; conserved Asp/Glu residue of Walker B motif is shown in dark red and the following residues are shown in pale red; Arg fingers are shown in blue/cyan. In amino acid residues shown as sticks, the oxygen atoms are colored red, and the nitrogen atoms are colored blue. In the MgF_3^- moiety, the fluoride atoms are colored light blue. In the AlF_4^- moiety, the Al atom is colored gray. All distances are given in ångströms.

A specific feature of most P-loop ATPases is their activation before each turnover, so that the NTP hydrolysis proceeds in two steps. First, an ATP or a GTP molecule binds to the Walker A motif and attains a configuration with eclipsed β- and γ-phosphates, as enforced by the Walker A motif and the Mg^{2+} ion, see Fig. 1B and [31, 36-40]. Then the P-loop domain interact with its cognate activating partner, which could be a domain of the same protein, a separate protein and/or a DNA/RNA molecule. Upon this interaction, specific stimulatory moieties, usually Arg or Lys residues ("Arg/Lys fingers", Fig. 1E-F), are inserted into the catalytic sites and promote the cleavage of γ-phosphate, see the accompanying article [41] and [4, 15, 16, 40, 42-49].

The energy of NTP binding drives the “closing” of the catalytic pocket, whereas the energy of hydrolysis is utilized for its “opening”; both these large-scale conformational changes can be coupled to useful mechanical work; they drive various cell motors, see, e.g. [4, 50-52].

Important hints for clarifying the catalytic mechanism of P-loop NTPases are provided by their structures with bound transition state (TS) analogs, such as NDP:AlF_4^- or NDP:MgF_3^- or NDP-VO_4^- complexes [4, 34, 42, 43, 46, 48, 53-56]. The crystal structures with NDP:MgF_3^- or

NDP:AlF_4^- bound (see Fig. 1E and 1F, respectively) revealed a "catalytic" water molecule W_{cat} near the analog of the P^G atom and almost in-line with its bond with the O^{3B} oxygen atom (see Fig. 1B for the atom names according to the IUPAC recommendations for nucleoside triphosphates [33]). In the NDP-VO_4^- complexes, one of the four oxygen atoms of vanadate occupies the position of the catalytic water molecule [4, 55]. These structures, in support to earlier suggestions, indicate that the ultimate cleavage of γ-phosphate is triggered by the apical nucleophilic attack on the terminal phosphorus atom P^G; the deprotonated state of W_{cat} (**OH^-_{cat}**) is thought to serve as a nucleophile in GTPases and ATPases, see Fig. 1E-F, Fig. S1 in Supplementary Materials and [15, 48, 56-63].

There is no consensus on how stimulatory moieties accelerate the NTP hydrolysis. It has been unclear whether they decrease the activation barrier of NTP hydrolysis by compensating for the developing negative charge on β-phosphate [62, 64] or by electrostatically stabilizing the TS [65] or by expulsing water from the catalytic pocket [66] or by some other impact.

It has remained also unclear how the interaction with the stimulating moiety initiates the deprotonation of W_{cat} and what is the fate of the proton that is released upon this deprotonation. The first TS-like crystal structures of small GTPases, such as shown in Fig. 1C, 1E, did not reveal potential bases among the ligands of W_{cat} [4, 42, 43, 53]. Thus, it was suggested that the proton is accepted directly by γ-phosphate [67-69]. In contrast, the crystal structures of many other P-loop NTPases showed that W_{cat} interacts with Glu or Asp residues; these “catalytic” residues were suggested to serve as proton acceptors in these NTPases, see e.g. Glu253 in Fig. 1F and [8, 54, 63, 70]. It remains unclear whether the proton is transferred from these bases to the triphosphate and, if so, how this transfer takes place.

In the accompanying article [41], by using cumulative computational approach, we inspected 3136 structures of Mg-NTP-containing catalytic sites of P-loop NTPases, identified the

structures with inserted stimulator(s) and analyzed the patterns of stimulatory interactions. In most cases, at least one stimulator, by linking the oxygen atoms of α- and γ-phosphates, appears to twist γ-phosphate counter-clockwise by 30-40º; the rotated γ-phosphate is stabilized by a H-bond with the backbone amino group of the fourth residue of the Walker A motif. In rest cases, the stimulator(s) only engage(s) the γ-phosphate group and likely pull(s) or twist(s) it. The mechanistic interaction between the stimulator(s) and γ-phosphate appears to be a common property of all examined P-loop NTPases, which points to the stimulator-induced twist of γ-phosphate as the trigger for NTP hydrolysis.

Here we have combined manual identification of structural elements specific to major classes of P-loop NTPases with global computational analysis of H-bonding around Walker A and Walker B motifs in the same set of 3136 catalytic sites. By focusing on TS-like structures, we tried to capture the structural transitions involved in catalysis.

We have found that major classes of P-loop ATPases and GTPases share the following common structural features:

(1) In most analyzed structures, a short H-bond (< 2.7 Å) connects Asp^{WB} and $[Ser/Thr]^{K+1}$; this bond is extremely short (2.4-2.5 Å) in those structures that contain NDP:AlF_4^- as a TS analog;

(2) In TS-like structures of P-loop NTPases of all classes, except those of TRAFAC class, the W_{cat}-coordinating "catalytic" Glu or Asp residue provides a proton pathway from W_{cat} to the nearest ligand of Mg^{2+}.

(3) The distance between neighboring ligands in the coordination shell of Mg^{2+} is 2.9-3.0 Å, which implies the possibility of proton exchange between all of them.

These common structural traits allowed us to specify a basic mechanism of stimulated catalysis for the whole superfamily of P-loop NTPases as follows:

(i) interaction with the activating partner and twisting γ-phosphate by stimulator(s) appear to affect the properties of Mg^{2+} ligands including $[S/T]^{K+1}$, so that, in the transition state, the $[S/T]^{K+1}$ – Asp^{WB} H-bond shortens, the functional pKs of $[S/T]^{K+1}$ and Asp^{WB} become leveled, and the proton relocates from $[S/T]^{K+1}$ to Asp^{WB};

(ii) the remaining proton vacancy at anionic $[Ser/Thr]^{K+1}$ alkoxide is refilled by a proton that comes from W_{cat} (or a sugar moiety in some kinases), after which the nascent anion attacks γ-phosphate;

(iii) upon the breakaway of γ-phosphate, the trapped on Asp^{WB} proton relays, via $[Ser/Thr]^{K+1}$, to β-phosphate and compensates for its developing negative charge.

2. **Results**

To ensure detailed analysis and to cover as many structures as possible, we combined (i) the manual inspection of catalytic machinery in selected representatives from the major classes of P-loop NTPases (as described in Section 2.2.) with (ii) systematic computational analysis of all available structures of P-loop NTPases with bound Mg-NTP-like molecules (see Section 2.3 and the accompanying article [41]).

2.1. Generic designation of structure elements in P-loop fold NTPases

In the accompanying article [41], we have introduced and used a generic amino acid numbering for the conserved regions of P-loop NTPases. Hereafter we use the same nomenclature and number the amino acids residues of the Walker A, Switch I, and Walker B motifs (including functionally relevant residues following the Walker B motif) relatively to strictly conserved

reference residues, namely Lys^{WA} (K^{WA}) of the Walker A motif, Asp^{WB} (D^{WB}) of the Walker B motif, and $[Thr/Ser]^{SwI}$ ($[T/S]^{SwI}$) of the Switch I motif, respectively, as shown in Fig. 1 (see the accompanying article [41] for further details).

For ease of reference, we also introduce and use hereafter a novel generic numbering for the strands of the β-pleated sheet (for comparison, the conventional numbering of β-strands is shown in Fig. S2 for major classes of P-loop NTPases). Indeed, in small P-loop NTPases, the Walker B motif is at the C-cap of the β_3-strand [9]. However, in other NTPases, it is at the C-cap of other β strands or even at the N-terminus [32]. Furthermore, larger P-loop NTPases can have additional β-strands which precede, in the amino acid sequence, the β_1-strand that turns into the P-loop. This variable position of the Walker B motif is confusing. For instance, the Walker B motif is located at the C-cap of the β_2-strand in the shikimate, gluconate, and adenosine phosphosulfate kinases [9]. The respective structures show that the conserved Asp^{WB} residue makes both canonical H-bonds with $[Thr/Ser]^{K+1}$ and the Mg^{2+}-coordinating water, respectively. And still, even recent review papers on these kinases indicate the Walker B motif in the β_3-strand, where it is conspicuously absent.

Therefore, in this article, for simplicity, we call the β-strand, which is in-line with the triphosphate chain, "*Walker B strand*" or *WB-strand*. This strand is easy to find in a structure because it carries an aspartate or, rarely, a glutamate residue at its C-cap; the carboxyl of this residue is usually H-bonded to the $[Thr/Ser]^{K+1}$ residue of the Walker A motif as shown in Fig. 1E-F. In addition, this carboxylic residue is usually preceded by four non-polar amino acids of the Walker B motif, see Fig. 1A and [1]. Other strands of the same β–pleated sheet, independently of their position in the amino acid sequence, can be numbered by their position relatively to WB-strand as WB-1, WB-2, or WB+1, WB+2 and so on, as shown in Fig. 1C. For

the sake of brevity, "WB" could be omitted, and the strands could be numbered -1, -2, 0 (for the WB strand), +1, +2 and so on, as depicted in Fig. 1D, S3, and S4.

In those cases where the crystal structures of NTPases with their cognate activating partners are available, these partners, according to our observations, usually interact with a stretch of amino acids that follows the Walker B motif and approximately corresponds to residues from Asp^{WB}+1 (aka D+1) to Asp^{WB}+12 (aka D+12); this stretch is colored red in Fig. 1C-D or pale red in Fig. 1E-F. In the case of small NTPases, this region corresponds to their α_3-helices (Fig. 1C). In some publications, the first few amino acids of this stretch are united with the Walker B motif into the "extended Walker B motif". However, the amino acids beyond the conserved Asp^{WB} residue show no conservation throughout P-loop NTPases (see Fig. S3); hence, they make no conserved motif. By its shape, this stretch resembles a cock's crest and usually rises above the neighboring β-strands as clearly seen in Fig. 1C-D. Therefore, hereafter we will name this structural element "*Walker B crest*" or *WB-crest*.

2.2. Catalytically relevant amino acids, stimulatory patterns, and activation mechanisms in different classes of P-loop NTPases.

The P-loop NTPases are thought to form two divisions, namely the Kinase-GTPase division and ASCE (Additional Strand Catalytic E (glutamate)) division, with both divisions containing several enzyme classes, see Fig. S2-S4 and [9, 10, 12, 14, 19].

For most classes of P-loop NTPases, we have selected representatives out of a set of proteins with available crystal structures in the Protein Data Bank (PDB) at www.rcsb.org [71, 72]. These structures are listed in Table 1. Each selected structure contains a Mg^{2+} cation and an NTP molecule or its analog bound; we preferred those structures that contain TS analogs. For these NTPases, after assessing the overall interaction with the activating partner, we checked the following features: (i) amino acids that coordinate the Mg-triphosphate moiety; (ii)

positively charged, potentially stimulatory moiety(ies) inserted into the catalytic site during the activation (their cumulative analysis is presented in the accompanying article [41]); (iii) amino acids that interact with $\mathbf{W_{cat}}$; and (iv) other auxiliary amino acids that interact with oxygen atoms of the γ-phosphate group (or its analogs). The results of this manual analysis are described below and summarized in Table 1.

2.2.1. Coordination of the Mg-triphosphate moiety

First, representative structures from different classes were superposed with the structure of AlF_4^--containing, K^+-dependent GTPase MnmE (PDB ID 2GJ8, resolution 1.7 Å [46]), the activation mechanism of which we scrutinized elsewhere [40]. We aligned 20 amino acids of the $ß_1$-strand, P-loop, and $α_1$-helix with the corresponding amino acids 217-236 of MnmE. The whole shape of the P-loop found to be strictly conserved across all classes of P-loop NTPases (Fig. 2A). Accordingly, the binding mode of the triphosphate chain, which is described below, appears to be conserved throughout P-loop NTPases.

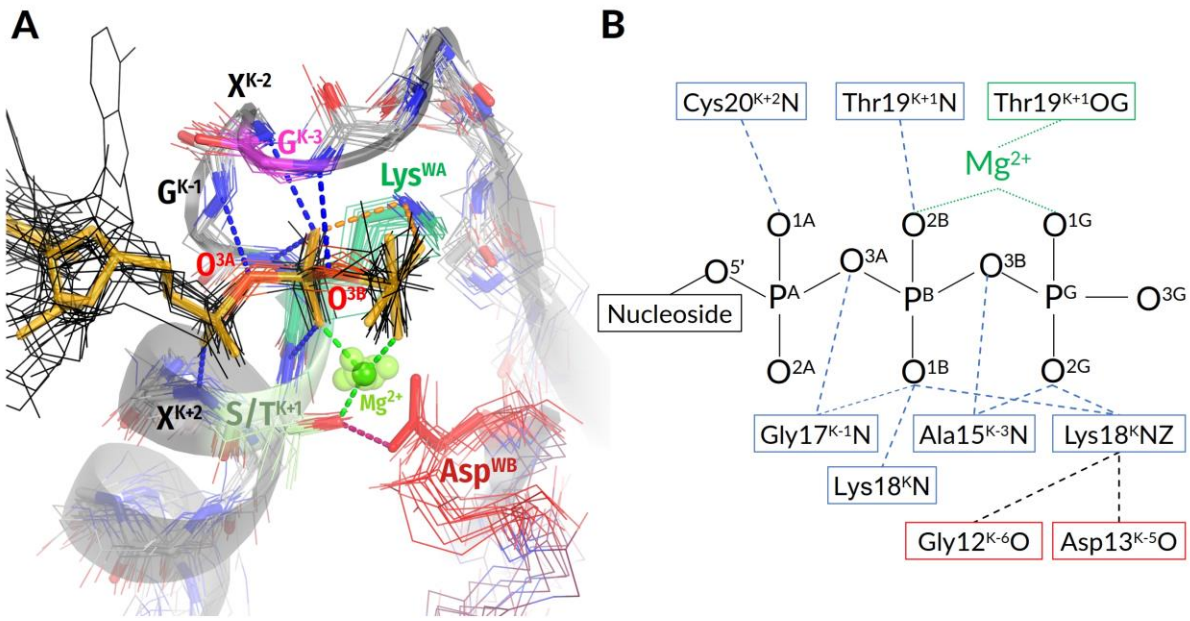

Figure 2. Conserved interaction between Walker A and Walker B motifs across classes of P-loop NTPases.
A. Structures of proteins, representing different classes of P-loop NTPases and described in Table 1 are shown superimposed on the P-loop region of the MnmE GTPase with a TS-analog

GDP:AlF_4^- bound (PDB ID: 2GJ8 [46]). For the MnmE GTPase, the P-loop region is shown as a cartoon. The bonding pattern is shown only for the MnmE GTPase. For all the proteins, the last seven residues from the motif GxxxxGK[S/T]x, as well as the Asp residue of the Walker B motif and NTP analogs are shown by lines and colored as follows: Lys^{WA} in green, Ser/Thr^{K+1} in pale green, $Gly/Ala/Asn^{K-3}$ in purple, Asp^{WB} in red; NTP molecules or their analogs are shown in black with bridging oxygen atoms in red. GDP:ALF_4^- from the MnmE structure is shown in orange. Other protein residues are shown in gray with backbone nitrogen and oxygen atoms shown in blue and red, respectively. Mg^{2+} ions are shown as green spheres. The phosphate chain is involved in numerous bonds with backbone HN groups of Walker A motif residues (the bonds are highlighted in blue), conserved Lys^{WA} contacts O^{2G} and O^{1B} atoms (orange bonds) and O^{2B} and O^{1G} atoms are part of the Mg^{2+} coordination shell (green bonds). **B.** Coordination bonds and H-bonds between the Walker A motif and Mg-NTP moiety in the MnmE GTPase (PDB ID: 2GJ8 [46]).

In all manually inspected structures, the NTP molecule (or its analog) is bound to the P-loop of the Walker A motif in an extended conformation which is supposedly catalytically prone (Fig. 1E-F, 2A); elsewhere we showed that this conformation is similar to those of Mg-ATP and Mg-GTP in water in the presence of large monovalent cations such as K^+ or NH_4^+ [40]. The configuration of the catalytic site is enforced by a plethora of conserved bonds that mostly involve the backbone amino group (hereafter **HN** groups) of the Walker A motif, see Fig. 1, 2A, B and [15, 31, 73]. The partial positive charges of these groups compensate for negative charges of the triphosphate chain oxygens. The structural elements responsible for stabilization of the triphosphate chain by amino acids of the Walker A motif are almost universally conserved (Fig. 2). The conservation of invariant residues in the [G/A]XXXXGK[T/S] motif has straightforward reasons: the Gly^{K-1} and Gly^{K-6} residues mark the beginning and end of the P-loop and enable the bending of the backbone; Gly^{K-1}, in addition, electrostatically stabilizes the O^{3A} atom of α-phosphate. The Lys^{WA} residue interacts with O^{1B} and O^{2G} atoms and additionally appears to stabilize the P-loop by interacting with backbone carbonyl oxygens of K-5 and K-6 residues (Fig. 2).

In NTPases of all classes except several families of nucleotide monophosphate kinases, the Walker A and Walker B motifs are linked by a H-bond between the side chains of $[Thr/Ser]^{K+1}$

and Asp^{WB} (Fig. 1E-F, 2A). This interaction is considered in more detail in Section 2.3.1. below where its comprehensive computational analysis is presented.

The same side chain of the conserved $[Ser/Thr]^{K+1}$ serves as the ligand #4 of Mg^{2+}. As shown in Fig. 1B, other strictly conserved ligands are O^{2B} and O^{1G} atoms of the triphosphate chain as ligands #1 and #2, respectively, and water molecules as ligands #5 (W5) and #6 (W6). The position #3 is taken either by water W3 or by diverse amino acid residues in different enzyme families, see [32] for details. The positions of Mg^{2+} ligands are similar over the entire superfamily of P-loop NTPases.

Fig. 2A, B show that the O^{2A} and O^{3G} atoms of the triphosphate are "free", not bound to P-loop residues. Not surprisingly, in many TS-like structures, they interact with stimulators (Fig. 1E-F). For the MnmE GTPase, our molecular dynamics (MD) simulations showed that the insertion of a K^+ ion and its simultaneous interaction with O^{2A}, O^{3B} and O^{3G} atoms rotates γ-phosphate and leads to formation of a new H-bond between the O^{2G} atom and **HN** of $Asn226^{K-3}$, see [40] and the accompanying paper [41]. Generally, the position of $\mathbf{HN}^{K-3}$ in the vicinity of the O^{2G} atom (or the corresponding atom of an NTP analog) is structurally conserved across P-loop NTPases, being determined by the highly conserved H-bond of $\mathbf{HN}^{K-3}$ with the bridging O^{3B} oxygen (Fig. 2). In manually inspected representative structures from Table 1, the distances between $\mathbf{HN}^{K-3}$ and the closest oxygen atom of γ-phosphate (or its structural analog) were shorter in the case of TS analogs. A comprehensive computational analysis of $\mathbf{HN}^{K-3}$-O^{2G} distances in all relevant PDB structures is presented in the accompanying paper [41].

2.2.2. Catalytically relevant amino acids, activating partners, stimulatory patterns, and coordination of W_{cat}

Other structural elements of P-loop NTPases, as well as their activating partners and stimulating moieties, vary among enzyme families; each class of P-loop NTPases is

characterized by its specific constellation(s) of stimulators and W_{cat}-coordinating residues. Since no detailed, comparative survey of catalysis-relevant structural attributes in all the multitude of P-loop NTPases is available, we provide here such a survey for the major classes of P-loop NTPases. Below we consider only those families and classes of P-loop NTPases for which the available structures allowed us to obtain unambiguous structural information. The results of this analysis are summarized in Table 1. Those classes of P-loop NTPases for which the structural information is ambiguous are discussed in the Supplementary File 1.

2.2.2.1. Kinase-GTPase division

The Kinase-GTPase division unites three classes of NTPases: the TRAFAC (from *tra*nslation *fac*tors) class of translational factors and regulatory NTPases, SIMIBI (*si*gnal recognition, *M*inD, and *Bi*oD) class of regulatory dimerizing ATPases and GTPases, and the class of nucleotide kinases (Fig. S2, S3).

In the NTPases of **the TRAFAC class,** the α_1-helix is followed by an elongated Switch I loop that is specific to the class. The elongated Switch I loop goes into the β-strand, which is antiparallel to all other β-strands of the core β-pleated sheet (Fig. 1C, S3). Apart from the TRAFAC class, other classes of P-loop NTPases have predominantly all-parallel core β-pleated sheets.

The Switch I loop contains the only strictly conserved $[Thr/Ser]^{SwI}$ reference residue with its side chain coordinating Mg^{2+} as the ligand #3 (Fig. 1C, 1E, and S3). In most TRAFAC NTPases, the **HN** group of $[Thr/Ser]^{SwI}$ forms a H-bond with γ-phosphate (Fig. 1E, 3). The backbone carbonyl group (hereafter **CO** group) of $[Thr/Ser]^{SwI}$ interacts with the W_{cat} molecule seen in TS-like crystal structures (Fig. 1E, 3).

The TRAFAC class NTPases show a remarkably broad variety of stimulatory interactions; they are shown in Fig. 1C, 1E, 3, listed in Table 1 and described below.

Monovalent cation-dependent NTPases, which we have considered elsewhere [40], are usually stimulated by K^+ ions, as the aforementioned GTPase MnmE, see Fig. 2, S3A, Table 1 and [46, 47]. The K^+ ion in MnmE GTPase is coordinated by O^{2A}, O^{3B}, and O^{3G} atoms of the triphosphate chain, two **CO** groups of the K-loop, and the side chain of Asn^{K-3}, see Fig. 2A, [40, 46] and the accompanying article [41].

In the unique eukaryotic protein family of dynamins, the NTP hydrolysis can be stimulated by either K^+ or Na^+ ions [74]. Here a Na^+ or a K^+ ion interacts only with the O^{3B} and O^{3G} atoms but does not reach the O^{2A} atom, see Fig. 3A, the accompanying article [41], and [40, 47] for details.

These K^+/Na^+-stimulated TRAFAC class NTPases belong to the family of HAS (hydrophobic aminoacid substitution) NTPases [75]. No hydrophilic side chains are present in the vicinity of W_{cat}; as indicated in Table 1, W_{cat} interacts only with the nearby atoms of the protein backbone, e.g. $\mathbf{CO}^{SwI}$, $\mathbf{HN}^{SwI}$, and $\mathbf{HN}^{D+2}$ in the case of the MnmE GTPase (see also the accompanying paper [41]). In dynamins (Fig. 3A), these are the side chain of Gln^{K-4}, $\mathbf{CO}^{SwI}$ and $\mathbf{HN}^{D+3}$.

The titular family of ***translation factors*** unites ribosome-dependent GTPases directly involved in the translation, such as elongation factors EF-Tu and EF-G (Fig. S3B, Table 1). These GTPases showed K^+-dependence both when studied in the absence of the ribosome [76, 77] and under conditions of protein synthesis [78-81]. Earlier, we suggested that these translational GTPases, alike K^+-dependent GTPases, are stimulated by a K^+-ion bound between the side chain of Asp^{K-3} and **CO** of Gly^{T-2} [82]. More recently, crystal structures of these GTPases indeed showed monovalent cations in the predicted position [83]. In the translational GTPases, W_{cat} is uniquely coordinated by the side chain of His^{D+4} residue in addition to **HN** of Gly^{D+3} and **CO** of Thr^{SwI}; the side chain of His turns towards W_{cat} in response to the activating interaction of the WB-crest with the small ribosomal subunit and tRNA [84].

In ***GB1/RHD3-type GTPases*** (e.g. atlastins) the stimulatory Arg finger is in the K-3 position of the P-loop and links the O^{2A} and O^{3G} atoms of GTP when two protein monomers dimerize in response to the interaction with the activating partner (PDB ID 4IDQ [85], Fig. 3B). In this case, Arg fingers stimulate GTP hydrolysis in the very same P-loop domain they belong to. In the case of atlastins, W_{cat} is seen stabilized by $\mathbf{CO}^{SwI}$ and $\mathbf{HN}^{D+3}$ (Table 1, Fig. 3B).

In the GTPase domains of ***α-subunits of heterotrimeric G-proteins***, the intrinsic Arg finger, as provided by a family-specific insertion domain, links O^{2A} and O^{3G} atoms of GTP and is on a H-bond compatible distance from the O^{3B} atom, see Fig. 3C and [43, 86]. The W_{cat} is stabilized by Gln^{D+4} and $\mathbf{HN}^{D+3}$ of the WB-crest, as well as by $\mathbf{CO}^{SwI}$, see Fig. 3C, Table 1 and [43, 86].

The family of ***Ras-like GTPases*** named after its oncogenic members (from *rat sarcoma*), is one of the best-studied groups in the TRAFAC class [15, 49, 50, 87]. In these proteins, the Switch I loop interacts with diverse physiological modulators of activity whereas the specific GTPase activating proteins (GAPs) bind to the WB-crest (also called Switch II in these proteins), see Fig. 1C, 1E, S3C and [15, 49, 88, 89]. As in α-subunits of heterotrimeric G-proteins shown in Fig. 3C, the NH2 group of the stimulatory Arg finger links the O^{2A} and O^{3G} atoms in most structures of Ras-like GTPases (Fig. 1C, 1E; see the accompanying article [41] for the discussion of apparent exceptions). The W_{cat} molecule is stabilized by the side chain of Gln^{D+4}, **HN** of Gly^{D+3}, and $\mathbf{CO}^{SwI}$, see Table 1 and [15, 88, 90].

In P-loop NTPases of the ***kinesin and myosin families*** a Ser residue (Ser^{SwI}) serves as a reference residue of Switch I; Ser^{SwI} provides its side chain oxygen atom to coordinate the Mg^{2+} ion as ligand #3 (Fig. 3D, S3D). In these proteins, the Asn^{S-4} residue inserts between α- and γ-phosphates [91-93], so that the side chain amino group of Asn^{S-4} links the O^{2A} and O^{3G} atoms, see Fig. 3D and the accompanying article [41]. Additional coordination of the γ-phosphate appears to be provided by the side chain of $[Ser/Thr]^{K-4}$ of the P-loop and Ser^{S-1} of Switch I.

The **CO**^{SwI} group and, likely, the side chain of Ser^{S-1} form H-bonds with W_{cat}. One more H-bond with W_{cat} is provided by **HN** of Gly^{D+3} (Table 1, Fig. 3D).

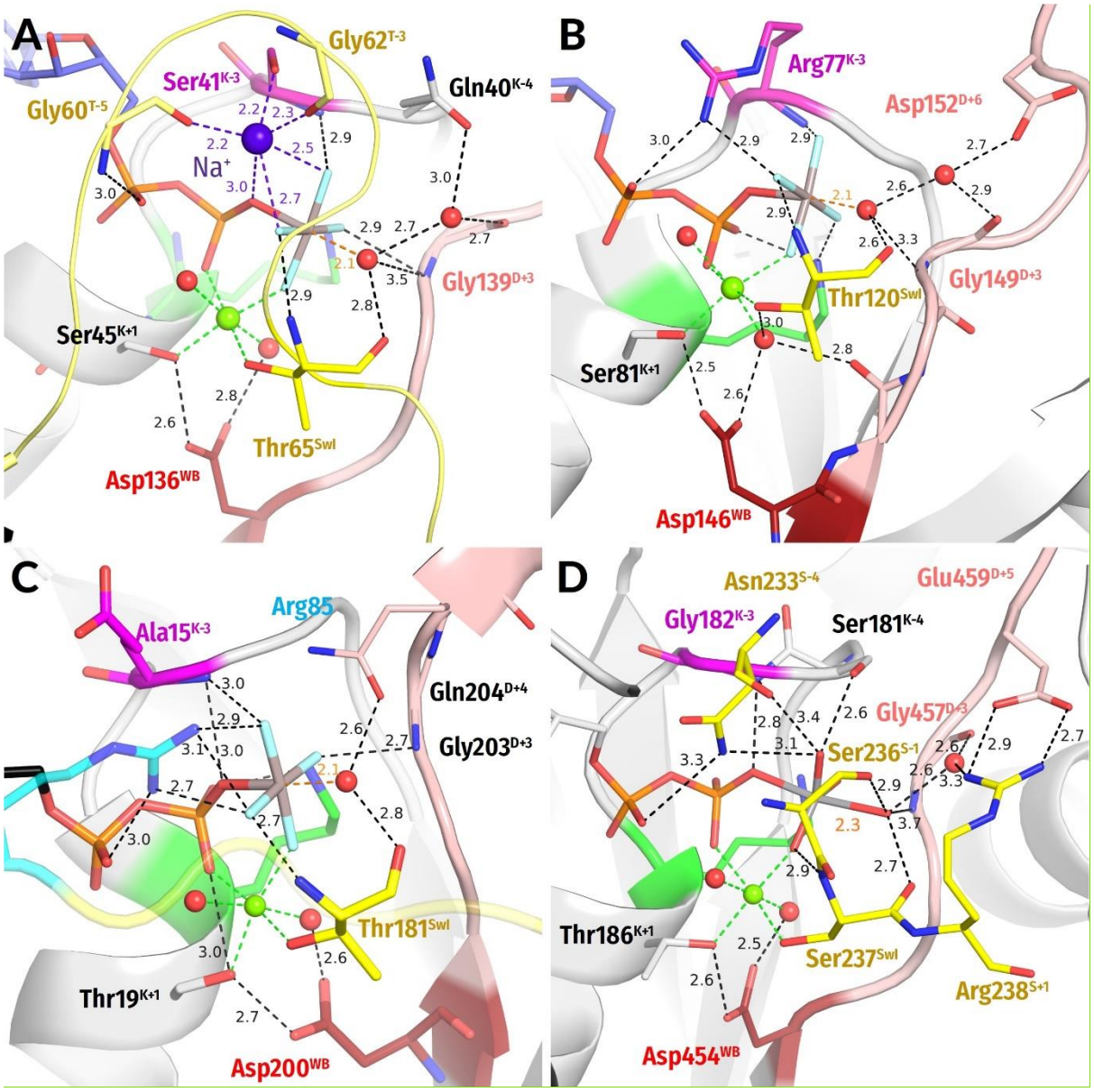

Figure 3. Representative NTPases of the TRAFAC class.
The residues of Switch I/K-loop are shown in yellow, nucleotides, their analogs, and functionally relevant residues are shown as sticks, water molecules and cations are shown as spheres: water in red, Mg^{2+} in lime, Na^{+} in blue. Other colors as in Fig. 1E-F. All distances are given in ångströms. **A,** Dynamin (PDB ID 2X2E, [74]); **B,** Atlastin-1 (PDB ID 6B9F, [94]); **C,** $G\alpha_{12}$ subunit of a heterotrimeric G-protein (PDB ID 2ODE, [86]); **D,** Myosin II, (PDB ID 1VOM [95]).

The SIMIBI class NTPases include ATPases and GTPases that dimerize upon interaction with the activating partner in such a way that catalytic sites of the monomers interact "face to face", see Fig. S3E and [96, 97] for reviews. Each monomer inserts either a Lys (Fig. 4A) or an Arg residue (Fig. 4B) into the catalytic site of the other monomer [96, 97]. Many SIMIBI class ATPases and GTPases contain the so-called "deviant" Walker A motif KGGxGK[S/T] with an additional conserved Lys^{K-5} residue that is inserted into the catalytic site of the partner subunit in a dimer [97]. Lysine fingers, as used by SIMIBI proteins, form H-bonds with both O^{2A} and O^{3G} atoms (Fig. 4A).

Signal recognition particles (***SRPs***) and their cognate receptors ***(SRs***) stand separately within the SIMIBI class. Their GTPase domains form a pseudo-homodimer, where the two GTP binding sites interact face-to-face, but GTP hydrolysis occurs in only one of the two monomers. These proteins employ Arg residues that are inserted reciprocally so that the guanidinium group interacts with the α- and γ-phosphate of the GTP molecule bound by "its" subunit and the α-phosphate of the GTP molecule bound by the other subunit (Fig. 4B).

Many SIMIBI proteins have a Gly^{D+3} residue which appears to provide its $\mathbf{HN}^{D+3}$ for coordination of the γ-phosphate, similarly to Gly^{D+3} in TRAFAC class proteins, see Fig. 4A-B and [10]. Additional coordination of γ-phosphate is provided by amino acids located outside of the conserved motifs. Such residues are protein family-specific and are often introduced into the catalytic site from the adjacent monomer upon the interaction with the activating partner and dimerization (Fig. 4A-B).

The W_{cat} molecule in SIMIBI NTPases is routinely stabilized by **HN** of Gly^{D+3} and the Asp/Glu residue at the C-cap of the WB+1 strand; the carboxy group of this "catalytic" residue links W_{cat} with the Mg^{2+}-coordinating W3 molecule (Fig. 4A-B). Also, the residues of the other monomer and even the ribose 3' hydroxyl group of the "other" GTP molecule can contribute to the coordination of W_{cat}, see Table 1, Fig. 4A-B. The NTP-bound SIMIBI dimer is believed

to require the interaction with an activating protein (or RNA in SRP/SR complexes) to bring these specific "catalytic" residue(s) closer to the catalytic site where they can contribute to the H-bond network around W_{cat} [96, 98].

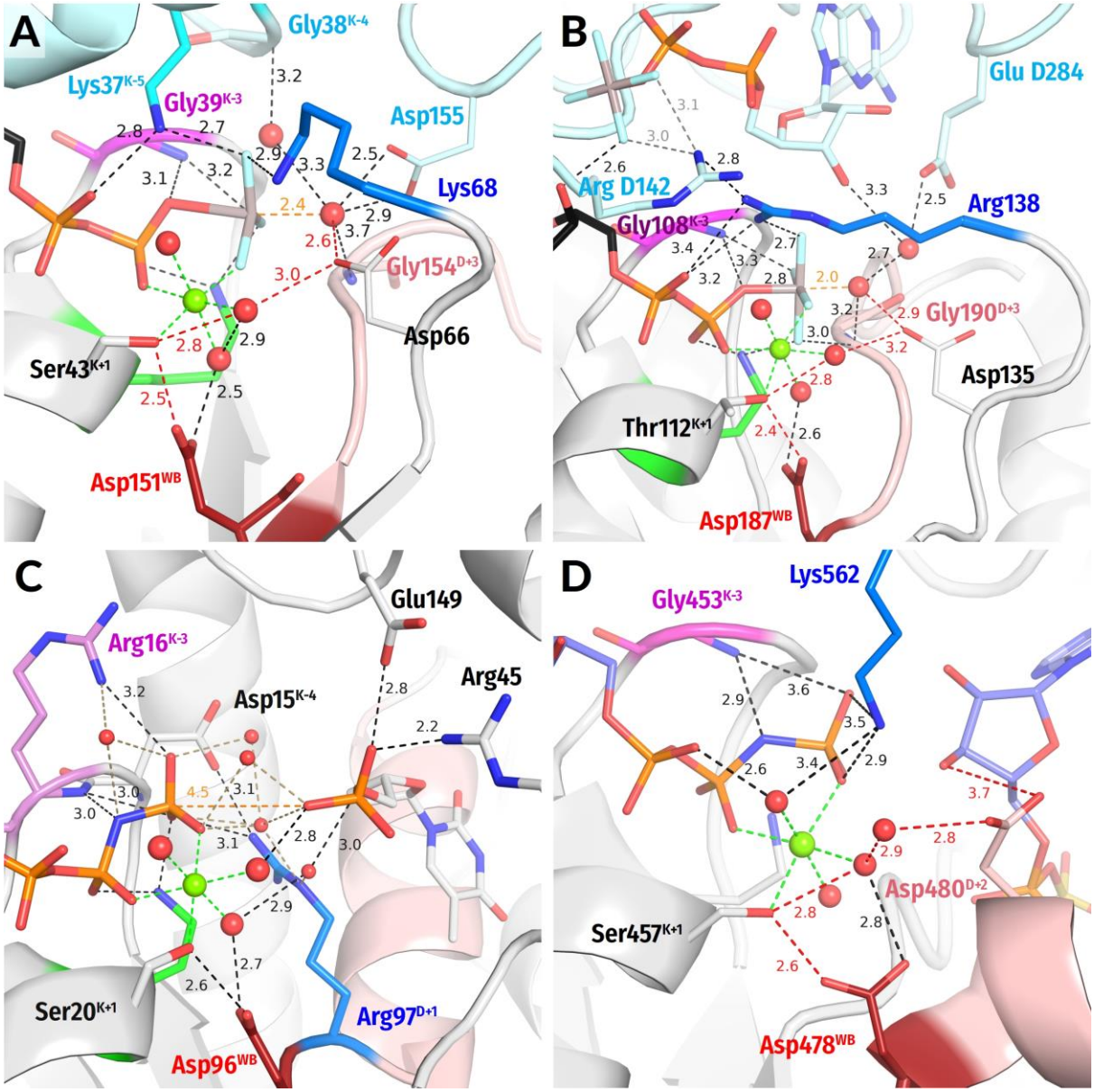

Figure 4. Representatives of the SIMIBI and kinase classes.
The residues of the adjacent monomers in dimers are shown in cyan. Arg and Lys residues belonging to the same protein chain as Walker A motif, i.e. to the lid domains in kinases are shown in blue. Red dashed lines mark protonic connections between W_{cat} and Asp^{WB}. Other colors as in Fig. 3. All distances are indicated in ångströms. **A.** ATP-binding component of the dark-operative protochlorophyllide reductase (PDB ID 2YNM, [99]). **B.** Signal recognition particle (FtsY/Ffh) complex (PDB ID 2CNW, [100]), **C**. Human thymidylate kinase (PDB ID 1NN5 [101]). **D**. Adenosine 5'-phosphosulfate kinase (PDB ID 4BZX, [102]).

Nucleotide Kinases are ubiquitous enzymes that usually transfer a γ-phosphoryl residue from ATP to a wide range of “second” substrates, primarily small molecules [9, 103], see Fig. S3F. The key roles in the catalysis by P-loop kinases are usually played by Arg or Lys residue(s) located in the so-called “LID” domain, a small helical segment that "covers" the catalytic site and often carries several positively charged residues [9, 103, 104], see Fig. 4C-D. In thymidylate kinases, these fingers are assisted by Arg^{K-3}, similarly to atlastines, cf Fig. 3B and 4C. Thus, P-loop kinases do not need other proteins or domains to provide stimulatory Arg/Lys fingers. Instead, binding of their second substrate is enough to trigger the Lid domain rearrangement that results in the insertion of Arg/Lys finger(s). While Arg residues serve as stimulatory moieties in most kinases (Fig. 4C), a Lys residue appears to be involved in adenylylsulfate kinases (Fig. 4D) [105].

One of the stimulatory fingers usually inserts between the α- and γ-phosphates. In the case of the adenosine-5'-phosphosulfate (APS) kinase, the lid domain inserts a Lys finger that interacts directly with the γ-phosphate and is connected to α-phosphate via a water molecule (Fig. 4D). As in many other P-loop NTPases, the catalysis in kinases is usually assisted by auxiliary arginine and lysine fingers that position the interacting molecules and neutralize the negative charges of phosphate groups, see Fig. 4C-D, Table 1 and [56, 106]. Some families of kinases use also an Arg residue of the WB-crest, see Fig. 4C and [9].

In kinases, the hydrolysis of the phosphoryl donor molecule is mediated by the acceptor molecule, which, similarly to W_{cat} in other reactions of NTP hydrolysis, appears to initiate the nucleophilic attack and formation of the pentavalent intermediate. In nucleotide monophosphate kinases, the attacking group is a negatively charged phosphate moiety requiring no specific proton acceptor (Fig. 4C). In those kinase families, where the deprotonation of the attacking molecule is needed to produce a nucleophile, the $[Asp/Glu]^{D+2}$ residue appears to serve as an immediate proton acceptor, see Fig. 4D and Table 1. This residue

links the would-be nucleophilic group with the Mg^{2+} ligand in position 3, usually a water molecule (Fig. 4D).

2.2.2.2. ASCE division

The NTPases of the ASCE division have all-parallel β-pleated sheets with an inserted, as compared to the sequences of the Kinase-GTPase division NTPases, β-strand in the WB+1 position, see Fig.1B, S2, and S4. In many enzyme classes of this division, further additional β-strands were identified, see Fig. S2, S4 and [14, 18, 19]. For coordination of W_{cat}, in addition to class-specific residues, ASCE NTPases typically use a "catalytic" glutamate residue that either directly follows the conserved Asp^{WB} or is located at the C-cap of the WB+1 strand, similarly to SIMIBI NTPases. These two features define the name of this division: *additional strand, catalytic E* (ASCE) [10, 12, 107, 108]. According to current views [14, 18, 19] and the most recent phylogenetic scheme depicted in Fig. S2, the ASCE NTPases are divided into two clades that differ by the number of β-strands in their P-loop domains. The group of "middle-size" domains with up to five-six β-strands includes AAA+ ATPases, helicases of superfamily 3 (SF3), as well as STAND and KAP ATPases. The clade of "large" ATPases domains, with many β-strands, includes helicases of superfamilies 1 and 2 (SF1/2), ABC-ATPases, RecA/F_1 ATPases, VirD/PilT-like ATPases, and FtsK-HerA-like ATPases.

AAA+ ATPases are *ATPases associated with various cellular activities*, where "+" stands for "extended", see Fig. 5A and S4A. These enzymes contain an N-terminal P-loop domain and an additional α-helical C-terminal domain, see [6, 12, 13, 16, 45, 109, 110] for comprehensive reviews. The P-loop domain of the AAA+ ATPases carries conserved Arg/Lys residue(s) from the side that is opposite to the P-loop. The P-loop domains interact upon oligomerization (most often a hexamer is formed), so that the nucleotide-binding site of one subunit receives the Arg/Lys finger(s) from the neighboring subunit (Fig. 5A-B) and/or, in some protein families,

an additional Arg/Lys residue from its own C-terminal helical domain (Fig. 5A), see [16]. One of the stimulatory residues interacts with γ-phosphate and is called "finger" whereas the other one occupies the space between α- and γ-phosphates and is called "sensor 2". We could not find structures of AAA+ ATPases with bound TS analogs; based on available data on site-specific mutants [16], W_{cat} appears to be coordinated by the "catalytic" $[Glu/Asp]^{D+1}$ residue, Arg/Lys finger, and, perhaps, Asn/Ser/Thr residue at the C-cap of the WB-1 strand ("sensor 1", see Fig. 5A). As shown in Fig. 5A, Glu^{D+1} connects a would-be W_{cat} with Mg^{2+}-coordinating W3 in the structure of N-ethylmaleimide sensitive factor (PDB ID 1NSF [111]).

AAA+ NTPases are rather diverse, they can use further polar residues to interact with W_{cat} or γ-phosphate. While the Arg/Lys finger that interacts with γ-phosphate is usually present, the sensor 1 or sensor 2 residues are absent in some enzyme families, as reviewed in [6, 12, 13, 16, 45, 109, 110]. Also, the topology of domains that interact with the P-loop domain can vary. For instance, the helicases of superfamily 3 (SF3 helicases) have different topology of their C-terminal helical domain [13]. Their other specific feature is the presence of a Glu^{WB}–Asp^{E+1} pair at the C-cap of the WB strand; the Asp^{E+1} residue builds a link to the Mg^{2+}-coordinating W3 molecule (Fig. 5B).

SF1/2 class helicases are mostly monomeric or dimeric with each polypeptide chain containing two P-loop fold domains, see [3, 112] for reviews. While SF1 and SF2 helicases differ in the structural motifs that couple their DNA/RNA binding sites with ATP-hydrolyzing catalytic pockets, the pockets proper are quite similar (cf Fig. 1F and 5C, respectively). Both in SF1 and SF2 helicases, the ATP molecule binds to the functional Walker A and B motifs of the N-terminal domain; the C-terminal domain, although it has a P-loop-like fold, lacks the Walker A and B motifs. Following the interaction with an RNA or a DNA molecule, two Arg residues of the C-terminal domain are usually inserted into the ATP-binding site [113]. One of these Arg residues forms H-bonds with both α- and γ-phosphates, whereas the other Arg residue

interacts with γ-phosphate (or its analog) and W_{cat} (Fig. 1F, 5C). The W_{cat} molecule is also coordinated by the "catalytic" Glu^{D+1} residue and class-specific Gln and Arg residues (Fig. 1F, 5C). The same Glu^{D+1} residue links W_{cat} with the Mg^{2+}-coordinating W3 molecule (Fig. 1F, 5C, Table 1).

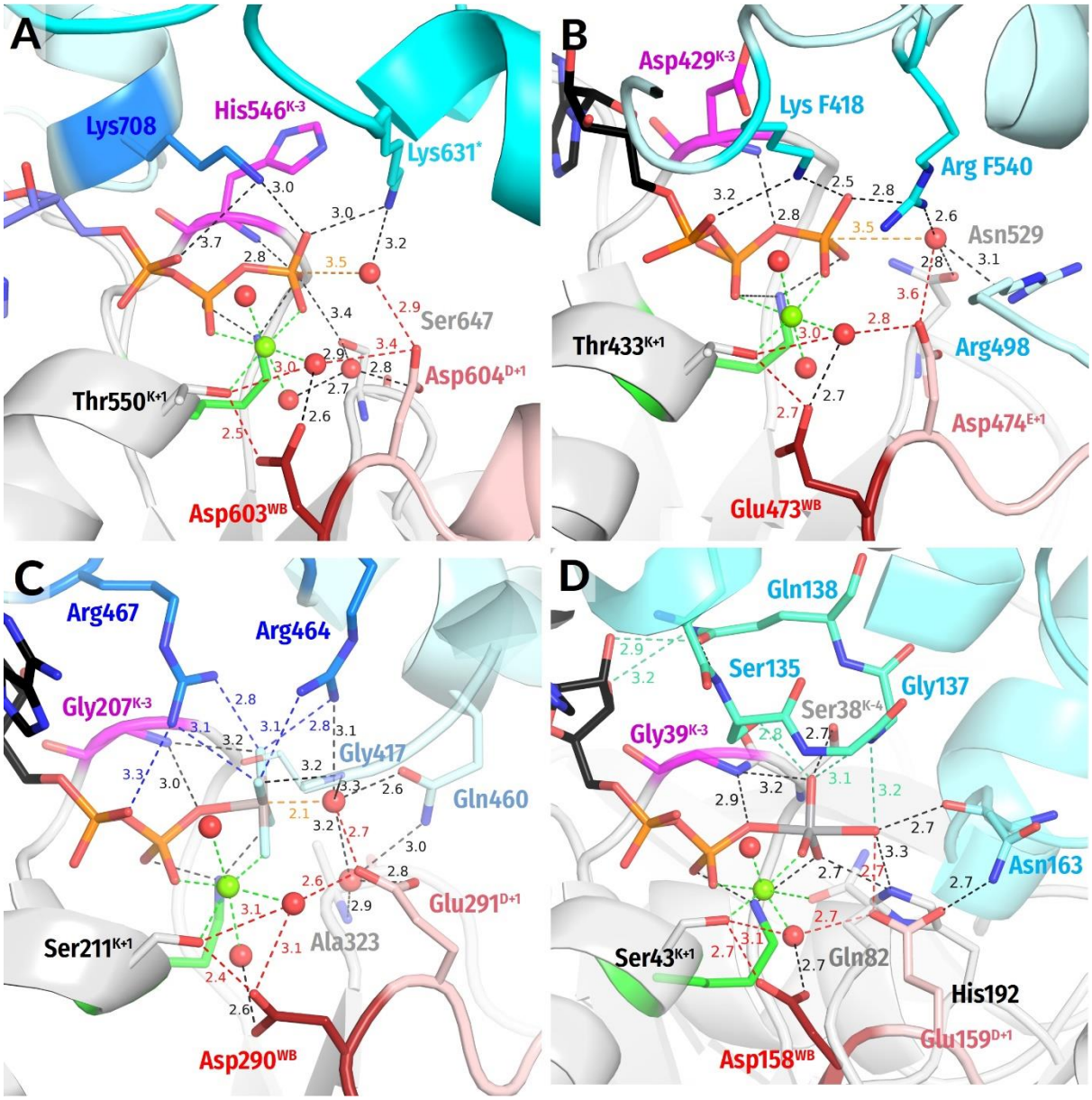

Figure 5. Representatives of AAA+ ATPases, SF3 helicases, SF2 helicases and ABC ATPases.

The adjacent monomers and their Arg and Lys residues are shown in cyan, residues of adjacent monomers labelled in light blue. The Arg residues from the C-terminal helical domain of the same monomer are shown in deep blue (panel C).

Red dashed lines mark protonic connections between W_{cat} and Asp^{WB}. Other colors as in Fig. 3. All distances are given in ångströms. **A,** N-ethylmaleimide sensitive factor (PDB ID 1NSF [111]); **B,** Replicative hexameric helicase of SV40 large tumor antigen (PDB ID 1SVM, [114]);

C, Hepatitis C virus NS3 SF2-helicase (PDB 5E4F [115]). **D,** Outward-facing maltose transporter complex with ADP:VO_4^{-} bound (PDB ID 3PUV, [116]). The LSGGQ motif is shown in green-cyan, the VO_4^{-} moiety by grey and red.

ABC (*ATP-binding cassette*) ATPases are multidomain proteins that usually operate as homo- or heterodimers, see Fig. 5D, S4B and [117, 118]. Their ATP-hydrolyzing domains are usually used to drive large scale conformational changes, e.g. in membrane-embedded ABC-transporters or water soluble complexes involved in DNA repair or translation [19, 119, 120]. In dimers of ABC-NTPases, the nucleotide-binding sites of P-loop domains are located on the interface between the monomers, in the same way, as in dimers of SIMIBI NTPases, cf. Fig. 5D with Fig. 4A-B. Instead of an Arg or Lys residue, each monomer inserts a whole signature motif L<u>S</u>G<u>G</u>Q into the catalytic pocket of the other monomer (Fig. 5D, S4B), see also the accompanying article [41] for details.

The structures with TS analogs bound are available for the maltose transporter complex, see Fig. 5D, Fig. 7D in the accompanying article [41], and [116]. In these structures, the side chain of serine and **HN** of the second glycine residue of the signature motif interact with the O^{3G} atom of γ-phosphate. The side chain of serine is located between the α- and γ-phosphates, in the position of the Na^{+} ion in dynamin-like proteins, cf Fig. 5D with Fig. 3A.

Several amino acids commonly found in the catalytic sites of ABC transporters can stabilize $W_{cat,}$ see Fig. 5D and Table 1. In the case of maltose transporter, these are a histidine residue at the C-cap of the WB-1 strand and Glu^{D+1}; the latter, in addition, links W_{cat} with the Mg^{2+}-coordinating W6 molecule. In the maltose transporter, the activating monomer in a dimer contributes to the coordination of W_{cat} by providing a backbone **CO** group of a residue that is located outside of the signature motif, see Fig. 5D and [116].

RecA/F_1 NTPases class encompasses oligomeric ATP-dependent motors involved in homologous recombination and DNA repair (RecA and RadA/Rad51), catalytic subunits of rotary F/N- and A/V-type ATP synthases, helicases of superfamilies 4 and 5 (SF4 and SF5), as

well as several other protein families [3, 107, 121]. In NTPases of this class, similarly to most AAA+ ATPases, the stimulatory moiety(is) is/are inserted in the catalytic site by the P-loop domain of the adjacent monomer (Fig. 6, S4C).

Our structure analysis showed that the stimulation mechanism appears to differ between rotary F_1-ATPases/SF5 helicases, on the one hand, and recombinases/SF4 helicases, on the other hand.

In the ***F_1-ATPases***, the stimulatory Arg residue of the adjacent monomer interacts with both α- and γ-phosphates, whereas an additional, intrinsic Arg residue coordinates γ-phosphate, approaching it apically (see Fig. 6A, S4C and Table 1). A similar stimulation mechanism is realized in ***SF5 helicases***, see e.g. the Rho helicase (PDB ID 6DUQ [122]).

The W_{cat} molecule is seen in the catalytic apical position only in the ADP:AlF_4^- -containing structure of the bovine F_1-ATPase (PDB ID 1H8E, Fig. 6A) [54]. While in most ASCE ATPases the W_{cat}-coordinating Glu^{D+1} residue directly follows the Asp^{WB} of the Walker B motif, the W_{cat}-coordinating Glu188 of the F_1-ATPase, similarly to SIMIBI NTPases, is at the C-cap of the WB+1 strand; within the ASCE division this feature is specific for the RecA/F_1 class members [8]. This glutamate residue also links W_{cat} with the Mg^{2+}-coordinating W3 molecule (Fig. 6A). In F_1-ATPase, W_{cat} is also stabilized by $Arg260^{D+4}$; this residue concurrently interacts with the activating neighboring monomer, which also provides a **CO** group to stabilize W_{cat} (Fig. 6A).

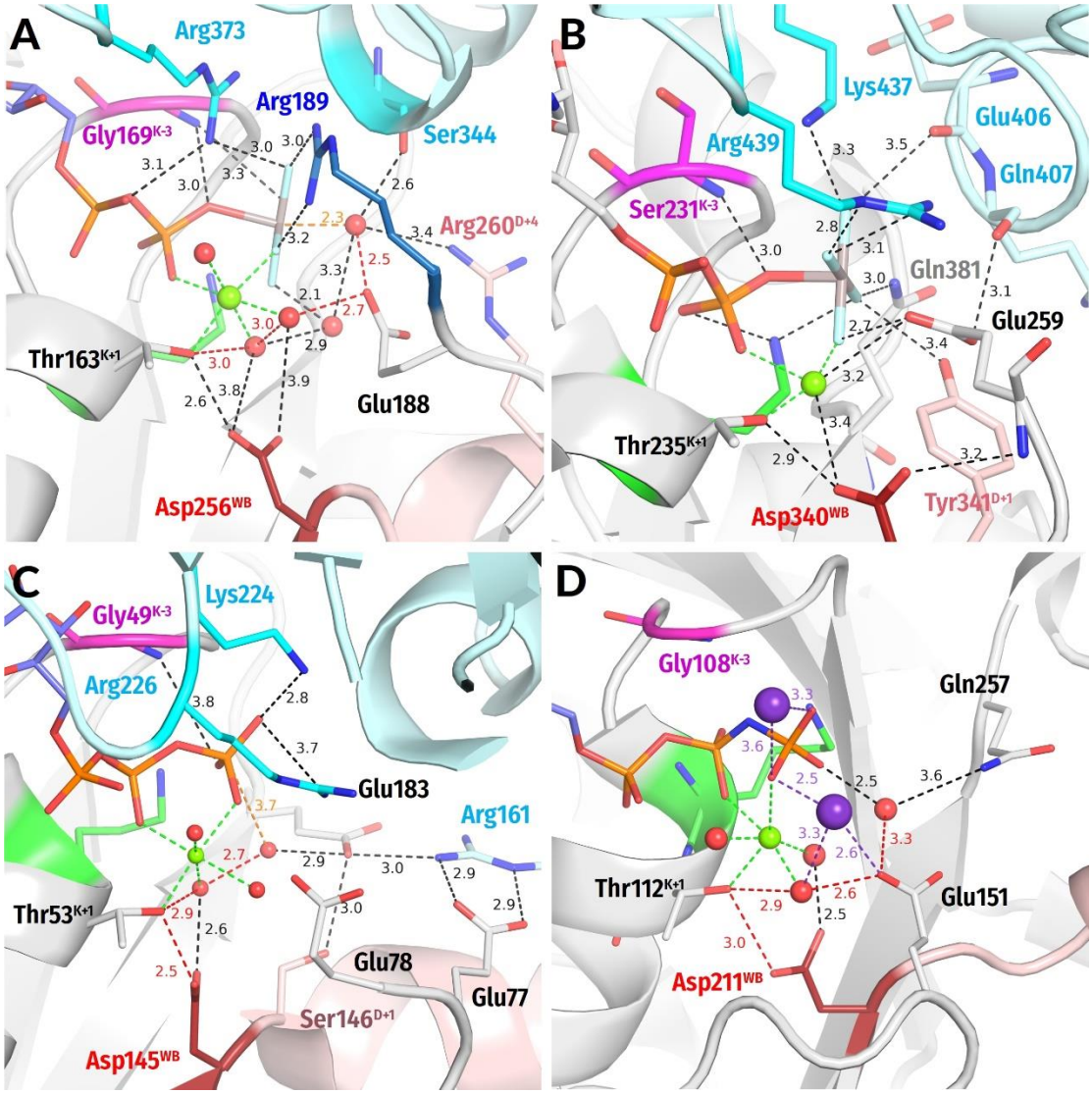

Figure 6. Representative proteins of the RecA/F$_1$-like class of the P-loop NTPases. The adjacent monomers and their Arg and Lys residues are shown in cyan, K^+ ions are shown as purple spheres. The Arg residue from the P-loop domain proper is shown in deep blue (panel A). Red dashed lines mark protonic connections between W_{cat} and Asp^{WB}. Other colors as in Fig. 3. All distances are in ångströms. **A,** Bovine F$_1$-ATPase (PDB ID 1H8E, [54]); **B,** DnaB replicative helicase from *Vibrio cholerae* (PDB 6T66 [123]); **C**, circadian clock protein KaiC (PDB ID 4TL7, [124]); **D,** RadA recombinase (PDB ID 3EW9, [125]).

In ***RecA-like recombinases*** and ***SF4 helicases***, two stimulatory positively charged moieties interact only with the γ-phosphate group, in contrast to F$_1$-ATPases. In several families, the adjacent subunit provides one Lys residue and one Arg residue that form a short KxR motif [126], with both residues reaching only γ-phosphate. These are, for instance, the bacterial helicase DnaB (Fig. 6B, see also [127]), circadian clock protein KaiC (Fig. 6C [124]), and gp4d helicase from the T7 bacteriophage (PDB ID 1E0J, [128]). In bacterial RecA recombinases,

the adjacent monomer in the homooligomer provides two Lys residues which approach the phosphate chain laterally and interact with γ-phosphate as in the RNA recombinase of *E. coli* (see Table 1 and PDB ID 3CMX, [129]). In archaeal and eukaryotic RadA/Rad51-like recombinases, the positions of terminal groups of stimulatory Lys/Arg residues are occupied by two K^+ ions, which appear to interact with γ-phosphate, see Fig. 6D and [126, 130].

In the case of RecA-like ATPases, the AlF_4^--containing structures of the bacterial DnaB helicase of *Vibrio cholerae* (Fig. 6B), *Bacillus stearothermophilus* (PDB ID 4ESV, [131]) and RecA recombinase of *E. coli* (PDB ID 3CMX, [129]) are available. However, the apical water molecule is absent from these structures, the possible reasons of which are discussed in [127]. Therefore, the full set of W_{cat}-coordinating groups remains unknown for RecA-like ATPases; the available structures imply the participation of glutamate residues at the C-terminus of the WB+1 strand (Fig. 6B-D), as in other RecA/F_1 class enzymes. The same residue appears to link the would-be W_{cat} with the Mg^{2+}-coordinating W3 molecule (Fig. 6B-D).

Generally, the H-bond networks around γ-phosphate and W_{cat} seem to be richer in RecA/F_1-NTPases than in other classes of P-loop NTPases. Specifically, the coordination of W_{cat} may potentially also involve the D+1 residue of the WB strand, which is usually a H-bonding Ser/Thr/Asn/Tyr, as well as other polar residues at the C-caps of the WB-1 and WB+1 strands [112, 124, 132].

2.2.3. Water molecules in the vicinity of the Mg^{2+} coordination shell

The W_{cat} molecule should be deprotonated on some stage of the catalytic cycle, see Fig. S1 and [15, 48, 56-59, 61-63, 133]. However, the pK_a value (hereafter pK for simplicity) of water is 14.0, which hinders the deprotonation both thermodynamically and kinetically.

The P-loop NTPases, in general, are not alone in their need to deprotonate a water molecule and to use the resulting hydroxyl for hydrolyzing the O-P bond. In various other, evolutionarily

unrelated Mg-dependent enzymes, Mg^{2+} ions are thought to decrease the pK value of potential nucleophilic water molecules [60, 134-137]. In such cases, usually, the would-be nucleophilic water molecule belongs to the first or second coordination shell of the metal cation. In the case of P-loop NTPases, the Mg^{2+} ion is remote from W_{cat} and can incite its deprotonation only if there is a protonic pathway between W_{cat} and the coordination shell of Mg^{2+}. Therefore, we manually searched for connections between W_{cat} (or the would-be W_{cat}) and the Mg^{2+}-coordinating ligands.

In many high-resolution structures of P-loop NTPases with bound substrate molecules or their analogs, water molecules are present in the vicinity of γ-phosphate and interact with the O^{1G}, O^{2G}, O^{3G} atoms of γ-phosphate, as seen in Fig. 7. In principle, a water molecule can interact with up to two oxygen atoms, which allows categorizing the γ-phosphate-bound water molecules as, for example, W_{12}, W_{13}, or W_{23}. Most likely, one of these molecules becomes the W_{cat} upon activation. For instance, Fig. 7A shows a structure of RadA from *Pyrococcus furiosus* that was post-soaked with ATP, see PDB ID 4A6X and [138]. The structure clearly shows W_{12} and W_{13} and resolves two conformations of the "catalytic" Glu174 of the WB+1 strand. In both conformations, Glu174 interacts with W_{13}, the apparent would-be W_{cat} in this enzyme. However, only in the Glu174A conformation, the side chain of Glu174 connects W_{cat} with the Mg^{2+}-coordinating W3 molecule.

Similarly, the "catalytic" Glu or Asp residues link W_{cat} with Mg^{2+}-ligands #3 or #6 in TS-like structures of NTPases of all classes (except the TRAFAC class), as already repeatedly noted throughout the Section 2.2. The tentative proton pathways from W_{cat} towards the Mg^{2+}-ligands are shown by red dashed lines in Fig. 4A-B, 4D, 5A-D, 6A, 6C-D.

In the case of TRAFAC class NTPases, which lack "catalytic" Glu/Asp residues, connections between W_{cat} and the Mg^{2+}-coordinating ligands are not so evident. The water molecules

around γ-phosphate appear to be highly mobile and hardly crystallizable. In the absence of TS-analogs, those water molecules that interact with γ-phosphate are usually resolvable in the structures only if constrained by additional interactions. For instance, in the ATP-soaked myosin structure (PDB ID 1FMW [139], see Fig. 7B), W_{12} is resolved because it is additionally bound to **CO** of Ser^{S-1}. This W_{12} molecule is at a H-bond-compatible distance from the Mg^{2+}-coordinating W6 molecule.

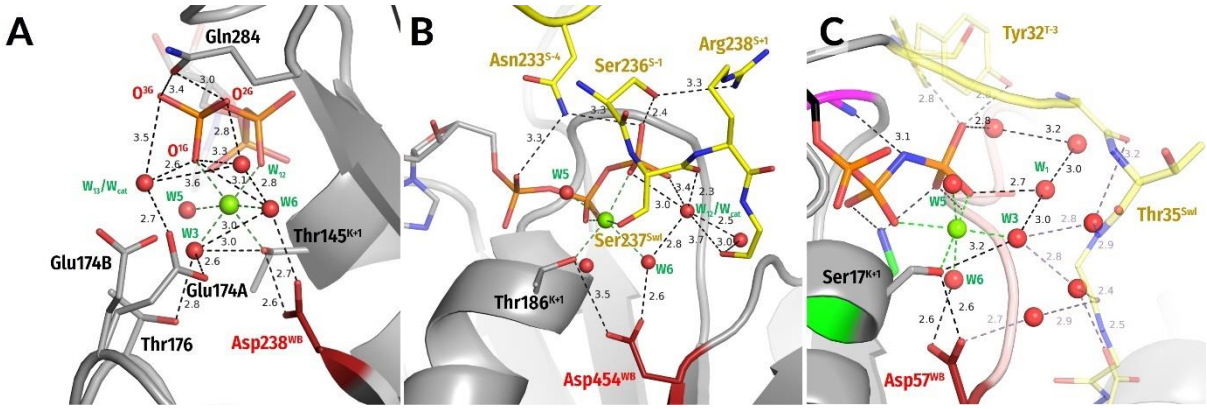

Figure 7. Networks of water molecules in the catalytic sites of P-loop NTPases. **A**, ATP-soaked ATPase domain of RadA from *Pyrococcus furiosus* (PDB ID 4A6X, [138]); **B**, ATP-soaked Myosin II from *Dictyostelium discoideum* (PDB ID 1FMW, [139]); C, human H-Ras GTPase (PDB ID 5B30 [140]). Colors as in figures 3-6.

In TS-like structures of small GTPases of the TRAFAC class, the closest to W_{cat} Mg^{2+}-coordinating ligand is $[Ser/Thr]^{SwI}$ of Switch I at about 4-5 Å (Fig. 1E, 3A-D). In these proteins, however, the Switch I motif is very dynamic so that the protein fluctuates between "open" and "closed" conformations even with a bound substrate or its analogs [140-142]. While in the closed conformation $[Ser/Thr]^{SwI}$ serves as ligand #3 for Mg^{2+}, in the open conformation the whole Switch I moves away from Mg^{2+} and a water molecule serves as ligand #3 (Fig. 7C, S5B). Notably, Matsumoto and colleagues succeeded to control the open to close transition in H-Ras GTPases by changing the humidity [140]. The crystal structure of H-Ras that crystalized in the open conformation at low humidity (PDB ID 5B30) reveal an additional water molecule next to W3 (Fig. 7C). It is depicted as W_1 in Fig. 7C and occupies approx. the same position as

W_{12} in the myosin structure in Fig. 7B. In the closed conformation (Fig. 1E, 3A-D), Switch I reaches Mg^{2+} and ousts W_1 and W3; only W_{cat} is present in the TS-like structure (cf Fig. 1E and 7C). As argued in section 3.2.2.4 of the Discussion, one of the two waters seen in the "open" structure may turn into W_{cat} whereas the other may transiently form a proton pathway between would-be W_{cat} and the Mg^{2+}-coordinating $[Ser/Thr]^{SwI}$.

2.2.4. Local molecular electric field in P-loop NTPases

In structures of P-loop NTPases that are shown in Fig. 1-7, the positive charged groups that stabilize the triphosphate chain, namely the Lys^{WA} residue, the backbone **HN** groups, the stimulatory moiety(ies), the auxiliary residues, and the positively charged N-terminus of the first α-helix are opposed by acidic residues that interact with W_{cat} either directly or via water bridges. Together with Asp^{WB}, these catalytic acidic residues form negatively charged clusters. Fig. 8 shows, for diverse P-loop NTPases, these positively and negatively charged clusters, which should produce a strong local electric field, as argued in the Discussion section.

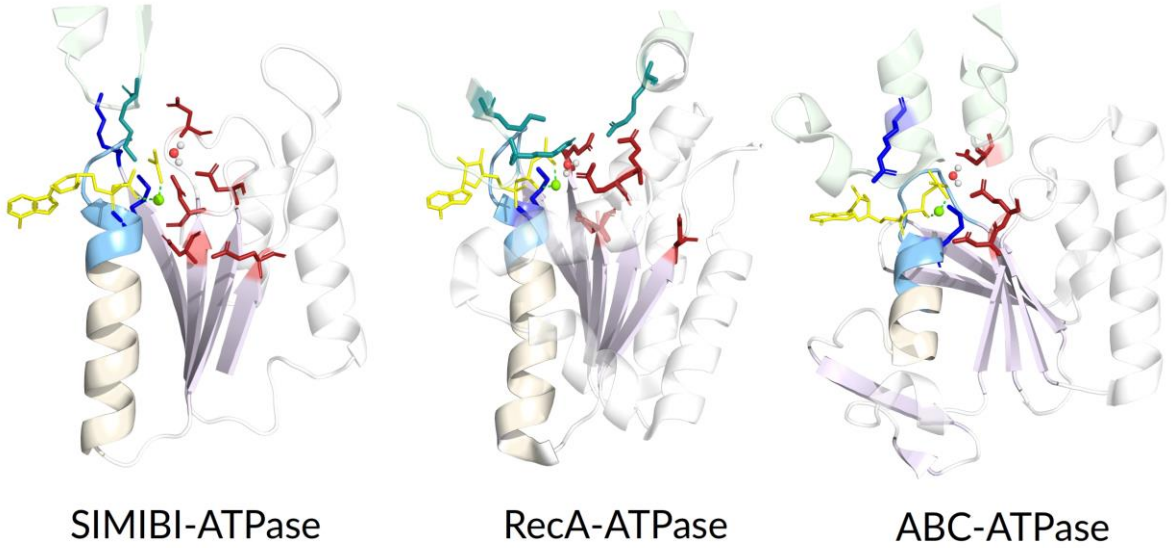

Figure 8. Uneven distribution of charged residues around nucleotide binding pockets in different classes of P-loop NTPases. Nucleotide analogs are shown in yellow, negatively charged residues are shown in red, positively charged residues are shown in blue and teal, the α_1 helix is shown in beige with its N-terminus and the P-loop shown in light blue.

A, SIMIBI class, light-independent protochlorophyllide reductase iron-sulfur ATP-binding protein chlL) (PDB ID 2YNM, [99]); **B**, RecA class, circadian clock protein kinase KaiC (PDB ID 4TL7, [124]); **C**, ABC-ATPase class, MBP-maltose transporter complex (PDB ID 3PUW,[116]).

2.3. Global structural analysis of hydrogen bonding between the Walker A and Walker B motifs in the whole set of P-loop NTPases with bound Mg-NTP complexes or their analogs

As described in the Methods section as well as in the in the accompanying article [41], we extracted from the Protein Data Bank (PDB) at www.rcsb.org [71, 72] those structures of P-loop NTPases that have substrates or their analogs bound together with a Mg^{2+} ion, yielding as many as 1383 structure entries with 3136 full-fledged catalytic sites (as of 11.0.2019; many of the structures contained several catalytic sites). The criteria for selection of full-fledged catalytic sites and the routine of their subsequent structural analysis are described and depicted in the Methods section of the accompanying article [41]. As discussed in Section 2.2 and depicted in Fig. 2, the shape of the P-loop and the spatial position of Asp^{WB} relatively to it are strictly conserved among P-loop NTPases. Building on that, we were able, here and in the accompanying article [41], to use the atomic coordinates of the Mg-triphosphate to pinpoint the catalytically relevant residues in an almost sequence-agnostic way, as described in the Methods sections of both articles. We applied this approach to perform analysis of nucleotide-binding sites in thousands of structures of P-loop NTPases. Relevant data on all these catalytic sites are cumulated in Supplementary Table 1 (hereafter Table S1).

Based on the type of the molecule bound, the catalytic sites could be sorted into four groups: 1043 sites contained native ATP/GTP molecules; 1612 sites contained bound non-hydrolyzable NTP analogs such as Adenosine 5′-[β,γ-imido]triphosphate, (AMP-PNP), Guanosine 5′-[β,γ-imido]triphosphate (GMP-PNP), Adenosine 5′-[*β*,*γ*-methylene]triphosphate (AMP-PCP),

Guanosine 5′-[β,γ-methylene]triphosphate (GMP-PCP), Adenosine 5′-[γ-thio]triphosphate (ATP-γ-S), and Guanosine 5′-[γ-thio]triphosphate (GTP-γ-S); 234 sites contained NDP:fluoride complexes mimicking the substrate state, such as NDP:BeF_3 and NDP:AlF_3, and 247 sites were with TS analogs NDP:AlF_4^-(204), NDP:MgF_3^- (10) and ADP:VO_4^- (33).

2.3.1. The H-bond between Asp^{WB} and $[Ser/Thr]^{K+1}$ is shorter in the presence of transition state analogs

The H-bond between Asp^{WB} and $[Ser/Thr]^{K+1}$ is special because it links the Walker A and Walker B motifs. Consequently, the length of this bond is a good measure of the catalytic site constriction. Upon our manual analysis, we noted that this H-bond is particularly short in the NDP:AlF_4^--containing representative structures (see Fig. 1-6). Therefore, we measured the distances between the two residues to characterize their H-bonding in all the available structures of P-loop NTPases with bound substrates or their analogs, as described in the Methods section. The results of these measurements for all the analyzed structures are presented in Table S1. Fig. 9 summarizes the data on best resolved structures (with resolution of 2.5 Å or less). The data for the three TS analogs are plotted separately for the sake of clarity. We consider as short the H-bonds of < 2.7 Å [143]; the range of short H-bonds is highlighted by cyan. As seen in Fig. 9, the length of the H-bond between Asp^{WB} and $[Ser/Thr]^{K+1}$ is, on average, < 2.7 Å in all groups of structures and < 2.6 Å in structures with ATP/GTP, nonhydrolyzable NTP analogs and NDP:MgF_3^- or NDP:AlF_4^- as TS analogs. Specifically, in NDP:AlF_4^--containing structures the H-bond distance is on average as short as 2.5 Å. It is noteworthy that improper binding of AlF_4^- can distort the coordination sphere of Mg^{2+}, as documented in the accompanying article [41]. Therefore, for the plot in Fig. 9, we selected only the sites with a correct Mg^{2+} coordination; the cut-off for the distance between Mg^{2+} and $[Ser/Thr]^{K+1}$ was 2.5 Å. When comparing only TS analogs, fluoride complexes were superior to vanadate complexes in their ability to constrict the catalytic site, as can be judged from the

distributions of the Asp^{WB}–$[Ser/Thr]^{K+1}$ bond lengths (Fig. 9). From the same data it follows that the NDP:AlF_4^- complexes "overperform" other metal fluorides complexes in the ability to constrict the catalytic pocket.

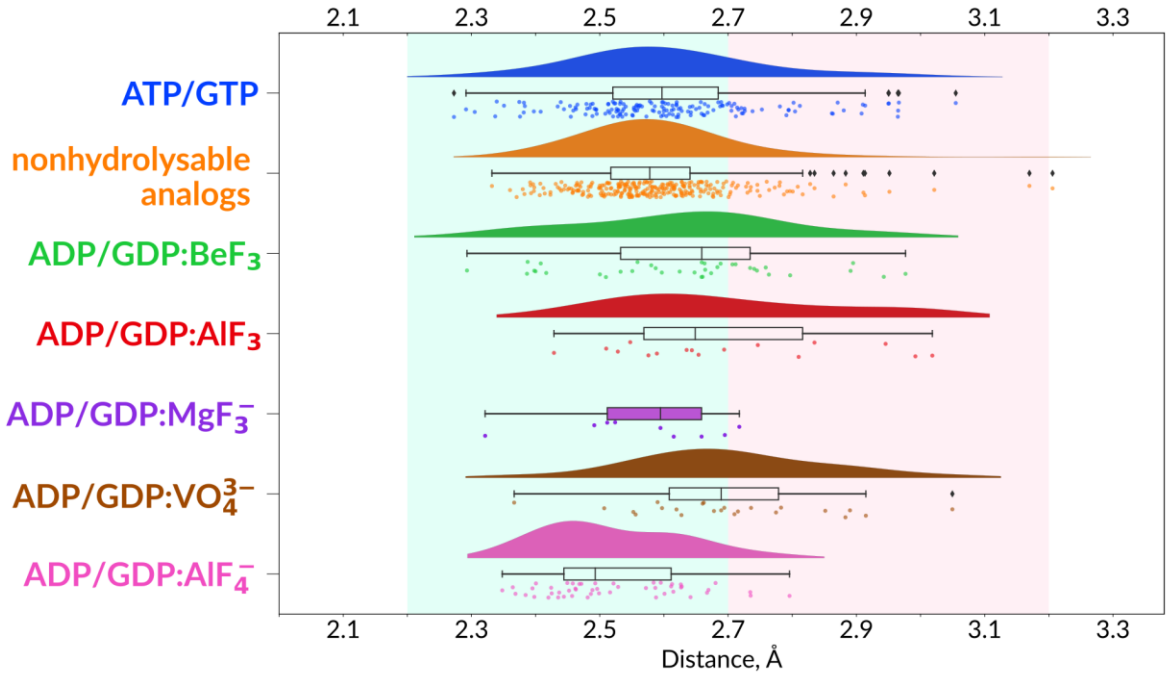

Figure 9. Distances between the side chains of $[Asp]^{WB}$ and $[Ser/Thr]^{K+1}$. For each type of complexes, distances are visualized as a kernel density estimate (KDE) plot, a boxplot and individual data points, each point representing one catalytic site in one structure. For ADP/GDP:MgF_3^- complexes the density plot is not shown owing to the scarcity of data. Data are shown only for structures with resolution ≤ 2.5 Å (see Table S1 for the whole data set). The integrity of catalytic sites was checked by two criteria: the $[Ser/Thr]^{K+1}$ – Mg^{2+} distance ≤ 2.5 Å and Mg^{2+} – Asp^{WB} distance ≤ 6 Å. The range of short H-bonds (2.2 Å-2.7 Å) is highlighted in cyan, the typical H-bond range (2.7 Å-3.2 Å) is highlighted in pale pink.

2.3.2. The TS analog AlF_4^- makes more bonds within the catalytic site than MgF_3^- or AlF_3

We hypothesized that the unique ability of AlF_4^- to pull the catalytic site together may correlate with its ability to enter more bonds than MgF_3^-, AlF_3 or BeF_3. We tested this hypothesis by comparing the structures of the same activated complexes with bound NDP:AlF_4^- and NDP:MgF_3^-/AlF_3, respectively. We counted and measured all the bonds in catalytic sites for the two pairs of such structures. One pair of structures consisted of RhoA GTPases in complex with their activator RhoGAP and GDP:AlF_4^- (PDB ID 1TX4, resolution 1.65 Å [144]) or GDP:MgF_3^- (PDB ID 1OW3, resolution 1.8 Å [34]), respectively, bound. The other pair was made up of catalytic sites of bovine mitochondrial F_1-ATPase with bound ADP:AlF_4^- (PDB ID 1H8E, resolution 2.0 Å [54]) or ADP:AlF_3 (PDB ID 1E1R, resolution 2.5 Å [70]), respectively. In the latter case, the fluoride derivative can be identified as a genuine ADP:AlF_3 by the similarity of its geometry to that of the Mn-ADP:AlF_3 complex in the Zika virus helicase (PDB ID 5Y6M [145]), see the accompanying paper [41] for details.

The findings are summarized in Supplementary Table S2 (hereafter Table S2), which shows that AlF_4^- forms more bonds with surrounding residues than MgF_3^- or AlF_3. Specifically, AlF_4^- usually makes two H-bonds, one moderate and one weak, with Lys^{WA}, whereas MgF_3^- or AlF_3 make only one bond. In addition, AlF_4^- makes two H-bonds with $\mathbf{HN}^{K-3}$, whereas MgF_3^- or AlF_3 make only one (cf Table S1 and S2). Furthermore, many of the AlF_4^- bonds are shorter than those of MgF_3^-, see Fig. 9 and Tables S1 and S2. Apparently, the NDP:AlF_4^- complexes have more potency to constrict he catalytic site than other TS analogs.

3. Discussion

Here and in the accompanying article [41], we reported the results of a comparative structural analysis of more than 3136 catalytic sites of P-loop NTPases with nucleoside triphosphates or their analogs bound. The aim of the analysis was to deduce the main structural features common to the catalytic sites of P-loop NTPases and use them to elucidate the mechanism(s) of stimulated NTP hydrolysis.

In our work, we used the tools of evolutionary biophysics, which assumes that certain structural elements are conserved by evolution because of their functional importance and that the degree of conservation of the structural elements involved should be taken into account when choosing from several possible biophysical mechanisms consistent with the structural data, see [126, 146-150] for some examples of this approach. In the case of P-loop NTPases, the *in silico* approach is particularly justified since the experimental investigation of all members of this vast superfamily would be unrealistic. In addition, P-loop NTPases are unique in that their catalytic repertoire is unusually narrow for such a vast superfamily [11], which increases the chances of finding a common catalytic mechanism.

3.1. Structure comparison of P-loop NTPases

3.1.1. Constriction of the catalytic site in the transition state

The data presented here, as well as data from the accompanying article [41], show that binding of TS analogs leads to greater constriction of catalytic sites than binding of ATP, GTP, or their analogs. In some cases, this constriction can be revealed by comparing the structures of same P-loop NTPases with bound substrate/substrate analogs and TS-analogs, respectively (Fig. S5). In the presence of a TS analog, the WB-crest moves closer to γ-phosphate (Fig. S5).

Furthermore, the Switch I of TRAFAC class NTPases undergoes dramatical conformational changes (see Fig. S5B, cf Fig 1E and 7C).

The constriction also manifests itself in the convergence of the Walker A and Walker B motifs. As it follows from Fig. 9 and Table S1, the most H-bonds between the side chains of Asp^{WB} and $[Ser/Thr]^{K+1}$ residues can be categorized as short in those structures that contain ATP/GTP or their non-hydrolyzable analogs. Apparently, these short H-bonds form upon "closing" of the catalytic site in response to the substrate binding. Still, these H-bonds are even shorter in the presence of NTP:AlF_4^- and NTP:MgF_3^- (Fig. 9, Table S1), which indicates a further constriction of the catalytic pocket in the presence of these TS analogs.

Noteworthy, our structural analysis initially revealed Asp^{WB} – $[Ser/Thr]^{K+1}$ distances of ≥ 4.0 Å in several NTP:AlF_4^--containing structures (see Table S1). Further inspection of these structures, however, has shown that AlF_4^- moiety is "improperly" bound; it makes two bonds with Mg^{2+} in all such structures but one (Table S1). When AlF_4^- makes two bonds with Mg^{2+}, the bond between Mg^{2+} and $[Ser/Thr]^{K+1}$ can get lost and the whole catalytic site undergoes distortion, as detailed and illustrated in the accompanying article [41]. In these cases, (all marked pink in Table S1), the structure of the catalytic site cannot be considered as analogous to the TS.

After we excluded these cases, the Asp^{WB} – $[Ser/Thr]^{K+1}$ distances found to be H-bond compatible in all TS-analog-containing structures (about 200) but one, which is depicted in Fig. S6 and discussed in its caption (Table S1). Hence, AlF_4^--containing P-loop NTPases can be used as reliable models of transition states, in support of earlier suggestions [48, 53, 56, 151], provided that the "properness" of the interaction between AlF_4^- and Mg^{2+} is checked in each particular case.

Earlier, our MD simulations of the MnmE GTPase showed that γ-phosphate, after its twisting by the stimulatory K^+ ion, was stabilized by a new H-bond between NH^{K-3} and O^{2G} [40]. Our structural analysis, as presented in the accompanying article [41], strongly indicates that the counter-clockwise twist of γ-phosphate correlates with the formation of a new H-bond with O^{2G} indeed. Specifically, H-bond-compatible distances between $\mathbf{HN}^{K-3}$ and the nearest oxygen/fluorine atom are seen in most structures with TS analogs bound, see Table S1 and the accompanying paper [41].

Twisted γ-phosphates and H-bond compatible $\mathbf{HN}^{K-3}$ - O^{2G} distances are also seen in diverse NTP-containing NTPases which were crystalized in their pre-transition configurations because of mutated W_{cat}-coordinating residues and/or their impaired interaction with W_{cat}, see Table S1 and Fig. 3 in the accompanying paper [41].

In sum, as it follows from Fig. 9, S5, Table S1, and the data in the accompanying article [41], the structures with TS analogs bound have particularly short H-bonds between $\mathbf{HN}^{K-3}$ and O^{2G}, as well as between Asp^{WB} and $[Ser/Thr]^{K+1}$, which suggests an additional constriction of the catalytic site in the TS.

3.1.2. Transition state analogs and energetics of P-loop NTPases

The observation of the shortest H-bonds within the catalytic sites in the presence of $NDP:AlF_4^-$ (see Fig. 9, Table S1 and S2) helps to clarify why these complexes are most potent functional TS-mimics in P-loop NTPases [34, 42, 43, 48, 49, 53, 54, 56, 90, 151-160]. Beginning in 1987, that is, even before the first $GDP:AlF_4^-$-containing structures were resolved in 1994 [42, 43], metal fluorides were shown to promote binding of various P-loop NTPases to their activating partners. Generally, many NTPases interacted with their activators only in the presence of

metal fluorides [48, 49, 53, 56, 90, 151-154, 156, 161, 162]. Crystal structures of P-loop NTPases with NDP:AlF_4^- or NDP:AlF_3/NDP:MgF_3^- complexes bound [34, 42, 43, 48, 54, 56, 90, 155, 160] show that metal-fluorides have planar (AlF_4^- and MgF_3^-) or almost planar (NDP:AlF_3) structures with W_{cat} in the apical attack position, see respective panels in Fig. 1-6 and the accompanying paper [41]. While the shape and electric charge of MgF_3^- is the same as that of γ-phosphate in the anticipated TS (see Fig. S1), the shape of AlF_4^- differs significantly, it is tetragonal instead of trigonal. Nevertheless, NDP:AlF_4^- complexes are more potent functional analogs of the TS than NDP:MgF_3^- or NDP:AlF_3, as follows from their superiority in promoting binding of P-loop NTPases to their activators [48, 49, 53, 56, 90, 151-154, 156, 161, 162]. In addition, the distances between W_{cat} and the metal atom are shorter (2.0-2.1 Å) in the case of NDP:AlF_4^- complexes than NDP:MgF_3^- (approx. 2.5 Å) or NDP:AlF_3 complexes (approx. 3.0 Å) see the accompanying article [41] and [48, 56]. The reason why NDP:AlF_4^- performs better than other substrate and TS analogs in all these cases has remained obscure, see e.g. [151].

The reason could be, however, understood by considering the energetics of P-loop NTPases. Our earlier MD simulations have shown that the linking of α- and γ-phosphates by an inserted stimulatory cationic moiety is an endergonic reaction; about 20-25 kJ/mol appear to be needed to twist the γ-phosphate by straining its bonds with Mg^{2+} and Lys^{WA} [40, 163]. This activation barrier prevents haphazard NTP hydrolysis due to accidental insertion of a K^+ ion or an Arg residue in the catalytic site, as argued elsewhere [40, 163]. These estimates from MD simulations corroborate earlier considerations of Warshel and colleagues that the stimulation of hydrolysis in P-loop NTPases by their cognate activators requires an input of about 20-25 kJ/mol of free energy, see e.g. [65, 133].

A specific problem of P-loop NTPases is the source of a such free energy input. In most enzymes, the free energy for lowering the activation barrier – by destabilizing the substrate-bound ground state and/or stabilizing the TS – is usually provided by substrate binding [164]. In P-loop NTPases, where the substrate binding step is separated from the ultimate catalytic step in most cases, the energy of substrate binding is partly used to bring the NTP molecule into its extended, catalytically prone conformation with eclipsed β- and γ-phosphates [36, 38, 165]. Another part of the binding energy is used to pre-organize the catalytic site, with the conformational changes that accompany catalytic site closure often being coupled with useful mechanical work, e.g. in myosins [92, 166]. While increasing the rate of NTP hydrolysis as compared to that in water (by five orders of magnitude in the case of Ras GTPase [39, 167]), the free energy of NTP binding to the P-loop is spent without achieving physiologically relevant hydrolysis rates. For the further acceleration of hydrolysis, additional source(s) of free energy is/are needed.

The source of additional free energy is evident in the case of ring-forming oligomeric P-loop NTPases, such as many AAA+ ATPases (see Fig. 5A and [109, 168]), helicases (see Fig. 5B-C and [14, 112]), or rotary ATPases/synthases of the RecA/F_1 class (see Fig. 6A and [169-171]). In such complexes, the free energy for the cleavage of a bound ATP molecule in one monomer is provided by the binding of another ATP molecule to another monomer. Part of the substrate binding energy at this other site drives a molecular motion that is transferred, for example, to the Arg finger; in the case of rotational F_1-ATPases, Paul Boyer called this kind of coupling "binding change mechanism" [171].

The same reasoning can be applied to ABC transporters (Fig. 5D), where ATP-hydrolysis appears to be coupled to the binding of the translocated molecule. Also, the activation of kinases (Fig. 4C-D) appears to be driven by binding of their phosphate-accepting substrates.

In other cases, however, P-loop NTPases, with an NTP molecule bound, do not bind further small molecules, but only the cognate activating partners, which are protein/RNA/DNA molecules (Table 1). These NTPases, per exclusionem, can harness only the free energy of binding to their activating partner(s). Indeed, there is evidence that the strength of such protein-protein binding does affect the catalytic activity of some P-loop NTPases [4, 172-174], making them easy to regulate via protein-protein interactions, as observed with small GTPases.

In all these cases, we are dealing with thermodynamic coupling where the free energy of binding is used for endergonic constriction of the catalytic site. Such a thermodynamic coupling is reversible by definition. Consequently, if we find a way to exergonically constrict the catalytic site, it will lead to the spontaneous assembly of the complex between P-loop NTPase and its cognate activator(s). Apparently, the binding of TS analogs such as NDP:AlF_4^- or NDP:MgF_3^-, which form multiple strong bonds within the catalytic site, is an exergonic reaction that leads to a TS-like configuration of the catalytic site by "constricting it from the inside", which can happen even in the absence of an activating partner (as in the NDP:AlF_4^--containing separately crystallized dimer of GTPase domains of the MnmE protein (Fig. 1F in the accompanying paper [41]) or SIMIBI NTPases (Fig. 4A-B). If cognate activators are also present, the “from-the-inside constriction” drives their interaction with the NTPase domain yielding a full-fledged activated complex, as described in the literature [48, 49, 53, 56, 90, 151-154, 156, 161, 162].

If this assumption is correct, then the assembling "efficiency" of the TS analogs will depend on the amount of free energy that becomes available upon their binding. As it follows from Fig. 9 and Fig. 2 of the accompanying paper [41], fluoride complexes are superior to vanadate complexes in their ability to constrict the catalytic site. This is consistent with the fact that the more electronegative fluorine atoms form stronger H-bonds than oxygen atoms. Also

NDP:AlF_4^- complexes are superior to NDP:MgF_3^- complexes (Fig. 9 and Fig. 2 of the accompanying paper [41]) because, as documented in Table S2, they enter into more bonds. Not surprisingly, NDP:AlF_4^- complexes, which "raise" more binding energy despite their "unphysiological" geometry, are the most efficient in assembling activated complexes *in vitro*.

In sum, the extent of H-bonding of TS analogs within catalytic sites of P-loop NTPases (Fig. 9, Tables S1, S2 and Fig. 2 of the accompanying paper [41]) appear to correlate with their ability to induce self-assembly of activated complexes [48, 49, 53, 56, 90, 151-154, 156, 161, 162], which implies that these H-bonds stabilize the TS upon hydrolysis of ATP or GTP.

3.1.3. Coordination of W_{cat} and auxiliary interactions

The W_{cat} molecule is usually stabilized by the combined action of evolutionary conserved and variable moieties. The conserved part is represented by residue(s) of the WB-crest and contains residues that bind either W_{cat} alone or W_{cat} and γ-phosphate, such as Gly^{D+3} and Gln^{D+4} of small GTPases (Fig. 3), or Asp^{D+2} of many kinases (Fig. 4 C-D), or Glu^{D+1} of many ASCE ATPases (Fig. 5). Variable residues are provided by the C-caps of the β-strands, family-specific protein loops, or even external activating proteins/domains, as documented in Table S1.

In the Kinase-GTPase division, not only the position but also the nature of W_{cat}-coordinating residues varies between classes and families (Fig. 1E, 3, 4, S2); specifically, residues and/or **HN** groups in different positions of WB-crest are involved (Fig. 1E-F, 3, 4, Table 1). In most members of the ASCE division, W_{cat} interacts with the "catalytic" Glu^{D+1} residue of WB-crest (Fig. 5, Table 1). In Rec/F1 ATPases, the "catalytic" Glu residue is provided by the WB+1 strand and complemented by varying residues of WB-crest (Fig. 6, Table 1).

In addition, polar, W_{cat}-stabilizing ligands may be provided by the activating partners. In some Ras-like NTPases, GAPs can provide both the Arg finger and the W_{cat}-stabilizing Gln [175]. In SIMIBI NTPases, the "activating" monomer of the dimer provides not only the Lys finger, but also the Asp or a Glu residue that stabilizes W_{cat} (Fig. 4A-B). In maltose transporter ABC ATPase (Fig. 5D) and F_1-ATPases (Fig.6A), the adjacent monomer that provides the stimulator also provides the backbone **CO** atom to coordinate W_{cat} (Fig. 5D, 6A). Such behavior, where both the stimulator and the W_{cat}-stabilizing residue(s) are controlled by the interaction with the activating partner, might represent a kind of a "two-key mechanism" to better control and prevent accidental unwanted NTP hydrolysis.

In most cases, other auxiliary positively charged groups, such as **HN** groups and/or additional Arg/Lys residues, are involved in the coordination of the oxygen atoms of γ-phosphate and/or W_{cat} in addition to the "main" stimulator. This is observed in AAA+ NTPases (Fig. 5A), many helicases (Fig. 1F, 5B, 5C), ABC NTPases (Fig. 5D), hexamers of F_1/RecA-like ATPase (Fig. 6), PilT-like proteins (Fig. SF1_2A in the supplementary File 1), see also the accompanying article [41]. These auxiliary residues, indicated for the various classes of P-loop NTPases in Tables 1 and S1, are poorly conserved even within individual families of P-loop NTPases.

The abundance and variety of such auxiliary interactions could be related to the energetics of P-loop NTPases, which was discussed in section 3.1.3. Many of H-bonding interactions between oppositely charged moieties of the P-loop domain and its activator, which often invoke residues of WB-crest, may provide the free energy needed for catalysis. If so, elimination – for example through mutations – of such interactions, even if they are not involved in the chemistry of catalysis, would still slow the enzyme reaction, which is consistent with some experimental observations [4, 49, 172]. Therefore, a case-by-case analysis is needed to

understand whether specific auxiliary residues contribute directly to catalysis or only to the exergonic interaction of the NTPase domain with its activator.

3.1.4. Common structural traits of P-loop NTPases.

Comparative structural analyses, as performed here, in the accompanying article [41], and in our earlier paper [40], unraveled the following common structural features of P-loop NTPases:

i) in P-loop NTPases of different classes, the NTP molecule (or its analog) is bound by the Walker A motif in a same extended conformation (Fig. 2A); this conformation is likely to be catalytically prone [40];

ii) our structure analyses showed, in agreement with previous data (see e.g. [50, 176]) that the activating partner usually binds to the P-loop domain by making new H-bonds and salt bridges with the residues of the WB-crest, see Fig. 1C-D, S5. In all inspected structures for which TS-like structures are available, some of the amino acid residues that immediately follow Asp^{WB} (at the D+1 – D+5 positions of the WB-crest) are involved in catalytic interactions with W_{cat} (Fig. 1-7, S5, Table 1 and Table S1). The energy of binding of the activation partner seems to be used for pushing W_{cat} towards the P^G atom of γ-phosphate, constricting the catalytic site, and inserting the stimulatory moiety;

iii) in the accompanying article [41], we provide evidence that the common trait of all inspected stimulators is their mechanistic interaction with the oxygen atom(s) of γ-phosphate;

iv) comparing the structures with analogs of ATP/GTP and TS, respectively, we noticed that the binding of TS-analogues results in greater constriction of catalytic sites than the binding of ATP or GTP. The constriction manifests itself in the shorter distances between Asp^{WB} and $[Ser/Thr]^{K+1}$ which are as short as 2.5 Å on average in the presence of $ADP:AlF_4^-$ (Fig.

1-6, 9). Also the distances between **HN**$^{K-3}$ and the analogs of γ-phosphate are shorter in the TS-like structures, see Fig. 1-6 and the accompanying article [41].

v) In TS-like configurations of P-loop NTPases of all major classes, except the TRAFAC NTPases, the W_{cat}-coordinating "catalytic" Glu or Asp residue links W_{cat} with Mg^{2+}-ligands in positions 3 and/or 6, see Fig. 1E, 1F, 4-6, 7A.

These common structural traits, which are shared by P-loop NTPases of different classes, have been mostly overlooked so far. We believe that these features are of key importance for understanding the common mechanism of P-loop NTPases.

3.2. Common mechanistic traits in P-loop NTPases

3.2.1. Background on the catalysis by P-loop NTPases

The cleavage of γ-phosphate by P-loop NTPases is thought to involve a nucleophilic attack of W_{cat}/OH^{-}_{cat} on the P^{G} atom (Fig. S1). However, it is yet unclear whether the reaction proceeds in two steps separated by formation of a metastable intermediate (Fig. S1A-B), or in one concerted transition with the pentavalent trigonal bipyramidal (tbp) transition state, see Fig. S1C and [15, 48, 56-63, 133]. In the case of two-step mechanism, it is also unclear whether the reaction follows the dissociative S_N1 pathway (Fig. 1SA) or the associative S_N2 pathway (Fig. S1B). In the S_N1 mechanism, the rate-limiting step is dissociation of the terminal O^{3B}–P^{G} bond to form a metaphosphate intermediate, which interacts with OH^{-}_{cat} yielding inorganic phosphate (P_i), see Fig. S1A. In the S_N2 mechanism, the rate-limiting reaction is the nucleophilic attack by OH^{-}_{cat} on P^{G} and the formation of the pentavalent tbp intermediate, which then dissociates into NDP and P_i, see Fig. S1B.

The research community is roughly evenly divided between proponents of these three mechanisms, see e.g. [63, 133, 177]. However, it is not clear whether the difference between

the mechanisms is fundamental in this case. It was experimentally shown that the mechanism of ATP hydrolysis varies even in water; it changes from dissociative in pure water to associative in the presence of positively charged chelators for γ-phosphate [178].

Therefore, instead of focusing on these differences, we would like to emphasize the universally recognized common features of the reaction pathways shown in Fig. S1, namely:

1) in any model, the covalent bond between O^{B3} and P^{G} must be destabilized [57-59];

2) the γ-phosphate group undergoes a steric inversion when forming a covalent bond with the nucleophile, see Fig. S1 and [57]. Therefore, catalytic interactions should planarize the γ-phosphate [179, 180];

3) Negative charges of the oxygen atoms of γ-phosphate must be compensated to increase the electrophilicity of the P^{G} atom and make it prone to nucleophilic attack [15, 48, 56-59, 61-63, 133, 180];

4) Conditions in the catalytic site should enable deprotonation of W_{cat} by a suitable proton acceptor [57-61];

5) Upon dissociation of the O^{B3} – P^{G} bond, a large negative charge on the O^{3B} atom must be effectively compensated as it contributes significantly to the activation barrier [62, 64].

By correlating the results of our structural analysis with the literature, we outline below how P-loop NTPases may handle these five tasks.

3.2.2. Main catalytic factors in P-loop NTPases

3.2.2.1. Destabilization of the O^{3B} – O^{3G} bond

Even prior to activation, the NTP molecule is bound within the closed catalytic site in a conformation more extended compared to its conformation in water, as noted earlier for particular enzymes [39, 40, 180, 181]. As Figure 2A shows, this extended conformation of the bound NTP molecule is common to all major families of P-loop NTPases. In enzyme-bound NTP molecules, the β- and γ-phosphates are in an almost perfectly eclipsed conformation due to interactions with Mg^{2+} and Lys^{WA} (see Fig. 1D), in contrast to their staggered configuration in water [40, 181]. The repulsion of the eclipsed oxygen atoms has the potential to destabilize the O^{3B} – P^{G} bond [36, 62, 165, 182].

Our finding that stimulators always interact with γ-phosphate indicates that this interaction may contribute further to destabilization of the O^{3B} – O^{3G} bond. For example, the twisted γ-phosphate may become more eclipsed relative to the α-phosphate, so that the oxygen atoms of the α- and γ-phosphate repel each other, as suggested by Rudack and colleagues [183]. Moreover, any twisting or pulling γ-phosphate can destabilize the entire Mg-NTP system, inevitably disturbing the coordination sphere of Mg^{2+}, since the O^{1G} atom of γ-phosphate is one of the Mg^{2+} ligands (Fig. 1D, 2).

3.2.2.2. Planarization of γ-phosphate

Already in the absence of the stimulator, the oxygen atoms of the γ-phosphate are already "pulled up" to the β-phosphate by Lys^{WA}, which interacts with O^{1B} and O^{2G}, and by Mg^{2+}, which interacts with O^{2B} and O^{1G}, see Fig. 1B and [184]. The stimulatory moiety in the AG site further planarizes γ-phosphate by drawing the O^{3G} atom toward O^{2A} and enabling the

interaction between **HN**$^{K-3}$ and O^{2G} (Fig. 1-6, Table S1). Indeed, in the presence of stimulatory moieties – for example in the pre-TS structures shown in Fig. 3 of the accompanying article [41] – the O^{3B}-P^{G}-O^{1G}, O^{3B}-P^{G}-O^{2G}, and O^{3B}-P^{G}-O^{3G} angles are mostly less than the 109° expected for an ideal tetrahedron, see also [184].

Even when interacting only with γ-phosphate, the stimulator is often located between α- and γ-phosphates, as in dynamins (Fig. 3A) or ABC transporters (Fig. 5D) and can planarize γ-phosphate by tying O^{3G} to the "head" of the NTP molecule. For instance, the Na^{+} ion in dynamins, while not reaching the α-phosphate directly, is connected to it via two noncovalent bonds (Fig. 3A). The signature motif of ABC-NTPases is H-bonded via conserved Ser and Gln residues to the O2' atom of the ribose (Fig. 5D).

Notably, the twisted or tilted γ-phosphate becomes more eclipsed relative to α-phosphate, but *less* eclipsed relative to β-phosphate [40], which might be a prerequisite for inversion of the γ-phosphate group (otherwise, in the case of an ideal eclipse, the oxygen atoms of β-phosphate would prevent the inversion of γ-phosphate).

3.2.2.3. Electrostatic compensation of the negative charge of the phosphate groups

The positive charges of amino group of Lys^{WA}, the Mg^{2+} ion, and several **HN** groups of the P-loop compensate for the negative charges of phosphate oxygen atoms (see Fig. 2B) so that electrons are "pulled away" from the P^{G} atom, see for example [36, 65, 176-178, 180, 183]. Notably, the phosphate chain "sits" on the last N-terminal turn of the α_1-helix, which generally carries a dipole positive charge of about 0.5 [36, 185]. This positive charge should also contribute to electrostatic compensation. The positions of the groups involved are strictly conserved (Fig. 2), so that such a compensation is common to all major families of P-loop NTPases and may, at least partly, explain why the very binding of the GTP molecule to the catalytic site of Ras GTPase accelerated hydrolysis by five orders of magnitude, as compared

to hydrolysis in water, even in the absence of an activating partner [39, 167]. In addition to these common positively charged moieties, class-specific auxiliary residues could be involved, as, for instance, “sensors 3” in some AAA+ ATPases.

On activation, the negative charges of the γ-phosphate oxygen atoms are additionally compensated by the positive charges provided by most stimulators, see Fig. 1-6 and the accompanying article [41]. The additional electrostatic compensation significantly increases the electrophilicity of the P^G atom. Rudack and colleagues showed in their QM/MM calculations that the insertion of the arginine finger alone increases the partial positive charge on P^G to 1.46 elementary charges [183]. The interaction of O^{2G} with $\mathbf{HN}^{K-3}$, as described in the accompanying article [41] and in [40] should further increase the positive charge on P^G in the pre-transition state.

Furthermore, Fig. 8 shows that the electrostatic potential at the catalytic sites of diverse P-loop NTPases is distributed unevenly, which has already been noted for particular enzymes of this family, see, e.g., [186]. The strength of the local electric field can be roughly estimated using the Coulomb’s equation as ~ 10^8 V/m under the very modest assumptions that (i) the resulting electric charge difference at a distance of 10 Å (between the acid residues and the P-loop) corresponds to one elementary charge and (ii) the effective dielectric permittivity of the catalytic pocket is about 10 [187, 188]. Such an electric field strength, albeit large, is compatible with those measured in the catalytic pockets of other enzymes [189]. Notably, the local electric field is directed approximately from the P-loop to Asp^{WB}. Hence, the catalytic pocket is strongly polarized in P-loop NTPases, which also can contribute to catalysis, as discussed below.

Consequently, in those cases where the stimulator is positively charged, its positive charge not only secures the bonding with particular oxygen atom(s) of triphosphate and increases the positive charge on P^G, but additionally polarizes the whole catalytic pocket.

3.2.2.4. Does the [Ser/Thr]$^{K+1}$ – Asp^{WB} pair accept a proton from W_{cat}?

In their comprehensive review on enzymatic mechanisms of phosphate transfer, Cleland and Hengge wrote: "The problem for an ATPase … is thus to position a water molecule so that it *is* in a position to attack the γ-phosphorus. This requires steric restraints as well as organized hydrogen bonding networks. And more specifically, there must be a path for one proton of the attacking water molecule to reach a suitable acceptor " (quoted from [60]). In P-loop NTPases, the proton from W_{cat} is commonly thought to be taken up either by γ-phosphate in TRAFAC class NTPases [67, 133] or by W_{cat}-coordinating, „catalytic" Glu or Asp residues in other classes of P-loop NTPases [8, 54, 99, 102, 114, 116, 125, 129, 190-192]. Still, our comparative structure analysis showed that such Glu/Asp residues, present in all classes of NTPases except the TRAFAC class, are non-homologous. In SIMIBI NTPases, W_{cat}-coordinating Glu or Asp residues are at the C-tip of their WB+1 β-strands (Fig. 4A-B). In most classes of ASCE ATPases, the "catalytic" Glu^{D+1} follows Asp^{WB}, see Fig. 5, and [14, 16, 32]. In F_1/RecA ATPases, the "catalytic" Glu residue is located at the C-tip of the WB+1 β-strand, see Fig. 6 and [8, 14, 19]. Also, those kinases that require deprotonation of the second substrate have usually an Asp^{WB}-Leu^{D+1}-[Asp/Glu]$^{D+2}$ motif where the D+2 residue interacts with the prospective nucleophilic group, see Fig. 4D and sequence alignments in [9]. Such an absence of homology is unusual for catalytically critical residues.

More importantly, neither γ-phosphate, nor W_{cat}-coordinating Glu/Asp residues can hold the proton from W_{cat}. Indeed, the inverse solvent isotope effect on the GAP-activated hydrolysis by the Ras GTPase upon H/D substitution [193] indicates that deprotonation is likely to occur

before the rate-limiting step of bond cleavage [60]. The bond cleavage time by P-loop NTPases is in the millisecond range (100 ms at 260°K in a Ras GTPase activated by the RasGAP [194]). During this time, the proton must be "detained" in such a way as to prevent its return to OH^{-}_{cat} and the reversal of the reaction. In general, the ability to keep the proton is seen as a prerequisite for the completion of enzymic reactions with participation of deprotonated nucleophiles, as discussed e.g. for the eukaryotic cAMP-dependent protein kinase [195, 196].

The common belief of proton trapping from water (pK_a=14.0) either by a "catalytic" Glu or Asp residue in a polar environment (with expected pK_a in the range of 2.0-5.0) or by γ-phosphate (with pK < 3.0 [197, 198]) is at odds with the basic rules of proton transfer as formulated by Eigen [199, 200]. After Eigen, if the donor and acceptor of the proton are connected by a "hydrogen bridge", proton transfer between them is "practically unhindered *provided the difference* $pK_{acceptor} - pK_{donor}$ *is positive*" (quoted from [200]). In the case of γ-phosphate and W_{cat}-coordinating Glu/Asp residues, the respective difference is strongly negative so the proton will promptly (in picoseconds) return to W_{cat}.

It was speculated that the W_{cat}-coordinating groups may facilitate its catalytic deprotonation by decreasing the proton affinity of W_{cat}, see e.g. [201]. Our structural analysis of TS-like structures showed that positively charged side chains of Lys or Arg, which could significantly lower the pK value of W_{cat}, interact with it only in a few classes of P-loop NTPases, e.g. in some AAA+ ATPases, see Section 2.2.2.2 and Table 1. Even in these cases, their positive charges can hardly decrease the apparent pK of W_{cat} by >10 pH units, which is needed for sustainable protonation of a "catalytic" Glu/Asp residue or γ-phosphate. Hence, neither "catalytic" acidic residues, nor γ-phosphate can trap a proton from W_{cat} per se.

As early as in 2004, some of these problems were recognized by Frick and colleagues [202, 203] who calculated the pK values for ionizable residues of the SF2 class Hepatitis C virus

(HCV) NS3 helicase by using the MCCE software [204]. Frick and colleagues wrote about supposedly W_{cat}-coordinating Glu291^{D+1} and its preceding Asp290^{WB}: "to function as a catalytic base, the pKa of Glu291 would need to be much higher than that of a typical Glu in a protein. However, electrostatic analysis of all HCV helicase structures reveals that neither Glu291, nor any nearby Glu, has an abnormally high pKa. In contrast, Asp290 has a pKa as high as 10 in some structures and as low as 3 in others. Interestingly, in structures in the open conformation (such as 8OHM), the pKa of Asp290 is low, and in the closed conformation (ex. 1A1V), the pKa of Asp290 is higher than 7, suggesting that Asp290 picks up a proton (like a catalytic base) when the protein changes from the open to the closed conformation. Thus, Asp290 could serve as a catalytic base…" (quoted from [203]). Frick and colleagues made their calculations with crystal structures of helicases that contained neither Mg-ATP nor its analogs. Therefore, they were unaware of the exact positions of Asp290^{D} and Glu291^{D+1} relative to the bound substrate and could only guess by analogy with known structures of related P-loop NTPases. The two subsequently resolved ADP:AlF_4^--containing, TS-like crystal structures of HCV NS3 helicase (PDB IDs 3KQL [205] and 5E4F [115]) show a typical for SF2 helicases arrangement of Asp290^{WB} and Glu291^{D+1} (see Fig. 5C). Furthermore, both structures show short 2.4 Å H-bonds between Ser211^{K+1} and Asp290^{WB}, as seen in Fig. 5C.

Unlike "catalytic", W_{cat}-coordinating Glu/Asp residues, Asp^{WB} is strictly conserved in P-loop NTPases. Equally strictly conserved is the [Ser/Thr]$^{K+1}$ residue [9, 10, 12, 206]. Both these residues can translocate protons. Therefore, building on our comparative structure analysis and following Frick and colleagues who suggested Asp290^{WB} as a catalytic base in the HCV NH3 helicase [202, 203], we propose here that the buried, H-bonded pair of strictly conserved [Ser/Thr]$^{K+1}$ and Asp^{WB} serves as a universal module that accepts the proton from W_{cat} and holds it as long as needed in P-loop NTPases of all classes.

It can be countered that the $[Ser/Thr]^{K+1}$ – Asp^{WB} pair does not interact directly with W_{cat}. However, direct tracing of intra-protein displacements of protons in energy converting enzymes and chemical models (see [199, 200, 207-219] for reviews) showed that fast proton transfer over a distance of up to 20 Å can be mediated by water bridges, provided that the distance between the groups involved is ≤ 3.0 Å, in accordance with Eigen [200]. Thereby it does not matter that water molecules are equally poor proton acceptors (with pK_b of 0.0) and proton donors (with pK_a of 14.0) because protons pass water by so-called von Grotthuss mechanism [220-222]. According to the modern version of this relay mechanism, the bridging molecule receives an external proton simultaneously with the transfer of its own proton to the next carrier at picoseconds [221, 222]. Apart from water molecules, the side chains of serine, threonine, tyrosine, and neutral histidine are suitable for proton transfer by the von Grotthuss mechanism: they have a proton-accepting lone pair of electrons and also their own proton to transfer on [223]. In addition, protons are transferred very fast between carboxy groups when they are bridged by single water molecules [199, 200, 213, 217]. Zundel and colleagues showed that such systems are highly polarized [207, 224], which lowers the activation barriers for proton transfer.

The best-studied examples of such proton-conducting chains are known from the photochemical reaction center (PRC) of α-proteobacterium *Rhodobacter sphaeroides* (as shown in Fig. 10A and described in its caption) and bacteriorhodopsin of an archaeon *Halobacterium salinarum* (as shown in Fig. 10B and described in its caption).

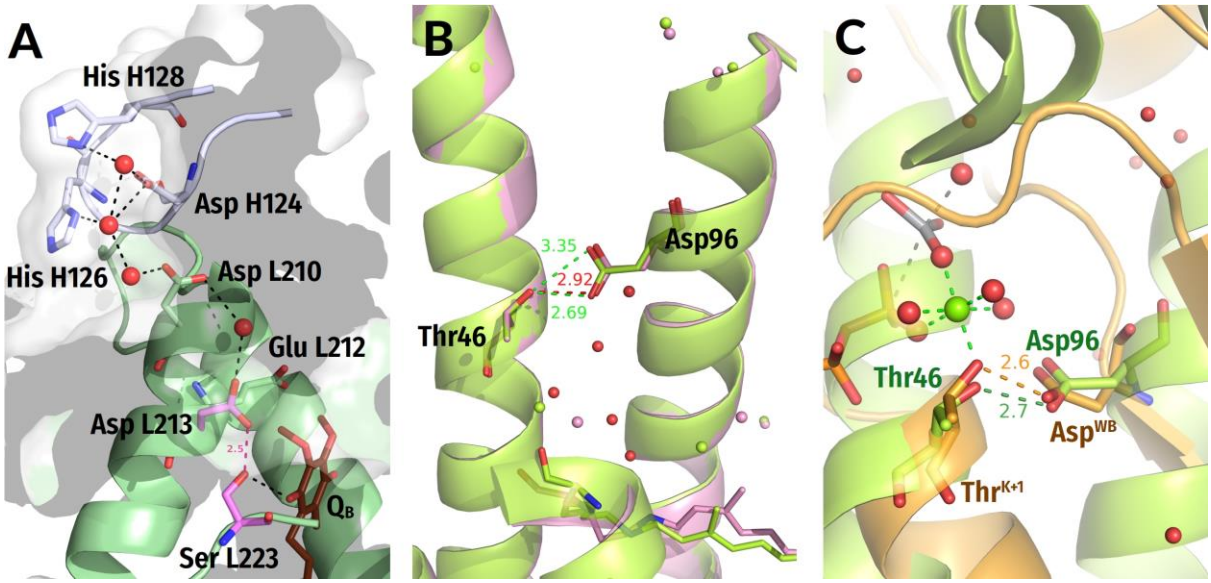

Figure 10. Proton traps in the photochemical reaction center and bacteriorhodopsin as compared with the Thr^{K+1}-Asp^{WB} pair of P-loop NTPase. Distances are given in ångströms. **A**, a high-pK proton trap in the photosynthetic reaction center (PRC) from *Rhodobacter sphaeroides*. Shown is the PRC in the charge-separated state (PDB ID 1DV3 [225]). Here, a proton path connects the protein surface with the buried binding site of the secondary ubiquinone acceptor Q_B. The proton is translocated over more than 20 Å via amino acid residues of the two PRC subunits, L and H. The proton pathway begins at the two His residues on the surface (His-H126 and His-H128); they are thought to have pK values of about 7.0 and to harvest protons which are ejected onto the photosynthetic membrane surface by the ATP synthase. From these histidine residues, the proton goes, via water-bridged carboxy groups of Asp H-124 and Asp-L210, to the Q_B -binding pocket. Proton transfer from the surface to the more hydrophobic interior of the protein becomes possible after the Q_B molecule docks to the Glu-L212 – Asp-L213 – Ser-L223 cluster [226] and turns it into a buried, high-affinity proton acceptor (a *membrane proton trap* according to Mitchell [227]), with a functional pK of about 9.5 – 10.0 [228-232]. This high functional pK is apparently due to the expulsion of water upon Q_B binding, the negative charge on the Glu-L212 – Asp-L213 pair, and the H-bond between Asp-L213 and Ser-L223, through which the proton passes to Q_B. The functional pK value of the trap increases to > 12.0 after the appearance of an electron at Q_B and the formation of the $Q_B^{-\cdot}$ anion radical, which attracts further protons into the buried catalytic site [212]. Mutations of either Glu-L212, or Asp-L213, or Ser-L223 block proton transfer from the surface [228, 233, 234]. For further details, see [216, 225, 235-237].

B, a high-pK proton trap in bacteriorhodopsin (BR), a membrane protein that pumps a proton across the membrane in response to the photoexcitation of its retinal pigment, see [209, 210, 238, 239] for reviews. Shown is the superposition of femtosecond X-ray laser-captured structures of bacteriorhodopsin from [240] in a closed resting state (PDB ID 6G7H, light-green) and in an "open" state 8.3 ms after illumination (PDB ID 6G7L, pink). Additional red-colored water molecules were taken from a high-resolution crystal structure of the V49A bacteriorhodopsin mutant that was crystalized in an "open" state (PDB ID 1P8U, [241]). In the BR, the key proton carrier Asp-96 has pK of ~12.0 owing to the absence of water in the vicinity

and a H-bond with Thr-46 of the nearby α-helix. Replacement of Thr46 by a valine decreased the apparent pK of Asp96 by approximately two pH units [242], which may characterize the contribution of the H-bond between Thr46 and Asp96 to the unusually high apparent pK of the latter. The photoisomerization of the retinal twists the α-helices and lets water molecules in the space between them, see the pink structure [209, 218, 219, 243-246, 247. The pK value of Asp-96 shifts to 7.1, which allows its deprotonation and proton transfer, via a transiently formed water chain, to the Schiff base of retinal at about 10 Å, see {Luecke, 2000 #3390, 248, 249]. Later, the cleft between helices closes again, the pK of Asp-96 returns to 12.0, and it is re-protonated from the surface [209, 210, 239, 244].

C, the Thr46-Asp96 pair of bacteriorhodopsin it its resting closed state (the green structure from panel 10B, PDB ID 6G7H) superimposed with the Thr^{K+1}—Asp^{WB} pair from the transition-state like, VO_4^--containing structure of myosin shown in Fig. 3D, orange (PDB ID 1VOM [95]).

The two proton transfer routes shown in Fig. 10A-B were reconstructed from direct electrometric tracking of flash-induced proton displacements [209, 250-254], kinetic IR and UV/Vis spectroscopy data [209, 210, 230, 231, 248, 251, 255, 256], kinetic ESR measurements [238, 243, 245, 257], and comparative structure analyses [218, 226, 236, 244]. These are the two best-understood cases of intra-protein proton transfer by far.

In the case of PRC (Figs. 10A), the buried proton acceptor must have a functional pK value greater than 9.0 to compensate for the desolvation penalty of about three pH units, which must be "paid" for delivery of a proton from a pK-neutral “antenna” group at the protein surface into the hydrophobic membrane [258, 259]. However, if such a buried group is equilibrated with the protein surface, its pK value can hardly exceed the ambient pH, which is usually neutral, because the groups with even higher pK values are already protonated. Hence, the strong proton acceptor shown in Fig. 10A is not fully equilibrated with the surrounding solution. In this case, it is better to speak about the *apparent/functional* pKa or high *proton affinity*. Such very strong proton acceptors usually emerge only transiently [232, 260].

The proton traps in Fig. 10A, B include H-bonded [Ser/Thr] – Asp pairs (modules). These examples show that proper H-bonding of a protein-buried Asp residue with a nearby Ser/Thr

residue in a hydrophobic environment can generate a trap with a high proton affinity; such traps can, in principle, accept protons even from water. Specifically, in the absence of pH-buffers and protons from the ATP synthase, the protons that pass through the PRC to compensate the negative charge at the Q_B site (Fig. 10A) appear to detach from surface water molecules, presumably polarized by surface charges [256].

Our suggestion that a similarly H-bonded $[Ser/Thr]^{K+1}$ – Asp^{WB} pair accepts the proton from W_{cat} in P-loop NTPases of different classes challenges the current ideas on catalytic proton transfer in P-loop NTPases. Therefore, we further substantiate the suggested mechanism below and illustrate it in Fig. 11 and 12:

1) In TS-like structures of P-loop NTPases of various classes (except the TRAFAC class), the "catalytic" Glu/Asp residues were found to connect W_{cat} with ligands of Mg^{2+} in positions #3 or #6, see Fig. 1F, 4-6, 7A. Notably, the six ligands of Mg^{2+} form a regular octahedron with edges 2.9-3.0 Å long, so that the ligands # 3 and #6 are on a H^+-transfer distance from $[Ser/Thr]^{K+1}$ (Fig. 11). The short H-bond between $[Ser/Thr]^{K+1}$ and Asp^{WB} completes the proton-conducting pathway that connects W_{cat} with Asp^{WB}. The proton pathways from W_{cat} to Asp^{WB}, which resemble proton translocation systems of PRC and BR (cf Fig. 10), are shown by the red dashed lines for P-loop NTPases of different classes in Fig. 4-6 and by dashed arrows in Fig. 11.

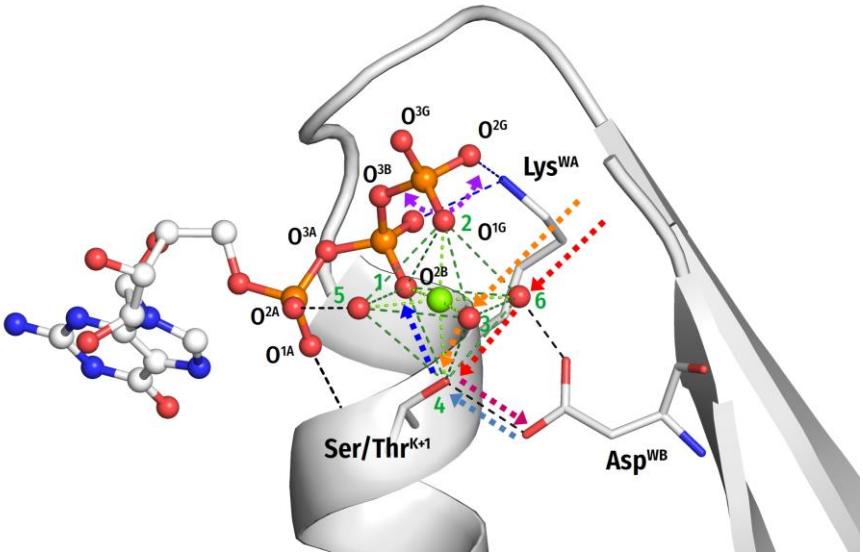

Figure 11. Schematic presentation of tentative proton routes along the edges of the octahedral coordination shell of Mg^{2+} ion. The Mg^{2+} ligand #3 is assumed to be a water molecule. Proton entry points via ligand #6 or ligand #3 are shown by red and orange arrows, respectively. Protonic connection between $[S/T]^{K+1}$ and Asp^{WB} are shown by magenta and light blue arrows, the route from $[S/T]^{K+1}$ to O^{2B} of β-phosphate is shown as a dark blue arrow. The movement of the O^{1G} atom as a result of γ-phosphate twist is shown by purple arrows.

2) The pKa of an aspartate residue in water is about 4.0, much lower than that of water (14.0). However, unlike the "catalytic" Glu/Asp residues or γ-phosphate surrounded by charged residues (Fig. 1E, 1F, 3-6), Asp^{WB} is in a nonpolar environment and its functional pK is likely to be high when the catalytic site is closed. Asp^{WB} is in the middle of an αβα sandwich, on the interface between the β-pleated sheet and the α_1-helix; such interfaces are stabilized by hydrophobic interactions [185]. In addition, Asp^{WB} is preceded by four hydrophobic residues of the Walker B motif (Fig. 1); the adjacent β strands, as well as the α_1-helix, also contain many hydrophobic residues, see the sequence alignments in [9, 10, 12, 206]. Upon constriction of the catalytic pocket and expulsion of eventually present water molecules, the hydrophobic environment should elevate the proton affinity of the H-bonded Asp^{WB}, as it happens with similarly H-bonded Asp96 which has a functional pKa of ~ 12.0 in a

hydrophobic environment of the ground-state BR. Fig. 10C shows that the structure of the Ser186^{K+1} – Asp454^{WB} pair of myosin overlaps nicely with Thr46 – Asp96 pair of BR.

3) In contrast, the pK of [Ser/Thr]$^{K+1}$, which is about 13.0 in water, is likely to be reduced when [Ser/Thr]$^{K+1}$ serves as a Mg^{2+} ligand. Coordination of a Zn^{2+} ion by a serine side chain is known to decrease the pK value of the latter up to 5.5 yielding a serine anion (alkoxide) at neutral pH, see [60] and references therein. The impact of a Mg^{2+} ion should be weaker; still, within a closed/constricted catalytic site, the low dielectric permittivity would enhance electrostatic interactions. [Ser/Thr]$^{K+1}$ is the most deeply buried of the Mg^{2+} ligands (see Fig. 1-6, 11), so it should be the most sensitive to electrostatic effects. As a result, the functional pK value of [Ser/Thr]$^{K+1}$ may dramatically decrease upon constriction of the catalytic site.

4) The found shortening of H-bonds in the TS-like structures (Fig. 9) enables estimation of the difference in functional pK values of [Ser/Thr]$^{K+1}$ and Asp^{WB} in the TS. It is well established, based on ample experimental evidence, that hydrogen bonds "generally shorten as ΔpKa, the difference in the donor and acceptor pKa values, decreases" (quoted from [261]). Specifically, Herschlag and colleagues observed, on various systems, that the Δp*K*a decreases linearly from 20 to 0 with the decrease in the O—H••••O distance from 2.9 Å to 2.4 Å, with a slope of 0.02 Å/p*K*a unit, [261, 262]. In NDP:AlF_4^--containing structures with constricted catalytic site, the length of the H-bonds between [Ser/Thr]$^{K+1}$ and Asp^{WB} varies around 2.5 Å (Fig. 1E-F, 3, 4A-B, 5C-D, 6A, 9), which corresponds to ΔpK < 3.0 and indicates a low-barrier hydrogen bond [261, 262]. Hence, [Ser/Thr]$^{K+1}$ and Asp^{WB} may have comparably high proton affinities in a constricted catalytic site.

5) Limbach and colleagues combined low-temperature UV-Vis and $^{1}H/^{13}C$ NMR spectroscopy (UVNMR) to study the effect of solvent polarity on the proton equilibrium between phenols and carboxylic acids [263-265], which system can be viewed as a model of

the [Ser/Thr]$^{K+1}$—Asp^{WB} H-bonded pair. These authors have shown that proton relocates from the hydroxy group to the carboxyl with decrease in polarity.

6) In the octahedral coordination shell of Mg^{2+}, the O^{1G} atom of γ-phosphate is the ligand opposite to [Ser/Thr]$^{K+1}$ (Figure 11). Therefore, the stimulator-induced rotation of γ-phosphate, by moving O^{1G} in *any* direction (as shown by dashed purple arrows in Fig. 11), would inevitably increase the distance between O^{1G} and the hydroxyl of [Ser/Thr]$^{K+1}$. Pulling away the negatively charged O^{1G} will increase the cumulative positive charge at [Ser/Thr]$^{K+1}$ prompting the relocation of its proton to Asp^{WB}, e.g. in response to a thermal fluctuation [265] (Fig. 12A).

7) We suggest that the resulting Mg^{2+}-coordinated Ser/Thr anion (alkoxide), used as a proton acceptor from water by many enzymes [60, 164, 266, 267], withdraws the proton from W_{cat} (or the sugar moiety in some kinases) via proton pathways shown in Figs. 4-6, 7A, 11, 12B; this proton transfer is additionally driven by strong local electric field (see Fig. 8 and Section 2.2.4). The resulting state where both [Ser/Thr]$^{K+1}$ and Asp^{WB} are protonated corresponds to the ground state of the Thr46-Asp96 pair in the BR (see the light-green structures in Fig. 10B-C).

8) The formed anionic nucleophile (e.g. $\mathbf{OH^{-}_{cat}}$) stabilized and polarized by its ligands, is attracted by the electrophilic P^{G} atom (Fig. 12B). The proton affinity of the anionic nucleophile decreases as it gets closer to P^{G}, so that proton return from the [Ser/Thr]$^{K+1}$—Asp^{WB} couple becomes increasingly unfavorable, eventually satisfying the Eigen's condition for proton transfer and making it complete.

9) In diverse P-loop NTPases, mutations of Asp^{WB} or [Ser/Thr]$^{K+1}$ diminished the enzyme activity dramatically, see e.g. [203, 268-275]. More specifically, mutations of Asp^{WB} to Asn retarded the activated hydrolysis without affecting the NTP binding [203, 268-272]. In the

case of *E.coli* F_1-ATPase, the mutation even increased the affinity for ATP [270]. The Asp^{WB} to Asn mutation mimics the charge state of a protonated Asp^{WB}. Hence, the protonation of Asp^{WB} is unlikely to distort the catalytic pocket and be the cause of the universal catalytic incompetence of the Asp^{WB} to Asn mutants. We attribute this incompetence to the inability of Asn^{WB} to trap a proton from $[Ser/Thr]^{K+1}$.

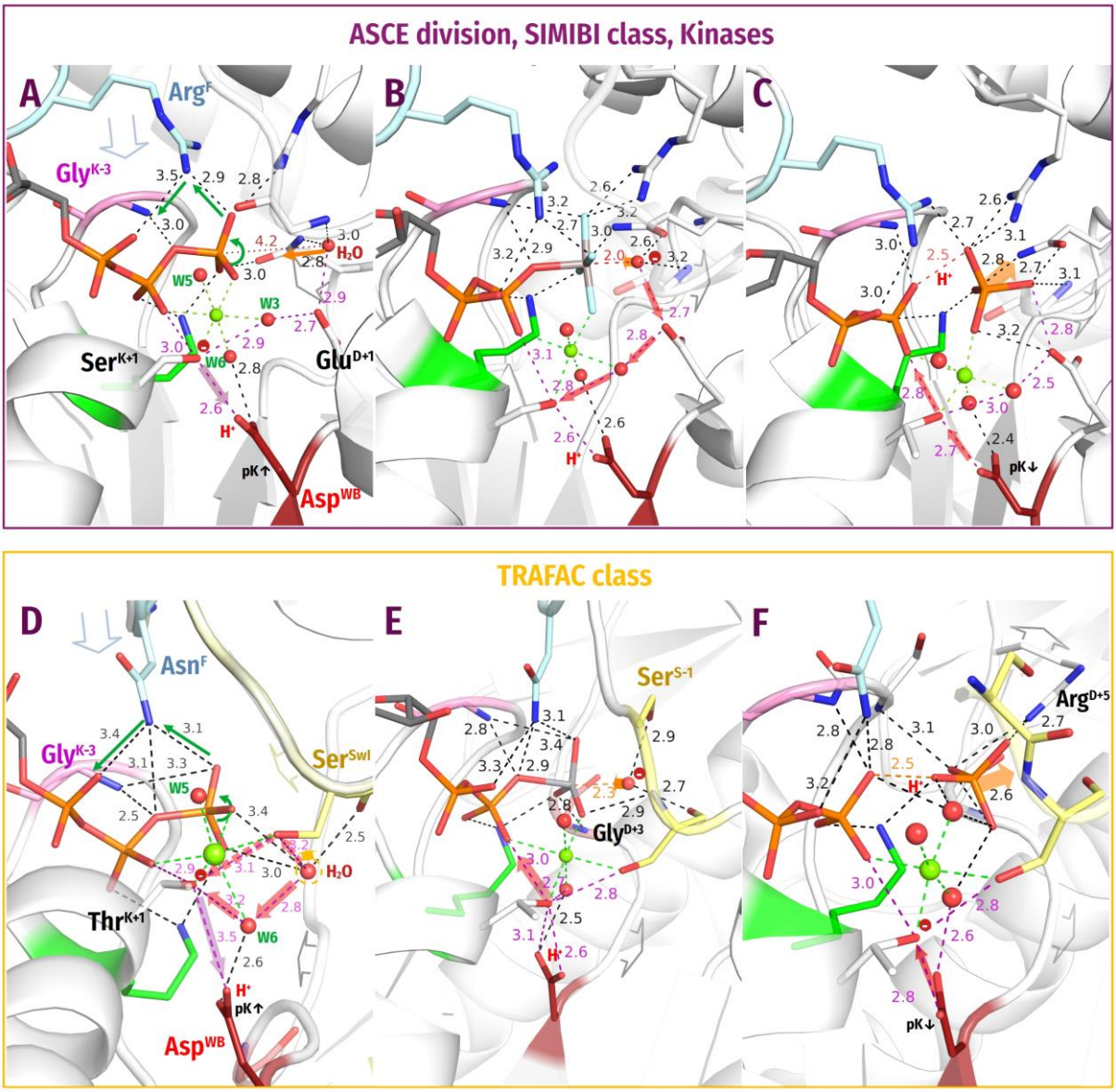

Figure 12. Two tentative mechanisms of proton transfer from W_{cat} to Asp^{WB} in P-loop NTPases. The shade of the red arrows of proton transfers varies through panels A-C and D-F to emphasize that the kinetic coupling of these steps with each other and reactions in the catalytic site could vary depending on the thermodynamics of particular enzymes. Other colors as in Fig. 3-6.

Top (**A-C**): Tentative mechanism of proton transfer via the **W_{cat}**-coordinating Glu/Asp residue in all classes of P-loop NTPases but TRAFAC class enzymes, as illustrated by structures of the SF1 helicase Pif1.

A, In the pre-catalytic state, which is exemplified by a structure with a bound non-hydrolyzable ATP analog ANP (PDB ID 6HPH [276]), the binding of ATP and closure of the catalytic site increases the proton affinity of Asp^{WB}. Activation-induced constriction of the catalytic site and twist of γ-phosphate prompt the proton redistribution from $[Ser/Thr]^{K+1}$ to Asp^{WB}; **B**, in the TS, which is exemplified by a structure with a bound TS analog ADP:AlF_4^- (PDB ID 5O6B [192]), a proton from W_{cat} repletes the vacancy at the anionic $[Ser/Thr]^{K+1}$ by going via the W_{cat}-coordinating Glu^{D+1} and W3; the resulting **OH^-_{cat}** attacks γ-phosphate; **C**, in the post-TS, which is exemplified by a structure with ADP:MgF_4^{2-} bound (PDB ID 6S3I [277]), where we replaced the $H_2PO_4^{2-}$ mimic MgF_4^{2-} by $H_2PO_4^{2-}$, the proton goes from Asp^{WB}, via Ser^{K+1}, to β-phosphate to compensate its negative charge (see the main text).

Bottom (**D-F**): Tentative mechanism of proton transfer from W_{cat} to Asp^{WB} in TRAFAC class NTPases, as illustrated by structures of myosin.

D, For the pre-catalytic state we used the ATP-soaked crystal structure of myosin II (PDB ID 1FMW [139]) where the Switch I loop was taken from the structure of Myosin V complexed with ADP-BeF_3 (PDB ID 1W7J [278]) and superimposed via Lys^{WA} and Mg^{2+}. In this state, the binding of ATP and closing of the catalytic site increases the proton affinity of Asp^{WB}. Constriction of the catalytic site upon activation and twist of γ-phosphate prompt the proton redistribution from Thr^{K+1} to Asp^{WB} (purple arrow). The anionic Thr^{K+1} accepts a proton from W6 that, in turn, takes a proton from W_{12} (red arrows, cf. Fig. 7B-C); alternatively, the proton route from W_{12} to Thr^{K+1} may involve the conserved Ser^{Sw1} (dashed red arrows) The resulting **OH^-_{cat}** is brought into the apical position by residues of Switch I (colored yellow) and WB-crest; **E**, in the transition state, which is exemplified by a structure with a bound TS analog ADP:VO_4^- (PDB ID 1VOM [95]), **OH^-_{cat}** attacks P^G. In this constricted transition state, the protonic connection between **OH^-_{cat}** and the Mg^{2+}-coordinating water molecules appears to be broken. In the subsequent stage of the catalytic transition, the proton goes from $[S/T]^{WA}$ to β-phosphate and compensates for the large negative charge that builds up upon the detachment of γ-phosphate (the red arrow); **F**, in the post-transition state, which is exemplified by a structure with bound ADP and $H_2PO_4^{2-}$ (PDB ID 4PJK [52]), the negative charge on β-phosphate is compensated by a hydrogen bond between β- and γ-phosphate. Asp^{WB} repletes Thr^{K+1} concomitantly with the opening of the catalytic pocket (see also the main text).

In TRAFAC class NTPases, the H-bond between $[Ser/Thr]^{K+1}$ and Asp^{WB} is as short in the TS-like structures as in other classes of P-loop NTPases, see (Fig. 1F, 3) and Table S1. However, these NTPases have no "catalytic" W_{cat}-coordinating Glu/Asp residues. Instead,

they all have a strictly conserved [Thr/Ser]^{SwI} residue that coordinates Mg^{2+} by its side chain as ligand #3 and, in the same time, stabilizes W_{cat} with its **CO** group in the TS-like configuration (Fig. 1F, 3). In this configuration, the side chain oxygen of [Ser/Thr] ^{SwI} is exactly 2.9 Å away from the side chain oxygen of [Ser/Thr]$^{K+1}$, as they are neighboring ligands in the octahedral coordination shell of Mg^{2+} (see Fig. 11). In the absence of a bound TS-analog, however, [Thr/Ser]^{SwI}, as well as the whole Switch I loop, are highly mobile with water sporadically being involved as the Mg^{2+} ligand # 3 instead of [Thr/Ser]^{SwI}, see Fig. 7B-C, S5B and [140, 279]. It is tempting to speculate that the side chain of mobile [Thr/Ser]^{SwI} may be involved in a von Grotthuss-type proton transfer from the would-be W_{cat} to [Ser/Thr]$^{K+1}$ in the pre-TS state. Kumawat and colleagues, studying the small Rho GTPase by MD simulations, have shown that seven water molecules, on average, come within 4 Å distance from Thr37^{SwI} in a closed, GTP bound state [280]. This amount should be sufficient to transfer a proton from the would-be W_{cat} to anionic [Ser/Thr]^{SwI} over a distance of just 4–5 Å concomitantly with the constriction of the catalytic site. Alternatively, a W_{12} or W_{13} water molecule can give its proton to [Ser/Thr]^{SwI} and then move by 1-2 Å into the apical position turning into **OH^-_{cat}**. For myosin, where W_{12} is "visible" owing to extra bonds with residues of Switch I (Fig. 7D), we could reconstruct two tentative/alternative proton route(s), as shown by solid and dashed red arrows in Fig. 12D. Similar proton pathways can be proposed for Ras-like GTPases based on the "open" structure shown in Fig. 7C.

In TS-like structures, as already mentioned, [Ser/Thr]^{SwI} is fixed in a distinct position where it coordinates both the W_{cat} and Mg^{2+}; here the distance from its hydroxyl group to W_{cat} is about 4.5 Å (Fig. 3A-D), there appear to be no water molecules in between. It is tempting to speculate, that this configuration may hamper the unwanted return of a proton from Asp^{WB} to OH^-_{cat}.

3.2.2.5. Charge compensation at β-phosphate

According to Herschlag and colleagues [62, 64], the activation barrier of NTP hydrolysis is due to the strong negative charge that develops at β-phosphate as γ-phosphate breaks away; this charge should be compensated upon catalysis. The post-TS structures of the RhoA/RhoA-GAP complex (PDB ID 6R3V [201]) and activated myosin (PDB IDs 4PFP, 4PJK [52]) with NDP and detached P_i (Fig. 12F), as well as the structure of SF1 helicase Pif1 with a $H_2PO_4^{2-}$ mimic ADP:MgF_4^{2-} bound (Fig. 12C) show that the negative charge of β-phosphate is compensated by the joint action of Mg^{2+}, Lys^{WA}, Arg/Lys/Asn fingers and $\mathbf{HN}^{K-3}$. At this stage, the H-bond between $\mathbf{HN}^{K-3}$ and O^{2G} is lost so that $\mathbf{HN}^{K-3}$ is fully involved in compensating for the negative charge at β-phosphate. In addition, the structures show a short H-bond of 2.4-2.5 Å between the oxygen atoms of β-phosphate and P_i (see Fig. F12C, F and [52, 201, 277, 281]); this H-bond apparently also compensates for the negative charge at β-phosphate.

The proton for the H-bond between β-phosphate and P_i is thought to stem from W_{cat} [52, 201, 281] and should be somehow transferred to β-phosphate. In the octahedral coordination shell of Mg^{2+}, $[Ser/Thr]^{K+1}$ is 2.9 Å away from β-phosphate, so that its proton can directly pass on and compensate the negative charge (as shown in Fig. 11, 12C, 12E). The proton vacancy on $[Ser/Thr]^{K+1}$ could be then refilled by a proton from Asp^{WB} (Fig. 11, 12C, 12F), thus restoring the initial protonic configuration. Since the octahedral arrangement of Mg^{2+} ligands (Fig. 11) is similar in all P-loop NTPases, the proton can relocate from Asp^{WB} to β-phosphate, via $[Ser/Thr]^{K+1}$, in all of them.

3.2.3. Evidence for transient protonation of Asp^{WB} from infrared spectroscopy data

In PRC and BR shown in Fig. 10, the protonation of Asp/Glu residues was directly followed in the infrared (IR) spectral range [210, 230, 231, 239, 248, 255, 282]. In general, Asp and Glu residues are unique because the ν(C=O) vibration of their protonated carboxyl groups absorbs

in the 1710-1760 cm^{-1} spectral region that is free from overlap with absorption of other protein components [283]. Specifically, the protonated Asp-96 of BR has an absorption maximum at 1741 cm^{-1} [248], whereas the protonated GluL212-AspL213-Ser223 complex of PRC absorbs at 1728-1725 cm^{-1} [230, 231].

Application of the IR-spectroscopy to P-loop NTPases is complicated by the transient nature of Asp^{WB} protonation – proton passes through Asp^{WB} on the time scale of the NTPase turnover. Nevertheless, IR measurements in this spectral range were performed by Kim and colleagues who studied human Eg5, a kinesin-like motor protein of TRAFAC class, where $Asp265^{WB}$ and $Thr112^{K+1}$ are connected by a short H-bond of 2.59 Å (PDB ID 3HQD [284]). In their steady state experiments [285], Kim and colleagues investigated the action of monastrol, an allosteric inhibitor that binds some 12 Å away from the catalytic site [286] and increases the reversals in this enzyme by hampering the release of $H_2PO_4^{2-}$ [287]. In the presence of monastrol, an absorption maximum at 1726-1722 cm^{-1} was recorded and attributed to the protonation of a carboxylic group [285]. These data are consistent with proton trapping at $Asp265^{WB}$ when the overall equilibrium of ATP hydrolysis shifts to the left, as it happens in the presence of monastrol [287].

In kinetic experiments, the FTIR spectra of human Eg5 were monitored in real time and in response to the photorelease of caged ATP [288]. In the absence of microtubules, the hydrolysis by Eg5 proceeded at a time scale of seconds, which facilitated the IR measurements. A sharp absorption maximum at 1743 cm^{-1} appeared at approx. 3 s and then decayed, whereas $H_2PO_4^{2-}$, as measured at 1049 cm^{-1}, appeared at approximately 5 s and reached its maximum at 10 s (see Fig. 1 in [288]). According to the views of the time, the authors attributed the maximum at 1743 nm to an “organized water cluster undergoing protonation” (quoted from [288]). This attribution, however, seems far-fetched. In proteins, protonated water clusters absorb at higher

wave numbers of 1900 - 1800 cm^{-1} and show very broad continuum bands [282]. It is also unlikely that a protonated water cluster with pK around zero could have a lifetime of seconds at neutral pH of the experiment. It is tempting to suggest that the well-defined, sharp transient maximum at 1743 cm^{-1} was in fact due to the transient protonation of $Asp265^{WB}$ next to $Thr112^{K+1}$ in human Eg5 (cf with the maximum at 1741 cm^{-1} of Thr46-bound, protonated Asp96 in BR [248]).

3.2.4. Re-assignment of functions in and around the Walker motifs

In the framework proposed here, the Walker B motif serves as a trap for the proton from W_{cat}, whereas the coordination shell of the Mg^{2+} ion functions as an octahedral proton transfer hub with almost all Mg^{2+} ligands involved (Fig. 11). The proton is transferred from W_{cat} to Asp^{WB} in two steps: first, the proton shifts from $[Ser/Thr]^{K+1}$ to Asp^{WB} in response to the constriction of the catalytic site and stimulatory interaction, and then a proton from W_{cat} fills the proton vacancy at $[Ser/Thr]^{K+1}$, as shown in Fig. 12. Totally, one proton relocates from W_{cat} to Asp^{WB}. Still, the existence of separate proton transfer steps, as shown in Fig. 11, 12 by different shades, provides flexibility; the mechanism could be adapted to the dissociative, associative, or concerted mechanism of hydrolysis. For instance, if the reaction is concerted, the proton from W_{cat} can pass directly through the Mg^{2+}-coordinating ligands to β-phosphate, with the proton vacancy at $[Ser/Thr]^{K+1}$ being filled by Asp^{WB} later, concomitantly with the loosening of the catalytic site and decrease in proton affinity of Asp^{WB}, as shown in Fig. 12D-F.

The Asp^{WB} residue is almost strictly conserved throughout P-loop NTPases, see Table 1 and [9, 10, 12, 32, 107]. Only in several cases its function is performed by Glu, see [32] for details. Some of such cases are shown in Fig. S7 and described in its extended caption. The tentative interplay between Glu^{WB}, Asp^{E+1} and Glu^{E+4} residues in Vir/PilT-like ATPases is considered separately in the Supplementary File 1 together with other ambiguous cases.

Notably, the cause for the strict conservation of the entire Walker B motif has remained obscure so far; to our best knowledge, no function has been attributed to the motif as a whole. The here suggested scheme invokes Asp^{WB} as the common terminal acceptor of a proton from W_{cat}. Other four hydrophobic residues of the same motif serve as "hydrophobic protonic insulators". They may be needed to increase the proton affinity of Asp^{WB} in the constricted catalytic site and to prevent eventual unwanted proton escape from Asp^{WB}.

In our model, $[Ser/Thr]^{K+1}$ also acquires new key functions as a catalytic nucleophilic alkoxide and a von Grottuss-type proton carrier, which may explain its strict conservation, see Table 1. A few known exceptions are shown in Fig. S8 and described in its extended caption.

Most common outliers are glycine residues which substitute for $[Ser/Thr]^{K+1}$ in several distinct families of P-loop nucleotide monophosphate kinases [9]; in these cases, a water molecule serves as the Mg^{2+} ligand #4, see Fig. S8B. On the one hand, the successful involvement of a water molecule as the 4th ligand of Mg^{2+} in these kinases indicates that the conservation of $[Ser/Thr]^{K+1}$ in all other classes of P-loop NTPases may be unrelated to its function as a Mg^{2+} ligand. On the other hand, these multiple losses of $[Ser/Thr]^{K+1}$ provide additional support for here proposed mechanism. It is in these P-loop kinases that the attacking nucleophile – the anionic phosphate moiety of a nucleotide monophosphate – needs no deprotonation and, therefore, does not need a catalytic alkoxide. As noted earlier, kinases do not interact with separate activator proteins; they are activated by binding the second substrate, which causes covering of the catalytic site by the Lid domain and the insertion of stimulatory finger(s) (Fig. 4C-D, S8B). Therefore, there is always some danger that the insertion of the finger(s) will stimulate a nucleophilic attack on γ-phosphate not by the anionic phosphate group of the second substrate but by a haphazard water molecule, leading to a futile ATP hydrolysis. Within our proposed scheme, an unwanted ATP hydrolysis can be prevented by replacing $[Ser/Thr]^{K+1}$

with a residue incapable of accepting a proton from water. And that is what independently happened in several lineages of nucleotide monophosphate kinases, see Fig. S8B and multiple alignments in [9]. In particular, all the human adenylate kinases have glycine residues in the K+1 position except adenylate kinase 6, which has a threonine residue [289]. And it is for this kinase that both kinase and ATPase activities have been shown [290]. Hence, the consistent loss of $[Ser/Thr]^{K+1}$ – independently in several families of nucleotide monophosphate kinases [9] – finds a plausible explanation.

Neither of the exceptions in Fig. S7 and S8 calls into question the suggested mechanism where the buried $[Ser/Thr]^{K+1}$ – $[Asp/Glu]^{WB}$ module turns into a deep proton trap after the constriction of the catalytic site in most P-loop NTPases.

Why then the strictly conserved, H-bonded $[Ser/Thr]^{K+1}$ – Asp^{WB} pair has not established itself as a proton acceptor from W_{cat} so far? The theory of catalysis by P-loop NTPases was developed initially and intensively for small GTPases of TRAFAC class, such as G_{α}-proteins and Ras-like GTPases. Their W_{cat} molecules are stabilized not by a "catalytic" Glu/Asp, but by **CO**^{SwI}, Gly^{D+3} and Gln^{D+4} (Fig. 1F, 3C), so that Gln^{D+4} was initially suggested as the catalytic base. Warshel and colleagues challenged this view arguing that a Gln residue with pK < -2.0 is unlikely to accept a proton from water [67]. Among possible alternatives, they considered $Asp57^{WB}$ of Ras GTPase but discarded it because its mutation did not affect the slow "intrinsic" activity of the lone GTPase. Instead, the γ-phosphate group was proposed as a universal proton acceptor for W_{cat} [67] and has been considered as such ever since in TRAFAC class NTPases. Although just a year later it had been shown that mutations of Asp^{WB} slowed by orders of magnitude the fast activated hydrolysis by Ras/RasGAP complexes [272], the role of γ-phosphate as the proton acceptor was not revisited. After Cleland and Hengge noted that the direct proton transfer from W_{cat} to γ-phosphate is not possible "as the geometry does not permit

such a four center reaction" [60], the involvement of an additional water molecule between W_{cat} and γ-phosphate was hypothesized for TRAFAC class NTPases. In the case of other NTPase classes, the W_{cat}-coordinating Glu (Asp) residues were considered as "catalytic" bases. Unfortunately, the seminal work by Frick and colleagues on the suitability of buried Asp^{WB} as a proton acceptor from W_{cat} [202, 203], mentioned above, has not changed the common view. The inability either of γ-phosphate or "catalytic" Glu/Asp residues to serve as proton traps because of their low pK values has been overlooked.

Our suggestion that the proton affinity of Asp^{WB} depends on the length of its H-bond with $[Ser/Thr]^{K+1}$ explains why mutations of $Asp57^{WB}$ affect the fast RasGAP-activated GTP hydrolysis [272], but have no impact on the slow intrinsic hydrolysis by lone Ras GTPases [67]. In lone GTPases, the difference between the time of proton equilibration over the whole protein (microseconds) and the catalysis time (minutes/hours) is so large that the mere presence of a dedicated proton acceptor for W_{cat} is unlikely, see also [62]. Since the catalytic site is fully exposed in the absence of a GAP, W_{cat} eventually losses a proton to the neutral bulk solution. Analogously, some group with a pK value slightly higher than pH provides a proton for β-phosphate and then is repleted from the solution. Anyway, the terminal acceptor/donor of the proton is the neutral bulk solution so that the overall reaction is slow (as discussed elsewhere in relation to proton transfer in PRC [256]). Hence, the intrinsic hydrolysis in the absence of the GAP is insensitive to mutations of Asp^{WB} because this residue is unlikely to be specifically involved. In the exposed catalytic site of a lone Ras GTPase, the pK value of Asp^{WB} is expected to be ≤ 5.0 (which corresponds to the 2.6-2.7 Å length of the $[Ser/Thr]^{K+1}$ – Asp^{WB} H-bond in the structures that contain NTPs or their analogs, see Fig. 9 and [261]), so that $Ser17^{K+1}$ is protonated (see the neutron crystal structure of Ras, PDB ID 4RSG, [291]) and cannot accept a proton from W_{cat}. Both $[Ser/Thr]^{K+1}$ and Asp^{WB} can only be transiently visited by the "catalytic" proton as it redistributes over the protein on its way into the bulk solution. Such a

mechanism of slow, solution-controlled hydrolysis may also operate, even in the presence of an activator, in those P-loop NTPases where Asp^{WB} and/or $[Ser/Thr]^{K+1}$ were mutated [203, 268-275].

In a RasGAP-stimulated wild-type complex, the situation differs. Within the constricted catalytic site, the shortening of the H-bond with $Ser17^{K+1}$ up to 2.4-2.5 Å would increase the proton affinity of $Asp57^{WB}$ (see Fig. 9 and [261]), turning it into a deep trap for a proton from $Ser17^{K+1}$. The anionic alkoxide of $Ser17^{K+1}$ is thermodynamically much more favorable proton acceptor from W_{cat} than the pH-neutral solution. The same proton relays to β-phosphate when the latter is ready to accept it; there is no need to wait for a proton from the solution. As a result, hydrolysis is 10^5 times faster than in the case of the lone Ras GTPase. Expectedly, the $Asp57^{WB}$ to Asn mutation slowed the rate of the activated hydrolysis by Ras/RasGAP to the "intrinsic" level of hydrolysis observed in the absence of GAP [272].

By no way we state that γ-phosphate is banned for the "catalytic" proton from W_{cat}. Distance measurements indicate that the catalytic proton can pass to $[Ser/Thr]^{K+1}$ and Asp^{WB} also through the oxygen atom(s) of γ-phosphate in NTPases of all classes, which, to some extent, justifies numerous QM/MM models of water-mediated proton transfers from W_{cat} to γ-phosphate. These proton routes, however, involve "uphill" proton transfer from water to enzyme-bound triphosphate moiety with pK < 3.0 [197, 198]. Hence, these routes are thermodynamically very unfavorable and, therefore, very slow. Unfortunately, the QM modeling does not capture thermodynamic obstacles of this kind. It is this hindrance that may have prompted repeated independent emergence of γ-phosphate-bypassing proton pathways from W_{cat} to the $[Ser/Thr]^{K+1}$ – Asp^{WB} pair, which we identified in TS-like structures of diverse P-loop NTPases, see Fig. 3-7, 11, 12.

We turned towards the strictly conserved Asp^{WB} and $[Ser/Thr]^{K+1}$ as proton acceptors from W_{cat} after we realized that the "catalytic" Glu/Asp residues are provided by topologically diverse protein segments in different classes of P-loop NTPases see Fig. 1F, 4-6, 7A, Table 1, section 2.2. and [9, 10, 32, 292]. Our analysis shows that proton pathways via "catalytic" Asp or Glu residues, emerged independently in kinases, SIMIBI NTPases, "medium-size" ASCE ATPases, and large F_1/RecA-like ATPases, i.e. four times, at least.

This observation was unusual since catalytic bases are usually conserved within enzyme families. At the same time, the discovered amino acid residues that link W_{cat} to the coordination shell of Mg^{2+}, although non-homologous, strongly resemble each other as well as the proton path in the PRC (cf Fig. 4-6, 7A with Fig. 10A), which suggested that they constitute proton pathways. In the scheme proposed here, these non-homologous, "catalytic" Asp/Glu residues, as well as $[Ser/Thr]^{SwI}$ of TRAFAC class NTPases, are regarded as intermediate proton carriers, whereas thermodynamics of catalysis are determined by the difference in proton affinities between W_{cat} (or its analogs in kinases) and somewhat distantly located, but evolutionary conserved $[Ser/Thr]^{K+1}$ – Asp^{WB} module, which serves as a *catalytic base.*

3.2.5. Minimal mechanistic model of NTP hydrolysis by P-loop NTPases

Building on the comparative structure analysis of over 3100 catalytic sites presented here and in the accompanying article [41], as well as on the available experimental and theoretical data, we describe the activated catalysis typical for P-loop NTPases by a simple mechanistic model depicted in Fig. 13. We show the minimalistic version of the model that includes ubiquitous Walker A and Walker B motifs, Mg^{2+}-NTP, a simple stimulator, such as a K^+ ion or a Lys/Asn residue, and a few water molecules one of which serves as W_{cat}. The model, however, can be easily expanded/adapted to fit distinct NTPase families by adding further stimulatory

interactions, auxiliary and W_{cat}-coordinating residues, as well as by replacing W_{cat} by other nucleophiles.

According to the model, the catalytic transition proceeds in the following steps:

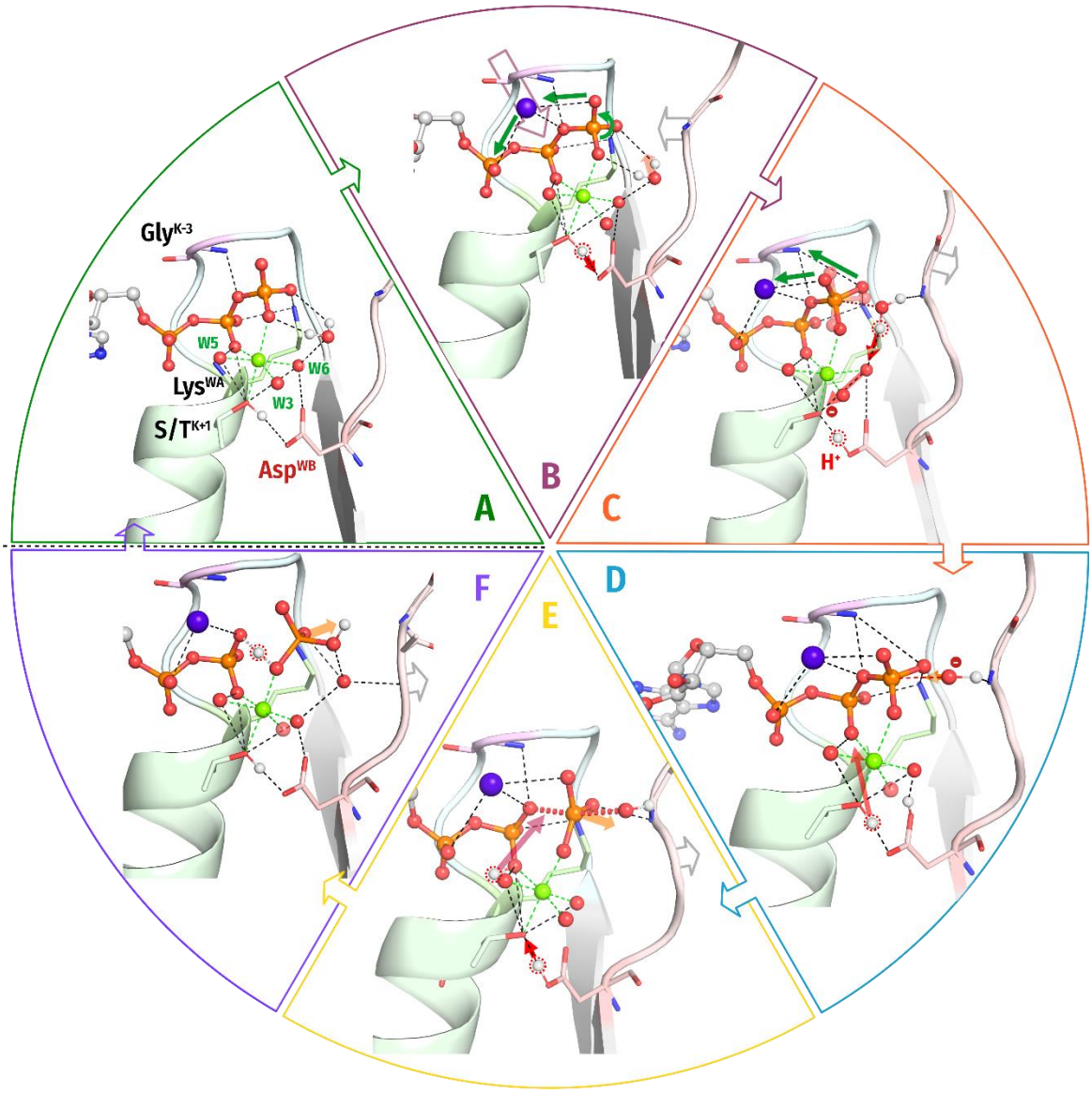

Figure 13. The common scheme of stimulated hydrolysis in P-loop NTPases. Empty purple arrow, movement of the stimulator (shown as a purple sphere); gray arrow, movement of the WB-crest; green arrows, twist and planarization of γ-phosphate; red arrows, proton displacements; orange arrows, detachment of Pi. The following crystal structures were used as templates: panels **A, B** – PDB ID 1FMW [139]; panels **C-E** – PDB ID 1VOM [95]; panel **F** – PDB ID 4PFP [52]. See the main text for a detailed explanation.

A) A Mg-NTP complex binds to the Walker A and Walker B motifs; the binding energy is used to bring the NTP molecule into an elongated conformation with eclipsed β- and γ-phosphates and to close the catalytic site by surrounding the triphosphate chain by positively charged groups that are provided by the P-loop, WB-crest and, only in TRAFAC NTPases, Switch I loop. The accompanying protein conformational changes can power useful mechanical work. The catalytic site is further stabilized by the H-bond between Asp^{WB} and $[Ser/Thr]^{K+1}$. The H-bond length is about 2.6-2.7 Å (Fig. 9); in this state Asp^{WB} is negatively charged.

B) An exergonic interaction between the activating partner (another protein domain and/or an RNA/DNA molecule) and the WB-crest (i) shields and constricts the catalytic site, (ii) moves the WB-crest residues closer to the γ-phosphate, (iii) inserts the stimulator(s) next to the phosphate chain. The constriction of the catalytic site shortens the H-bond between $[Ser/Thr]^{K+1}$ and Asp^{WB} to 2.4-2.5 Å, turning Asp^{WB} into a potent proton trap. In most cases, (one of) the stimulator(s) links the O^{2A} and O^{3G} atoms of the triphosphate (Fig. 1E, F, 3B-D, 4A-D, 5A-C, 6A) and twists γ-phosphate counterclockwise; the rotated γ-phosphate is stabilized by a new H-bond between O^{2G} and $\mathbf{HN}^{K-3}$. In other cases, the stimulators drag only γ-phosphate and, supposedly, twists it in some direction, see Fig. 3A, 5D, 6B-D. The interaction of stimulators with γ-phosphate (i) increases the electrophilicity of the P^G atom, (ii) weakens the O^{3B}–P^G bond, (iii) promotes the transition of γ-phosphate to a more planar conformation, and (iv) inevitably affects the coordination of the Mg^{2+} ion by displacing the O^{1G} atom. The increase of local positive charge at $[Ser/Thr]^{K+1}$ – after O^{1G} is moved aside by the stimulator – promotes the relocation of proton from $[Ser/Thr]^{K+1}$ to Asp^{WB}.

C) The anionic $[Ser/Thr]^{K+1}$ alkoxide withdraws a proton from the polarized W_{cat} molecule via intermediate proton carriers. Here we depicted the simplest proton route as envisioned for TRAFAC NTPases (see Fig. 12D-F and Section 3.2.2.4). More complex proton routes via W_{cat}-

coordinating Glu/Asp residues, as found in other classes of NTPases, are indicated by red dashed lines in Fig. 4-6 and differently shaded red arrows in Fig. 11, 12A-C.

D) The resulting **OH⁻$_{cat}$**, stabilized/polarized by its ligands, attacks the P^G atom. Although the simplified diagram in Fig. 13D shows only one stabilizing interaction of **OH⁻$_{cat}$** with the **HN** group of the WB-crest residue, several ligands are usually involved in the stabilization, see Fig. 1E-F, 3-6. During this step, the proton stays on Asp^{WB}. The formation of a covalent bond between **OH⁻$_{cat}$** and P^G increases the planarization of γ-phosphate; its oxygen atoms repel the β-phosphate oxygen atoms, resulting in a lengthening of the O^{3B}–P^G bond. With the inversion of γ-phosphate, increase in the O^{3B}–P^G distance, and γ-phosphate moving away from β-phosphate, $\mathbf{HN}^{K-3}$ detaches from γ-phosphate and, together with Lys^{WA}, Mg^{2+} and the stimulator, neutralizes the negative charge appearing on the O^{3B} atom, thereby lowering the activation barrier. In addition, the negative charge on β-phosphate attracts a proton from $[Ser/Thr]^{K+1}$.

E) The proton that comes from $[Ser/Thr]^{K+1}$ forms a new short H-bond between β- and γ-phosphate [52, 201, 281], which further stabilizes the negative charge on the β-phosphate. The proton at Asp^{WB} relocates to $[Ser/Thr]^{K+1}$.

F) The H-bond between β- and γ-phosphate gradually dissociates as $H_2PO_4^{2-}$ leaves the catalytic site. The departure of $H_2PO_4^{2-}$ is an exergonic reaction that may be coupled to conformational changes, detachment of the activating partner from the WB-crest, and useful mechanical work.

The simplified diagram in Figure 13 does not show the activation partner, as they are quite different in different families of P-loop NTPases. Accordingly, the exothermic interactions of the activator with the amino acid residues of the NTPase domain, which apparently result in the constriction of the catalytic site, are also not depicted. Some of them, however, are shown

in Fig. S9, where the proposed general scheme is applied to myosin. Despite several sets of excellent crystal structures available [52, 91, 139, 293-297], the mechanism of ATP hydrolysis by myosin remains unclear [166]. Using the entire set of myosin crystal structures and the scheme in Fig. 13, we tried to reconstruct the catalytic cycle of myosin, as shown in Fig. S9 and described in its caption.

3.3. Conclusions and Outlook

Here and in the accompanying article [41] we applied the tools of evolutionary biophysics to elucidate the mechanisms of catalysis by P-loop NTPases. This approach allowed us not only to find support for previous MD simulation data on twisting γ-phosphate by the stimulatory moiety in P-loop GTPases [40, 163], but also, rather unexpectedly, to suggest a common catalytic mechanism for P-loop NTPases. The key elements of the proposed mechanism are the activation-induced, oppositely directed changes in proton affinity of H-bonded $[Ser/Thr]^{K+1}$ and Asp^{WB}, which convert the latter into a deep trap for a proton from $[Ser/Thr]^{K+1}$ that, in turn, withdraws a proton from W_{cat} and converts it into a strong nucleophile OH^{-}_{cat}. The suggested mechanism rationalizes the strict evolutionary conservation of $[Ser/Thr]^{K+1}$ and Asp^{WB}, neither of which has been ascribed a specific catalytic function so far.

Indeed, Walker A and Walker B motifs — together — contain only two strictly conserved residues capable of proton transfer, namely $[Ser/Thr]^{K+1}$ and Asp^{WB}. It is amazing that this H-bonded pair has not been considered in relation to proton transfer from W_{cat} up to now.

As argued elsewhere, the ability to provide strong acids and bases timely is important for enzyme catalysis [232]. Specifically, enzymes were suggested to generate strong bases or acids – precisely when required – by transiently altering the length of relevant H-bonds [261, 262, 298-304]. In the case of P-loop NTPases, the mechanism is quite simple: the free energies of (i) substrate binding and (ii) interaction with the activation partner are used to close and

constrict the catalytic site, which shortens the H-bond between $[Ser/Thr]^{K+1}$ and Asp^{WB} and levels their functional pK values. Eventually, after γ-phosphate is rotated by the stimulator, proton relocates from $[Ser/Thr]^{K+1}$ to Asp^{WB} yielding a serine alkoxide as a strong nucleophile for W_{cat}.

The still prevalent notion that chemically different catalytic bases (phosphates vs glutamates) are used in different classes of apparently homologous P-loop NTPases is bizarre, to say the least. Furthermore, neither phosphates nor glutamates are common as catalytic bases in the other families of phosphate transferases. In one of the most comprehensive reviews on their mechanisms, Cleland and Hengge even pointed out the oddness of anticipated catalytic bases in P-loop ATPases: "... more specifically, there must be a path for one proton of the attacking water molecule to reach a suitable acceptor. ATPases appear not to use general bases such as the aspartates usually found in kinase active sites...." (quoted from [60]). Our message is that P-loop NTPases are no exception, they do use aspartates as catalytic bases just like most other phosphate transferases.

The proposed mechanism of proton transfer from W_{cat} to Asp^{WB} via Mg^{2+}-coordinating ligands brings the P-loop NTPases into the general context of other Mg-dependent hydrolases and transferases [57, 58, 60, 136, 266, 305, 306]. The full range of theoretical approaches developed for such enzymes can now be applied to P-loop NTPases. In particular, the relationship between changes in the Mg^{2+} coordination shell, proton affinity of Mg^{2+} ligands, and catalysis is the subject of QM/MM modeling in this field, see e.g. [307]. Also, Nemukhin and colleagues, have recently suggested proton transfer via the Mg^{2+} coordination shell in adenylate cyclase [306], which corroborates with the here proposed mechanism of proton transfer in P-loop NTPases. Therefore, we think that a new generation of QM/MM models of P-loop NTPases, which will

include the entire Mg^{2+} coordination shell as well as proton transfer networks around Asp^{WB}, will help to quantitatively describe their catalytic mechanisms.

Our tentative identification of the anionic $[Ser/Thr]^{K+1}$ alkoxide as the proton acceptor from W_{cat} brings P-loop NTPases into another broad context of enzymes that generate a strong nucleophile by stripping a Ser/Thr residue of its proton [60, 164, 266, 267]. These are numerous families of serine proteases where, within apparently similar, but non-homologous "catalytic triads", proton is transferred from the catalytic Ser to proton-accepting Asp via a histidine residue that serves as a von Grotthuss-type proton carrier. It is less known that the proton-accepting Asp residue of serine proteases is usually H-bonded to another conserved Thr/Ser residue [299, 308, 309]. Also, the catalytic Ser/Thr of eukaryotic protein kinases gives its proton to the conserved Asp [196, 310, 311], which, in turn, is also H-bonded to another conserved Ser/Thr residue.

In essence, we argue that P-loop NTPases use the same (bio)chemical strategies to produce a strong nucleophile as many other enzymes do; there is no reason to consider them different or special in this respect.

Notably, serine proteases, serine-threonine kinases, Mg-dependent hydrolases and transferases, as well as P-loop NTPases considered here, form the largest known enzyme families. Many of them use H-bonded [Asp/Glu]–[Ser/Thr] functional modules in different roles, which feature they share with membrane-embedded PRC and BR, see Fig. 10 and [247]. We believe that further search for structural features common to distinct enzyme families is a very promising task.

Last but not least, protonation of Asp and Glu residues can be traced in real time by IR spectroscopy [210, 230, 231, 239, 248, 255, 282, 285, 288]. Therefore, we believe that the proton shuttling between $[Ser/Thr]^{K+1}$ and Asp^{WB} in various P-loop NTPases is worthy of being

traced using photoactivated, caged ATP/GTP substrates and modern IR spectroscopy techniques (see, e.g., [39, 194, 282, 312]). Also, the position of a hydrogen atom within a short H-bond can be identified by complementary X-ray and neutron crystallographic structure determination [302-304]. Investigation of P-loop NTPases by these methods will shed new light on enzyme mechanisms.

4. Methods

Manual comparative structure analysis: For each class of P-loop NTPases, representative structures were manually selected from the Protein Data Bank (PDB) at www.rcsb.org [71, 72] based on literature data and structure availability.

Cumulative computational structure analysis: As for the analysis in the accompanying paper [41], structures were selected among those PDB entries that matched the following criteria: (1) assigned to InterPro record IPR027417; (2) contained an ATP/GTP molecule, or non-hydrolyzable analog of NTP, or a transition-state analog; (3) contained at least one Mg^{2+}, Mn^{2+} or Ca^{2+} ion; (4) resolution of 5 Å or higher, if applicable. Proteins were assigned to major classes of P-loop NTPases according to membership in Pfam families (ftp://ftp.ebi.ac.uk/pub/databases/Pfam/mappings/pdb_pfam_mapping.txt) [9, 10], see the details in the accompanying paper [41]. This search yielded 1474 PDB structures with 3666 catalytic sites in them.

We checked the reliability of each catalytic site by assessing the integrity of the NTP analog/presence of γ-phosphate mimic, presence of a P-loop motif Lys residue within 5Å of the β-phosphate. This analysis yielded 3136 complexes in 1383 structures with various substrates: ATP and GTP, their nonhydrolyzable analogs, and ADP/GDP molecules associated with γ-phosphate-mimicking moieties, see Fig. 14 in the accompanying paper [41].

Also as a quality control, we have measured distances from $[Ser/Thr]^{K+1}$ to Mg^{2+}, to ensure the correct binding of the Mg^{2+} and general reliability of the structure resolution at the binding site (i.e, very long distance would indicate a disturbed catalytic site or resolution at the site that is insufficient for our purposes of comparative analysis), and from $[Asp/Glu]^{WB}$ to Mg^{2+}, to identify cases of direct coordination of Mg^{2+} by the acidic residue (short distances) or disassembled binding sites (long distances).In addition, we examined the presence of interactions of phosphate chain with NH^{K-3} group and positively charged moieties in those sites that passed the quality control (the details of analysis are described in the accompanying paper [41] and depicted in Fig. 14 of it.)

Putative $[Asp/Glu]^{WB}$ residue was identified as follows: distances from all Asp and Glu residues to $[Ser/Thr]^{K+1}$ were measured, and the closest residue that was preceded by at least three non-ionizable residues (Glu, Asp, Ser, Thr, Tyr, Lys, Arg and His were considered as ionizable) was chosen as the partner of $[Ser/Thr]^{K+1}$. If this failed, a closest Asp/Glu was selected without hydrophobicity check (data available in Table S1). Residues located further than 5Å were not considered. In those few cases where $[Asp/Glu]^{WB}$ residue is indicated in the Table S1 as "absent at the threshold distance", the catalytic site is likely to be fully "open". We have not checked all these cases manually.

Visualization: Structure superposition, manual distance measurements, manual inspection and structures visualization were performed by Mol* Viewer [313] and PyMol v2.5.0 [314].

Data availability:

Descriptions of each binding site are available in Table S1. Scripts used to generate and annotate the data and quickly visualize selected sites listed in Table S1 are available from github.com/servalli/pyploop.

5. Acknowledgements

Very fruitful discussions with Drs. D.A. Cherepanov, M.Y. Galperin, D.N. Frick, K. Gerwert, A. V. Golovin, Y.Kalaidzidis, E.V. Koonin, A. Lupas, B.H. Meier, N. Voskoboynikova, T. Wiegand and M. Zereal are highly appreciated. We also are thankful to Alexander Mulkidzhanyan for his help during the initial stage of the project. The research was supported by DFG, DAAD, and the Osnabrueck University (the EvoCell Program and Open Access Publishing Fund).

6. References

[1] J.E. Walker, M. Saraste, M.J. Runswick, N.J. Gay, Distantly related sequences in the alpha- and beta-subunits of ATP synthase, myosin, kinases and other ATP-requiring enzymes and a common nucleotide binding fold, EMBO J 1(8) (1982) 945-51.

[2] M. Saraste, P.R. Sibbald, A. Wittinghofer, The P-loop – a common motif in ATP- and GTP-binding proteins, Trends Biochem. Sci. 15(11) (1990) 430-4.

[3] A.E. Gorbalenya, E.V. Koonin, Helicases: amino acid sequence comparisons and structure-function relationships, Curr Opin Struc Biol 3(3) (1993) 419-429.

[4] C.A. Smith, I. Rayment, Active site comparisons highlight structural similarities between myosin and other P-loop proteins, Biophys J 70(4) (1996) 1590-602.

[5] S.R. Sprang, G protein mechanisms: insights from structural analysis, Annu Rev Biochem 66 (1997) 639-78.

[6] A.F. Neuwald, L. Aravind, J.L. Spouge, E.V. Koonin, AAA+: A class of chaperone-like ATPases associated with the assembly, operation, and disassembly of protein complexes, Genome Res 9(1) (1999) 27-43.

[7] E.V. Koonin, Y.I. Wolf, L. Aravind, Protein fold recognition using sequence profiles and its application in structural genomics, Adv. Protein Chem. 54 (2000) 245-275.

[8] E. Muneyuki, H. Noji, T. Amano, T. Masaike, M. Yoshida, F(0)F(1)-ATP synthase: general structural features of 'ATP-engine' and a problem on free energy transduction, Biochim Biophys Acta 1458(2-3) (2000) 467-81.

[9] D.D. Leipe, E.V. Koonin, L. Aravind, Evolution and classification of P-loop kinases and related proteins, J Mol Biol 333(4) (2003) 781-815.

[10] D.D. Leipe, Y.I. Wolf, E.V. Koonin, L. Aravind, Classification and evolution of P-loop GTPases and related ATPases, J Mol Biol 317(1) (2002) 41-72.

[11] V. Anantharaman, L. Aravind, E.V. Koonin, Emergence of diverse biochemical activities in evolutionarily conserved structural scaffolds of proteins, Curr. Opin. Chem. Biol. 7(1) (2003) 12-20.

[12] L.M. Iyer, D.D. Leipe, E.V. Koonin, L. Aravind, Evolutionary history and higher order classification of AAA+ ATPases, J. Struct. Biol. 146(1-2) (2004) 11-31.

[13] M. Ammelburg, T. Frickey, A.N. Lupas, Classification of AAA+ proteins, J Struct Biol 156(1) (2006) 2-11.

[14] N.D. Thomsen, J.M. Berger, Structural frameworks for considering microbial protein- and nucleic acid-dependent motor ATPases, Mol Microbiol 69(5) (2008) 1071-90.
[15] A. Wittinghofer, I.R. Vetter, Structure-function relationships of the G domain, a canonical switch motif, Annu. Rev. Biochem. 80 (2011) 943-971.
[16] P. Wendler, S. Ciniawsky, M. Kock, S. Kube, Structure and function of the AAA+ nucleotide binding pocket, Biochim. Biophys. Acta 1823(1) (2012) 2-14.
[17] A.M. Burroughs, L. Aravind, The Origin and Evolution of Release Factors: Implications for Translation Termination, Ribosome Rescue, and Quality Control Pathways, Int J Mol Sci 20(8) (2019).
[18] L.M. Longo, J. Jablonska, P. Vyas, M. Kanade, R. Kolodny, N. Ben-Tal, D.S. Tawfik, On the emergence of P-Loop NTPase and Rossmann enzymes from a Beta-Alpha-Beta ancestral fragment, Elife 9 (2020).
[19] A. Krishnan, A.M. Burroughs, L.M. Iyer, L. Aravind, Comprehensive classification of ABC ATPases and their functional radiation in nucleoprotein dynamics and biological conflict systems, Nucleic Acids Res 48(18) (2020) 10045-10075.
[20] R.D. Schaeffer, Y. Liao, H. Cheng, N.V. Grishin, ECOD: new developments in the evolutionary classification of domains, Nucleic Acids Res 45(D1) (2017) D296-D302.
[21] R.D. Finn, P. Coggill, R.Y. Eberhardt, S.R. Eddy, J. Mistry, A.L. Mitchell, S.C. Potter, M. Punta, M. Qureshi, A. Sangrador-Vegas, G.A. Salazar, J. Tate, A. Bateman, The Pfam protein families database: towards a more sustainable future, Nucleic Acids Res. 44(D1) (2016) D279-D285.
[22] A.N. Lupas, C.P. Ponting, R.B. Russell, On the evolution of protein folds: are similar motifs in different protein folds the result of convergence, insertion, or relics of an ancient peptide world?, J Struct Biol 134(2-3) (2001) 191-203.
[23] C.P. Ponting, R.R. Russell, The natural history of protein domains, Annual review of biophysics and biomolecular structure 31 (2002) 45-71.
[24] B.G. Mirkin, T.I. Fenner, M.Y. Galperin, E.V. Koonin, Algorithms for computing parsimonious evolutionary scenarios for genome evolution, the last universal common ancestor and dominance of horizontal gene transfer in the evolution of prokaryotes, BMC Evol Biol 3 (2003) 2.
[25] J. Söding, A.N. Lupas, More than the sum of their parts: on the evolution of proteins from peptides, BioEssays 25(9) (2003) 837-46.
[26] J.A. Ranea, A. Sillero, J.M. Thornton, C.A. Orengo, Protein superfamily evolution and the last universal common ancestor (LUCA), J. Mol. Evol. 63(4) (2006) 513-25.
[27] V. Alva, J. Soding, A.N. Lupas, A vocabulary of ancient peptides at the origin of folded proteins, eLife 4 (2015) e09410.
[28] T.F. la Cour, J. Nyborg, S. Thirup, B.F. Clark, Structural details of the binding of guanosine diphosphate to elongation factor Tu from E. coli as studied by X-ray crystallography, EMBO J 4(9) (1985) 2385-8.
[29] F. Jurnak, Induction of elongation factor Tu-GDP crystal polymorphism by polyethylene glycol contaminants, J Mol Biol 185(1) (1985) 215-7.
[30] V.N. Hingorani, Y.K. Ho, A structural model for the alpha-subunit of transducin. Implications of its role as a molecular switch in the visual signal transduction mechanism, FEBS Lett 220(1) (1987) 15-22.
[31] E.F. Pai, U. Krengel, G.A. Petsko, R.S. Goody, W. Kabsch, A. Wittinghofer, Refined crystal structure of the triphosphate conformation of H-ras p21 at 1.35 A resolution: implications for the mechanism of GTP hydrolysis, EMBO J. 9(8) (1990) 2351-9.
[32] M. Kanade, S. Chakraborty, S.S. Shelke, P. Gayathri, A Distinct Motif in a Prokaryotic Small Ras-Like GTPase Highlights Unifying Features of Walker B Motifs in P-Loop NTPases, J Mol Biol 432(20) (2020) 5544-5564.

[33] G.M. Blackburn, J. Cherfils, G.P. Moss, N.G.J. Richards, J.P. Waltho, N.H. Williams, A. Wittinghofer, How to name atoms in phosphates, polyphosphates, their derivatives and mimics, and transition state analogues for enzyme-catalysed phosphoryl transfer reactions (IUPAC Recommendations 2016), Pure Appl. Chem. 89(5) (2017) 653-675.
[34] D.L. Graham, P.N. Lowe, G.W. Grime, M. Marsh, K. Rittinger, S.J. Smerdon, S.J. Gamblin, J.F. Eccleston, MgF(3)(-) as a transition state analog of phosphoryl transfer, Chem Biol 9(3) (2002) 375-81.
[35] Y.S. Law, A. Utt, Y.B. Tan, J. Zheng, S. Wang, M.W. Chen, P.R. Griffin, A. Merits, D. Luo, Structural insights into RNA recognition by the Chikungunya virus nsP2 helicase, Proc Natl Acad Sci U S A 116(19) (2019) 9558-9567.
[36] A. Matte, L.W. Tari, L.T. Delbaere, How do kinases transfer phosphoryl groups?, Structure 6(4) (1998) 413-9.
[37] I.R. Vetter, A. Wittinghofer, Nucleoside triphosphate-binding proteins: different scaffolds to achieve phosphoryl transfer, Q. Rev. Biophys. 32(1) (1999) 1-56.
[38] C. Allin, K. Gerwert, Ras catalyzes GTP hydrolysis by shifting negative charges from gamma- to beta-phosphate as revealed by time-resolved FTIR difference spectroscopy, Biochemistry 40(10) (2001) 3037-46.
[39] C. Kotting, K. Gerwert, Time-resolved FTIR studies provide activation free energy, activation enthalpy and activation entropy for GTPase reactions, Chem Phys 307(2-3) (2004) 227-232.
[40] D.N. Shalaeva, D.A. Cherepanov, M.Y. Galperin, A.V. Golovin, A.Y. Mulkidjanian, Evolution of cation binding in the active sites of P-loop nucleoside triphosphatases in relation to the basic catalytic mechanism, Elife 7 (2018).
[41] M.I. Kozlova, D.N. Shalaeva, D.V. Dibrova, A.Y. Mulkidjanian, Patterns of hydrolysis initiation in P-loop fold nucleoside triphosphatases, BioRxiv (2022), DOI: 10.1101/2022.06.23.497298.
[42] D.E. Coleman, A.M. Berghuis, E. Lee, M.E. Linder, A.G. Gilman, S.R. Sprang, Structures of active conformations of Gi alpha 1 and the mechanism of GTP hydrolysis, Science 265(5177) (1994) 1405-12.
[43] J. Sondek, D.G. Lambright, J.P. Noel, H.E. Hamm, P.B. Sigler, GTPase mechanism of Gproteins from the 1.7-A crystal structure of transducin alpha-GDP-AIF-4, Nature 372(6503) (1994) 276-9.
[44] K. Scheffzek, M.R. Ahmadian, A. Wittinghofer, GTPase-activating proteins: helping hands to complement an active site, Trends Biochem Sci 23(7) (1998) 257-62.
[45] T. Ogura, S.W. Whiteheart, A.J. Wilkinson, Conserved arginine residues implicated in ATP hydrolysis, nucleotide-sensing, and inter-subunit interactions in AAA and AAA+ ATPases, J. Structural Biology 146(1-2) (2004) 106-12.
[46] A. Scrima, A. Wittinghofer, Dimerisation-dependent GTPase reaction of MnmE: how potassium acts as GTPase-activating element, EMBO J 25(12) (2006) 2940-51.
[47] M.-R. Ash, M.J. Maher, J.M. Guss, M. Jormakka, The cation-dependent G-proteins: in a class of their own, FEBS Lett. 586(16) (2012) 2218-24.
[48] Y. Jin, R.W. Molt, Jr., G.M. Blackburn, Metal fluorides: Tools for structural and computational analysis of phosphoryl transfer enzymes, Top. Curr. Chem. (Cham) 375(2) (2017) 36.
[49] R. Gasper, F. Wittinghofer, The Ras switch in structural and historical perspective, Biol Chem 401(1) (2019) 143-163.
[50] I.R. Vetter, A. Wittinghofer, Signal transduction - The guanine nucleotide-binding switch in three dimensions, Science 294(5545) (2001) 1299-1304.

[51] K. Nam, J. Pu, M. Karplus, Trapping the ATP binding state leads to a detailed understanding of the F1-ATPase mechanism, Proc Natl Acad Sci U S A 111(50) (2014) 17851-6.
[52] P. Llinas, T. Isabet, L. Song, V. Ropars, B. Zong, H. Benisty, S. Sirigu, C. Morris, C. Kikuti, D. Safer, H.L. Sweeney, A. Houdusse, How actin initiates the motor activity of Myosin, Dev Cell 33(4) (2015) 401-12.
[53] A. Wittinghofer, Signaling mechanistics: aluminum fluoride for molecule of the year, Curr. Biol. 7(11) (1997) R682-R685.
[54] R.I. Menz, J.E. Walker, A.G. Leslie, Structure of bovine mitochondrial F_1-ATPase with nucleotide bound to all three catalytic sites: implications for the mechanism of rotary catalysis, Cell 106(3) (2001) 331-41.
[55] D.R. Davies, W.G. Hol, The power of vanadate in crystallographic investigations of phosphoryl transfer enzymes, FEBS Lett. 577(3) (2004) 315-21.
[56] Y. Jin, N.G. Richards, J.P. Waltho, G.M. Blackburn, Metal fluorides as analogues for studies on phosphoryl transfer enzymes, Angew. Chem. Int. Ed. Engl. 56(15) (2017) 4110-4128.
[57] J.R. Knowles, Enzyme-catalyzed phosphoryl transfer reactions, Annu Rev Biochem 49 (1980) 877-919.
[58] F.H. Westheimer, Why Nature Chose Phosphates, Science 235(4793) (1987) 1173-1178.
[59] Z.A. Shabarova, A.A. Bogdanov, Advanced Organic Chemistry of Nucleic Acids, VCH, Weinheim, 1994.
[60] W.W. Cleland, A.C. Hengge, Enzymatic mechanisms of phosphate and sulfate transfer, Chem Rev 106(8) (2006) 3252-78.
[61] M.W. Bowler, M.J. GCliff, J.P. Waltho, G.M. Blackburn, Why did Nature select phosphate for its dominant roles in biology?, New Journal of Chemistry 34 (2010) 784-794.
[62] J.K. Lassila, J.G. Zalatan, D. Herschlag, Biological phosphoryl-transfer reactions: understanding mechanism and catalysis, Annu Rev Biochem 80 (2011) 669-702.
[63] F.A. Kiani, S. Fischer, Comparing the catalytic strategy of ATP hydrolysis in biomolecular motors, Phys Chem Chem Phys 18(30) (2016) 20219-33.
[64] K.A. Maegley, S.J. Admiraal, D. Herschlag, Ras-catalyzed hydrolysis of GTP: a new perspective from model studies, Proc. Natl. Acad. Sci. USA 93(16) (1996) 8160-6.
[65] T.M. Glennon, J. Villa, A. Warshel, How does GAP catalyze the GTPase reaction of Ras?: A computer simulation study, Biochemistry 39(32) (2000) 9641-9651.
[66] C. Kotting, A. Kallenbach, Y. Suveyzdis, A. Wittinghofer, K. Gerwert, The GAP arginine finger movement into the catalytic site of Ras increases the activation entropy, Proc. Natl. Acad. Sci. USA 105(17) (2008) 6260-5.
[67] R. Langen, T. Schweins, A. Warshel, On the mechanism of guanosine triphosphate hydrolysis in ras p21 proteins, Biochemistry 31(37) (1992) 8691-6.
[68] T. Schweins, R. Langen, A. Warshel, Why Have Mutagenesis Studies Not Located the General Base in Ras P21, Nat Struct Biol 1(7) (1994) 476-484.
[69] T. Schweins, M. Geyer, K. Scheffzek, A. Warshel, H.R. Kalbitzer, A. Wittinghofer, Substrate-assisted catalysis as a mechanism for GTP hydrolysis of p21ras and other GTP-binding proteins, Nat Struct Biol 2(1) (1995) 36-44.
[70] K. Braig, R.I. Menz, M.G. Montgomery, A.G. Leslie, J.E. Walker, Structure of bovine mitochondrial F(1)-ATPase inhibited by Mg(2+) ADP and aluminium fluoride, Structure 8(6) (2000) 567-73.
[71] H.M. Berman, J. Westbrook, Z. Feng, G. Gilliland, T.N. Bhat, H. Weissig, I.N. Shindyalov, P.E. Bourne, The Protein Data Bank, Nucleic Acids Res 28(1) (2000) 235-42.
[72] S.K. Burley, C. Bhikadiya, C. Bi, S. Bittrich, L. Chen, G.V. Crichlow, C.H. Christie, K. Dalenberg, L. Di Costanzo, J.M. Duarte, S. Dutta, Z. Feng, S. Ganesan, D.S. Goodsell, S.

Ghosh, R.K. Green, V. Guranovic, D. Guzenko, B.P. Hudson, C.L. Lawson, Y. Liang, R. Lowe, H. Namkoong, E. Peisach, I. Persikova, C. Randle, A. Rose, Y. Rose, A. Sali, J. Segura, M. Sekharan, C. Shao, Y.P. Tao, M. Voigt, J.D. Westbrook, J.Y. Young, C. Zardecki, M. Zhuravleva, RCSB Protein Data Bank: powerful new tools for exploring 3D structures of biological macromolecules for basic and applied research and education in fundamental biology, biomedicine, biotechnology, bioengineering and energy sciences, Nucleic Acids Res 49(D1) (2021) D437-D451.

[73] M.P. Mueller, R.S. Goody, Review: Ras GTPases and myosin: Qualitative conservation and quantitative diversification in signal and energy transduction, Biopolymers 105(8) (2016) 422-30.

[74] J.S. Chappie, S. Acharya, M. Leonard, S.L. Schmid, F. Dyda, G domain dimerization controls dynamin's assembly-stimulated GTPase activity, Nature 465(7297) (2010) 435-40.

[75] R. Mishra, S.K. Gara, S. Mishra, B. Prakash, Analysis of GTPases carrying hydrophobic amino acid substitutions in lieu of the catalytic glutamine: implications for GTP hydrolysis, Proteins 59(2) (2005) 332-8.

[76] O. Fasano, E. De Vendittis, A. Parmeggiani, Hydrolysis of GTP by elongation factor Tu can be induced by monovalent cations in the absence of other effectors, J. Biol. Chem. 257(6) (1982) 3145-50.

[77] C. Maracci, F. Peske, E. Dannies, C. Pohl, M.V. Rodnina, Ribosome-induced tuning of GTP hydrolysis by a translational GTPase, Proc Natl Acad Sci U S A 111(40) (2014) 14418-23.

[78] G. Chinali, A. Parmeggiani, The coupling with polypeptide synthesis of the GTPase activity dependent on elongation factor G, J. Biol. Chem. 255(15) (1980) 7455-9.

[79] R. Ivell, G. Sander, A. Parmeggiani, Modulation by monovalent and divalent cations of the guanosine-5'-triphosphatase activity dependent on elongation factor Tu, Biochemistry 20(24) (1981) 6852-9.

[80] A. Parmeggiani, G. Sander, Properties and regulation of the GTPase activities of elongation factors Tu and G, and of initiation factor 2, Mol Cell Biochem 35(3) (1981) 129-58.

[81] J. Voigt, G. Sander, K. Nagel, A. Parmeggiani, Effect of NH+4 and K+ on the activity of the ribosomal subunits in the EF-G- and EF-T-dependent GTR hydrolysis, Biochem Biophys Res Commun 57(4) (1974) 1279-86.

[82] A.Y. Mulkidjanian, A.Y. Bychkov, D.V. Dibrova, M.Y. Galperin, E.V. Koonin, Origin of first cells at terrestrial, anoxic geothermal fields, Proc. Natl. Acad. Sci. USA 109(14) (2012) E821-30.

[83] B. Kuhle, R. Ficner, A monovalent cation acts as structural and catalytic cofactor in translational GTPases, EMBO J. 33(21) (2014) 2547-2563.

[84] R.M. Voorhees, T.M. Schmeing, A.C. Kelley, V. Ramakrishnan, The mechanism for activation of GTP hydrolysis on the ribosome, Science 330(6005) (2010) 835-838.

[85] L.J. Byrnes, A. Singh, K. Szeto, N.M. Benvin, J.P. O'Donnell, W.R. Zipfel, H. Sondermann, Structural basis for conformational switching and GTP loading of the large G protein atlastin, EMBO J. 32(3) (2013) 369-384.

[86] M. Soundararajan, F.S. Willard, A.J. Kimple, A.P. Turnbull, L.J. Ball, G.A. Schoch, C. Gileadi, O.Y. Fedorov, E.F. Dowler, V.A. Higman, S.Q. Hutsell, M. Sundstrom, D.A. Doyle, D.P. Siderovski, Structural diversity in the RGS domain and its interaction with heterotrimeric G protein alpha-subunits, Proc Natl Acad Sci U S A 105(17) (2008) 6457-62.

[87] N.J. Gay, J.E. Walker, Homology between human bladder carcinoma oncogene product and mitochondrial ATP-synthase, Nature 301(5897) (1983) 262-4.

[88] S.R. Sprang, G proteins, effectors and GAPs: structure and mechanism, Curr Opin Struc Biol 7(6) (1997) 849-856.

[89] A. Wittinghofer, GTP and ATP hydrolysis in biology, Biopolymers 105(8) (2016) 419-21.
[90] K. Scheffzek, M.R. Ahmadian, W. Kabsch, L. Wiesmuller, A. Lautwein, F. Schmitz, A. Wittinghofer, The Ras-RasGAP complex: structural basis for GTPase activation and its loss in oncogenic Ras mutants, Science 277(5324) (1997) 333-8.
[91] A.J. Fisher, C.A. Smith, J.B. Thoden, R. Smith, K. Sutoh, H.M. Holden, I. Rayment, X-ray structures of the myosin motor domain of Dictyostelium discoideum complexed with MgADP.BeFx and MgADP.AlF4, Biochemistry 34(28) (1995) 8960-72.
[92] M.A. Geeves, Review: The ATPase mechanism of myosin and actomyosin, Biopolymers 105(8) (2016) 483-91.
[93] R.A. Cross, Review: Mechanochemistry of the kinesin-1 ATPase, Biopolymers 105(8) (2016) 476-82.
[94] J.P. O'Donnell, L.J. Byrnes, R.B. Cooley, H. Sondermann, A hereditary spastic paraplegia-associated atlastin variant exhibits defective allosteric coupling in the catalytic core, J Biol Chem 293(2) (2018) 687-700.
[95] C.A. Smith, I. Rayment, X-ray structure of the magnesium(II).ADP.vanadate complex of the Dictyostelium discoideum myosin motor domain to 1.9 A resolution, Biochemistry 35(17) (1996) 5404-17.
[96] G. Bange, I. Sinning, SIMIBI twins in protein targeting and localization, Nat. Struct. Mol. Biol. 20(7) (2013) 776-780.
[97] J. Lutkenhaus, The ParA/MinD family puts things in their place, Trends Microbiol 20(9) (2012) 411-418.
[98] S.F. Ataide, N. Schmitz, K. Shen, A. Ke, S.O. Shan, J.A. Doudna, N. Ban, The crystal structure of the signal recognition particle in complex with its receptor, Science 331(6019) (2011) 881-6.
[99] J. Moser, C. Lange, J. Krausze, J. Rebelein, W.D. Schubert, M.W. Ribbe, D.W. Heinz, D. Jahn, Structure of ADP-aluminium fluoride-stabilized protochlorophyllide oxidoreductase complex, Proc Natl Acad Sci U S A 110(6) (2013) 2094-8.
[100] P.J. Focia, J. Gawronski-Salerno, J.S.t. Coon, D.M. Freymann, Structure of a GDP:AlF4 complex of the SRP GTPases Ffh and FtsY, and identification of a peripheral nucleotide interaction site, J Mol Biol 360(3) (2006) 631-43.
[101] N. Ostermann, D. Segura-Pena, C. Meier, T. Veit, C. Monnerjahn, M. Konrad, A. Lavie, Structures of human thymidylate kinase in complex with prodrugs: implications for the structure-based design of novel compounds, Biochemistry 42(9) (2003) 2568-77.
[102] O. Poyraz, K. Brunner, B. Lohkamp, H. Axelsson, L.G. Hammarstrom, R. Schnell, G. Schneider, Crystal structures of the kinase domain of the sulfate-activating complex in Mycobacterium tuberculosis, PLoS One 10(3) (2015) e0121494.
[103] S. Cheek, K. Ginalski, H. Zhang, N.V. Grishin, A comprehensive update of the sequence and structure classification of kinases, Bmc Struct Biol 5 (2005) 6.
[104] C.P. Kenyon, R.L. Roth, C.W. van der Westhuyzen, C.J. Parkinson, Conserved phosphoryl transfer mechanisms within kinase families and the role of the C8 proton of ATP in the activation of phosphoryl transfer, BMC Res Notes 5 (2012) 131.
[105] E.B. Lansdon, I.H. Segel, A.J. Fisher, Ligand-induced structural changes in adenosine 5'-phosphosulfate kinase from Penicillium chrysogenum, Biochemistry 41(46) (2002) 13672-80.
[106] S.J. Kerns, R.V. Agafonov, Y.J. Cho, F. Pontiggia, R. Otten, D.V. Pachov, S. Kutter, L.A. Phung, P.N. Murphy, V. Thai, T. Alber, M.F. Hagan, D. Kern, The energy landscape of adenylate kinase during catalysis, Nat Struct Mol Biol 22(2) (2015) 124-31.
[107] L.M. Iyer, K.S. Makarova, E.V. Koonin, L. Aravind, Comparative genomics of the FtsK-HerA superfamily of pumping ATPases: implications for the origins of chromosome

segregation, cell division and viral capsid packaging, Nucleic Acids Res 32(17) (2004) 5260-79.
[108] L. Aravind, L.M. Iyer, D.D. Leipe, E.V. Koonin, A novel family of P-loop NTPases with an unusual phyletic distribution and transmembrane segments inserted within the NTPase domain, Genome Biol. 5(5) (2004) R30.
[109] A.N. Lupas, J. Martin, AAA proteins, Curr. Opin. Struct. Biol. 12(6) (2002) 746-753.
[110] J.M. Miller, E.J. Enemark, Fundamental Characteristics of AAA+ Protein Family Structure and Function, Archaea 2016 (2016) 9294307.
[111] R.C. Yu, P.I. Hanson, R. Jahn, A.T. Brunger, Structure of the ATP-dependent oligomerization domain of N-ethylmaleimide sensitive factor complexed with ATP, Nat Struct Biol 5(9) (1998) 803-11.
[112] M.R. Singleton, M.S. Dillingham, D.B. Wigley, Structure and mechanism of helicases and nucleic acid translocases, Annu Rev Biochem 76 (2007) 23-50.
[113] T. Sengoku, O. Nureki, A. Nakamura, K.I. Satoru, S. Yokoyama, Structural basis for RNA unwinding by the DEAD-box protein Drosophila vasa, Cell 125(2) (2006) 287-300.
[114] D. Gai, R. Zhao, D. Li, C.V. Finkielstein, X.S. Chen, Mechanisms of conformational change for a replicative hexameric helicase of SV40 large tumor antigen, Cell 119(1) (2004) 47-60.
[115] M. Gu, C.M. Rice, The Spring alpha-Helix Coordinates Multiple Modes of HCV (Hepatitis C Virus) NS3 Helicase Action, J Biol Chem 291(28) (2016) 14499-509.
[116] M.L. Oldham, J. Chen, Snapshots of the maltose transporter during ATP hydrolysis, Proc Natl Acad Sci U S A 108(37) (2011) 15152-6.
[117] M. Dean, A. Rzhetsky, R. Allikmets, The human ATP-binding cassette (ABC) transporter superfamily, Genome Res 11(7) (2001) 1156-66.
[118] D.C. Rees, E. Johnson, O. Lewinson, ABC transporters: the power to change, Nat Rev Mol Cell Biol 10(3) (2009) 218-27.
[119] I.D. Kerr, Sequence analysis of twin ATP binding cassette proteins involved in translational control, antibiotic resistance, and ribonuclease L inhibition, Biochem Biophys Res Commun 315(1) (2004) 166-73.
[120] K.P. Hopfner, Rustless translation, Biol Chem 393(10) (2012) 1079-88.
[121] D.V. Dibrova, K.A. Konovalov, V.V. Perekhvatov, K.V. Skulachev, A.Y. Mulkidjanian, COGcollator: a web server for analysis of distant relationships between homologous protein families, Biol Direct 12(1) (2017) 29.
[122] M.R. Lawson, W. Ma, M.J. Bellecourt, I. Artsimovitch, A. Martin, R. Landick, K. Schulten, J.M. Berger, Mechanism for the Regulated Control of Bacterial Transcription Termination by a Universal Adaptor Protein, Mol Cell 71(6) (2018) 911-922 e4.
[123] S. Marsin, Y. Adam, C. Cargemel, J. Andreani, S. Baconnais, P. Legrand, I. Li de la Sierra-Gallay, A. Humbert, M. Aumont-Nicaise, C. Velours, F. Ochsenbein, D. Durand, E. Le Cam, H. Walbott, C. Possoz, S. Quevillon-Cheruel, J.L. Ferat, Study of the DnaB:DciA interplay reveals insights into the primary mode of loading of the bacterial replicative helicase, Nucleic Acids Res 49(11) (2021) 6569-6586.
[124] J. Abe, T.B. Hiyama, A. Mukaiyama, S. Son, T. Mori, S. Saito, M. Osako, J. Wolanin, E. Yamashita, T. Kondo, S. Akiyama, Circadian rhythms. Atomic-scale origins of slowness in the cyanobacterial circadian clock, Science 349(6245) (2015) 312-6.
[125] Y. Li, Y. He, Y. Luo, Conservation of a conformational switch in RadA recombinase from Methanococcus maripaludis, Acta Crystallogr D Biol Crystallogr 65(Pt 6) (2009) 602-10.
[126] D.V. Dibrova, M.Y. Galperin, E.V. Koonin, A.Y. Mulkidjanian, Ancient systems of sodium/potassium homeostasis as predecessors of membrane bioenergetics, Biochemistry. Biokhimiia 80(5) (2015) 495-516.

[127] A.A. Malaer, N. Wili, L.A. Volker, M.I. Kozlova, R. Cadalbert, A. Dapp, M.E. Weber, J. Zehnder, G. Jeschke, H. Eckert, A. Bockmann, D. Klose, A.Y. Mulkidjanian, B.H. Meier, T. Wiegand, Spectroscopic glimpses of the transition state of ATP hydrolysis trapped in a bacterial DnaB helicase, Nat Commun 12(1) (2021) 5293.
[128] M.R. Singleton, M.R. Sawaya, T. Ellenberger, D.B. Wigley, Crystal structure of T7 gene 4 ring helicase indicates a mechanism for sequential hydrolysis of nucleotides, Cell 101(6) (2000) 589-600.
[129] Z. Chen, H. Yang, N.P. Pavletich, Mechanism of homologous recombination from the RecA-ssDNA/dsDNA structures, Nature 453(7194) (2008) 489-4.
[130] X. Qian, Y. He, Y. Wu, Y. Luo, Asp302 determines potassium dependence of a RadA recombinase from *Methanococcus voltae*, J. Mol. Biol. 360(3) (2006) 537-47.
[131] O. Itsathitphaisarn, R.A. Wing, W.K. Eliason, J. Wang, T.A. Steitz, The hexameric helicase DnaB adopts a nonplanar conformation during translocation, Cell 151(2) (2012) 267-77.
[132] Y. Yamaichi, H. Niki, Active segregation by the Bacillus subtilis partitioning system in Escherichia coli, Proc. Natl. Acad. Sci. USA 97(26) (2000) 14656-61.
[133] S.C. Kamerlin, P.K. Sharma, R.B. Prasad, A. Warshel, Why nature really chose phosphate, Q. Rev. Biophys. 46(1) (2013) 1-132.
[134] M. Fothergill, M.F. Goodman, J. Petrushka, A. Warshel, Structure-energy analysis of the role of metal ions in phosphodiester bond hydrolysis by DNA polymerase I, J Amer Chem Society 117 (1995) 11619-11627.
[135] J.F. Da Silva, R.J.P. Williams, The biological chemistry of the elements: the inorganic chemistry of life, Oxford University Press2001.
[136] D. Berta, P.J. Buigues, M. Badaoui, E. Rosta, Cations in motion: QM/MM studies of the dynamic and electrostatic roles of H(+) and Mg(2+) ions in enzyme reactions, Curr Opin Struct Biol 61 (2020) 198-206.
[137] T.P. Silverstein, How enzymes harness highly unfavorable proton transfer reactions, Protein Sci 30(4) (2021) 735-744.
[138] D.E. Scott, M.T. Ehebauer, T. Pukala, M. Marsh, T.L. Blundell, A.R. Venkitaraman, C. Abell, M. Hyvonen, Using a fragment-based approach to target protein-protein interactions, Chembiochem 14(3) (2013) 332-42.
[139] C.B. Bauer, H.M. Holden, J.B. Thoden, R. Smith, I. Rayment, X-ray structures of the apo and MgATP-bound states of Dictyostelium discoideum myosin motor domain, J Biol Chem 275(49) (2000) 38494-9.
[140] S. Matsumoto, N. Miyano, S. Baba, J. Liao, T. Kawamura, C. Tsuda, A. Takeda, M. Yamamoto, T. Kumasaka, T. Kataoka, F. Shima, Molecular Mechanism for Conformational Dynamics of Ras.GTP Elucidated from In-Situ Structural Transition in Crystal, Sci Rep 6 (2016) 25931.
[141] Y. Li, Y. Zhang, F. Grosseruschkamp, S. Stephan, Q. Cui, C. Kotting, F. Xia, K. Gerwert, Specific Substates of Ras To Interact with GAPs and Effectors: Revealed by Theoretical Simulations and FTIR Experiments, J Phys Chem Lett 9(6) (2018) 1312-1317.
[142] J.S. Johansen, D. Kavaliauskas, S.H. Pfeil, M. Blaise, B.S. Cooperman, Y.E. Goldman, S.S. Thirup, C.R. Knudsen, E. coli elongation factor Tu bound to a GTP analogue displays an open conformation equivalent to the GDP-bound form, Nucleic Acids Res 46(16) (2018) 8641-8650.
[143] S. Zhou, L. Wang, Unraveling the structural and chemical features of biological short hydrogen bonds, Chem Sci 10(33) (2019) 7734-7745.
[144] K. Rittinger, P.A. Walker, J.F. Eccleston, S.J. Smerdon, S.J. Gamblin, Structure at 1.65 A of RhoA and its GTPase-activating protein in complex with a transition-state analogue, Nature 389(6652) (1997) 758-62.

[145] X. Yang, C. Chen, H. Tian, H. Chi, Z. Mu, T. Zhang, K. Yang, Q. Zhao, X. Liu, Z. Wang, X. Ji, H. Yang, Mechanism of ATP hydrolysis by the Zika virus helicase, Faseb J 32(10) (2018) 5250-5257.
[146] A.Y. Mulkidjanian, M.Y. Galperin, K.S. Makarova, Y.I. Wolf, E.V. Koonin, Evolutionary primacy of sodium bioenergetics, Biol. Direct 3 (2008) 13.
[147] D.V. Dibrova, D.A. Cherepanov, M.Y. Galperin, V.P. Skulachev, A.Y. Mulkidjanian, Evolution of cytochrome *bc* complexes: from membrane-anchored dehydrogenases of ancient bacteria to triggers of apoptosis in vertebrates, Biochim. Biophys. Acta 1827(11-12) (2013) 1407-27.
[148] D.V. Dibrova, D.N. Shalaeva, M.Y. Galperin, A.Y. Mulkidjanian, Emergence of cytochrome bc complexes in the context of photosynthesis, Physiol Plant 161(1) (2017) 150-170.
[149] D.N. Shalaeva, D.A. Cherepanov, M.Y. Galperin, G. Vriend, A.Y. Mulkidjanian, G protein-coupled receptors of class A harness the energy of membrane potential to increase their sensitivity and selectivity, Biochim Biophys Acta Biomembr 1861(12) (2019) 183051.
[150] D.N. Shalaeva, M.Y. Galperin, A.Y. Mulkidjanian, Eukaryotic G protein-coupled receptors as descendants of prokaryotic sodium-translocating rhodopsins, Biol Direct 10 (2015).
[151] N.J. Baxter, G.M. Blackburn, J.P. Marston, A.M. Hounslow, M.J. Cliff, W. Bermel, N.H. Williams, F. Hollfelder, D.E. Wemmer, J.P. Waltho, Anionic charge is prioritized over geometry in aluminum and magnesium fluoride transition state analogs of phosphoryl transfer enzymes, J Am Chem Soc 130(12) (2008) 3952-8.
[152] N. Zhang, M. Buck, Formation of MgF3 (-)-dependent complexes between an AAA(+) ATPase and sigma(54.), FEBS Open Bio 2 (2012) 89-92.
[153] M. Chaney, R. Grande, S.R. Wigneshweraraj, W. Cannon, P. Casaz, M.T. Gallegos, J. Schumacher, S. Jones, S. Elderkin, A.E. Dago, E. Morett, M. Buck, Binding of transcriptional activators to sigma 54 in the presence of the transition state analog ADP-aluminum fluoride: insights into activator mechanochemical action, Genes Dev 15(17) (2001) 2282-94.
[154] T. Higashijima, K.M. Ferguson, P.C. Sternweis, E.M. Ross, M.D. Smigel, A.G. Gilman, The effect of activating ligands on the intrinsic fluorescence of guanine nucleotide-binding regulatory proteins, J Biol Chem 262(2) (1987) 752-6.
[155] I. Schlichting, J. Reinstein, pH influences fluoride coordination number of the AlFx phosphoryl transfer transition state analog, Nat Struct Biol 6(8) (1999) 721-3.
[156] L. Gremer, B. Gilsbach, M.R. Ahmadian, A. Wittinghofer, Fluoride complexes of oncogenic Ras mutants to study the Ras-RasGap interaction, Biol. Chem. 389(9) (2008) 1163-71.
[157] M. Chabre, Aluminofluoride and beryllofluoride complexes: new phosphate analogs in enzymology, Trends in biochemical sciences 15(1) (1990) 6-10.
[158] B. Antonny, J. Bigay, M. Chabre, A novel magnesium-dependent mechanism for the activation of transducin by fluoride, FEBS Lett 268(1) (1990) 277-80.
[159] D.L. Graham, J.F. Eccleston, C.W. Chung, P.N. Lowe, Magnesium fluoride-dependent binding of small G proteins to their GTPase-activating proteins, Biochemistry 38(45) (1999) 14981-7.
[160] B. Antonny, M. Sukumar, J. Bigay, M. Chabre, T. Higashijima, The mechanism of aluminum-independent G-protein activation by fluoride and magnesium. 31P NMR spectroscopy and fluorescence kinetic studies, J Biol Chem 268(4) (1993) 2393-402.
[161] R. Mittal, M.R. Ahmadian, R.S. Goody, A. Wittinghofer, Formation of a transition-state analog of the Ras GTPase reaction by Ras-GDP, tetrafluoroaluminate, and GTPase-activating proteins, Science 273(5271) (1996) 115-7.

[162] P.P. Chakrabarti, O. Daumke, Y. Suveyzdis, C. Kotting, K. Gerwert, A. Wittinghofer, Insight into catalysis of a unique GTPase reaction by a combined biochemical and FTIR approach, J Mol Biol 367(4) (2007) 983-95.
[163] D.N. Shalaeva, D.A. Cherepanov, M.Y. Galperin, A.Y. Mulkidjanian, Comparative analysis of active sites in P-loop nucleoside triphosphatases suggests an ancestral activation mechanism, BioRxiv 439992 [preprint] (2018).
[164] W.P. Jencks, Catalysis in chemistry and enzymology, Courier Corporation1987.
[165] L.T. Delbaere, A.M. Sudom, L. Prasad, Y. Leduc, H. Goldie, Structure/function studies of phosphoryl transfer by phosphoenolpyruvate carboxykinase, Biochim. Biophys. Acta 1697(1-2) (2004) 271-8.
[166] J.J. Frye, V.A. Klenchin, C.R. Bagshaw, I. Rayment, Insights into the importance of hydrogen bonding in the gamma-phosphate binding pocket of myosin: structural and functional studies of serine 236, Biochemistry 49(23) (2010) 4897-907.
[167] A. Shutes, C.J. Der, Real-time in vitro measurement of intrinsic and Ras GAP-mediated GTP hydrolysis, Methods Enzymol 407 (2006) 9-22.
[168] D.A. Hattendorf, S.L. Lindquist, Analysis of the AAA sensor-2 motif in the C-terminal ATPase domain of Hsp104 with a site-specific fluorescent probe of nucleotide binding, Proc. Natl. Acad. Sci. USA 99(5) (2002) 2732-7.
[169] J.E. Walker, The regulation of catalysis in ATP synthase, Curr Opin Struct Biol 4(6) (1994) 912-8.
[170] A.E. Senior, S. Nadanaciva, J. Weber, The molecular mechanism of ATP synthesis by F_1F_0-ATP synthase, Biochim. Biophys. Acta 1553(3) (2002) 188-211.
[171] P.D. Boyer, The ATP synthase--a splendid molecular machine, Annu. Rev. Biochem. 66 (1997) 717-49.
[172] P. Gideon, J. John, M. Frech, A. Lautwein, R. Clark, J.E. Scheffler, A. Wittinghofer, Mutational and kinetic analyses of the GTPase-activating protein (GAP)-p21 interaction: The C-terminal domain of GAP is not sufficient for full activity, Mol. Cell Biol. 12(5) (1992) 2050-6.
[173] J. Codina, L. Birnbaumer, Requirement for intramolecular domain interaction in activation of G protein alpha subunit by aluminum fluoride and GDP but not by GTP gamma S, J. Biol. Chem. 269(47) (1994) 29339-42.
[174] J. Cherfils, M. Zeghouf, Regulation of small GTPases by GEFs, GAPs, and GDIs, Physiol. Rev. 93(1) (2013) 269-309.
[175] S. Majumdar, A. Acharya, B. Prakash, Structural plasticity mediates distinct GAP-dependent GTP hydrolysis mechanisms in Rab33 and Rab5, Febs J 284(24) (2017) 4358-4375.
[176] N. Nassar, G.R. Hoffman, D. Manor, J.C. Clardy, R.A. Cerione, Structures of Cdc42 bound to the active and catalytically compromised forms of Cdc42GAP, Nat Struct Biol 5(12) (1998) 1047-52.
[177] M. Klahn, E. Rosta, A. Warshel, On the mechanism of hydrolysis of phosphate monoesters dianions in solutions and proteins, J Am Chem Soc 128(47) (2006) 15310-23.
[178] N.H. Williams, Magnesium ion catalyzed ATP hydrolysis, JACS 122(48) (2000) 12023-12024.
[179] G. Li, X.C. Zhang, GTP hydrolysis mechanism of Ras-like GTPases, J. Mol. Biol. 340(5) (2004) 921-32.
[180] T. Rudack, F. Xia, J. Schlitter, C. Kotting, K. Gerwert, The role of magnesium for geometry and charge in GTP hydrolysis, revealed by quantum mechanics/molecular mechanics simulations, Biophys J 103(2) (2012) 293-302.
[181] J.C. Liao, S. Sun, D. Chandler, G. Oster, The conformational states of Mg.ATP in water, Eur Biophys J 33(1) (2004) 29-37.

[182] J.F. Cannon, AMBER force-field parameters for guanosine triphosphate and its imido and methylene analogs, LJ Comput Chem 14 (1993) 995-1005.
[183] T. Rudack, F. Xia, J. Schlitter, C. Kotting, K. Gerwert, Ras and GTPase-activating protein (GAP) drive GTP into a precatalytic state as revealed by combining FTIR and biomolecular simulations, Proc. Natl. Acad. Sci. USA 109(38) (2012) 15295-300.
[184] H. Cheng, S. Sukal, H. Deng, T.S. Leyh, R. Callender, Vibrational structure of GDP and GTP bound to RAS: an isotope-edited FTIR study, Biochemistry 40(13) (2001) 4035-43.
[185] A. Finkelstein, B. Ptitsyn, Protein Physics, Academic Press2016.
[186] D. delToro, D. Ortiz, M. Ordyan, J. Pajak, J. Sippy, A. Catala, C.S. Oh, A. Vu, G. Arya, D.E. Smith, C.E. Catalano, M. Feiss, Functional Dissection of a Viral DNA Packaging Machine's Walker B Motif, J Mol Biol 431(22) (2019) 4455-4474.
[187] B. Garcia-Moreno, J.J. Dwyer, A.G. Gittis, E.E. Lattman, D.S. Spencer, W.E. Stites, Experimental measurement of the effective dielectric in the hydrophobic core of a protein, Biophys Chem 64(1-3) (1997) 211-24.
[188] P. Kukic, D. Farrell, L.P. McIntosh, E.B. Garcia-Moreno, K.S. Jensen, Z. Toleikis, K. Teilum, J.E. Nielsen, Protein dielectric constants determined from NMR chemical shift perturbations, J Am Chem Soc 135(45) (2013) 16968-76.
[189] S.D. Fried, S. Bagchi, S.G. Boxer, Extreme electric fields power catalysis in the active site of ketosteroid isomerase, Science 346(6216) (2014) 1510-4.
[190] F. Voigts-Hoffmann, N. Schmitz, K. Shen, S.O. Shan, S.F. Ataide, N. Ban, The structural basis of FtsY recruitment and GTPase activation by SRP RNA, Mol Cell 52(5) (2013) 643-54.
[191] Y. Dong, S. Zhang, Z. Wu, X. Li, W.L. Wang, Y. Zhu, S. Stoilova-McPhie, Y. Lu, D. Finley, Y. Mao, Cryo-EM structures and dynamics of substrate-engaged human 26S proteasome, Nature 565(7737) (2019) 49-55.
[192] K.Y. Lu, W.F. Chen, S. Rety, N.N. Liu, W.Q. Wu, Y.X. Dai, D. Li, H.Y. Ma, S.X. Dou, X.G. Xi, Insights into the structural and mechanistic basis of multifunctional S. cerevisiae Pif1p helicase, Nucleic Acids Res 46(3) (2018) 1486-1500.
[193] T. Schweins, A. Warshel, Mechanistic analysis of the observed linear free energy relationships in p21ras and related systems, Biochemistry 35(45) (1996) 14232-43.
[194] C. Allin, M.R. Ahmadian, A. Wittinghofer, K. Gerwert, Monitoring the GAP catalyzed H-Ras GTPase reaction at atomic resolution in real time, Proc Natl Acad Sci U S A 98(14) (2001) 7754-9.
[195] M. Valiev, R. Kawai, J.A. Adams, J.H. Weare, The role of the putative catalytic base in the phosphoryl transfer reaction in a protein kinase: first-principles calculations, J Am Chem Soc 125(33) (2003) 9926-7.
[196] M. Valiev, J. Yang, J.A. Adams, S.S. Taylor, J.H. Weare, Phosphorylation reaction in cAPK protein kinase-free energy quantum mechanical/molecular mechanics simulations, J Phys Chem B 111(47) (2007) 13455-64.
[197] H. Cheng, S. Sukal, R. Callender, T.S. Leyh, Gamma-phosphate protonation and pH-dependent unfolding of the Ras.GTP.Mg2+ complex: a vibrational spectroscopy study, J Biol Chem 276(13) (2001) 9931-5.
[198] D. Mann, J. Guldenhaupt, J. Schartner, K. Gerwert, C. Kotting, The protonation states of GTP and GppNHp in Ras proteins, J Biol Chem 293(11) (2018) 3871-3879.
[199] M. Eigen, W. Kruse, Über den Einfluß von Wasserstoffbrücken-Struktur und elektrostatischer Wechselwirkung auf die Geschwindigkeit protolytischer Reaktionen, Z. Naturforsch. B. 18b (1963) 857-865.
[200] M. Eigen, Proton transfer, acid-base catalysis, and enzymatic hydrolysis. Part I: elementary processes, Angewandte Chemie International Edition in English 3(1) (1964) 1-19.

[201] R.W. Molt, Jr., E. Pellegrini, Y. Jin, A GAP-GTPase-GDP-Pi Intermediate Crystal Structure Analyzed by DFT Shows GTP Hydrolysis Involves Serial Proton Transfers, Chemistry 25(36) (2019) 8484-8488.
[202] D.N. Frick, R.S. Rypma, A.M. Lam, C.M. Frenz, Electrostatic analysis of the hepatitis C virus NS3 helicase reveals both active and allosteric site locations, Nucleic Acids Res 32(18) (2004) 5519-28.
[203] D.N. Frick, The hepatitis C virus NS3 protein: a model RNA helicase and potential drug target, Curr Issues Mol Biol 9(1) (2007) 1-20.
[204] E.G. Alexov, M.R. Gunner, Incorporating protein conformational flexibility into the calculation of pH-dependent protein properties, Biophys J 72(5) (1997) 2075-93.
[205] M. Gu, C.M. Rice, Three conformational snapshots of the hepatitis C virus NS3 helicase reveal a ratchet translocation mechanism, Proc Natl Acad Sci U S A 107(2) (2010) 521-8.
[206] D.D. Leipe, L. Aravind, N.V. Grishin, E.V. Koonin, The bacterial replicative helicase DnaB evolved from a RecA duplication, Genome Res 10(1) (2000) 5-16.
[207] G. Zundel, Proton polarizability of hydrogen bonds: infrared methods, relevance to electrochemical and biological systems, Methods Enzymol 127 (1986) 439-55.
[208] B. Brzezinski, G. Zuńdel, The role of water and proton-transfer processes in hydrogen-bonded chains with large proton polarizability, Faraday Discussions 103 (1996) 363-370.
[209] A.D. Kaulen, Electrogenic processes and protein conformational changes accompanying the bacteriorhodopsin photocycle, Biochim Biophys Acta 1460(1) (2000) 204-19.
[210] J. Heberle, Proton transfer reactions across bacteriorhodopsin and along the membrane, Biochim Biophys Acta 1458(1) (2000) 135-47.
[211] T.E. Decoursey, Voltage-gated proton channels and other proton transfer pathways, Physiol Rev 83(2) (2003) 475-579.
[212] C.A. Wraight, Chance and design--proton transfer in water, channels and bioenergetic proteins, Biochim Biophys Acta 1757(8) (2006) 886-912.
[213] A.Y. Mulkidjanian, Proton in the well and through the desolvation barrier, Biochim Biophys Acta 1757(5-6) (2006) 415-27.
[214] A.Y. Mulkidjanian, J. Heberle, D.A. Cherepanov, Protons @ interfaces: implications for biological energy conversion, Biochim. Biophys. Acta 1757(8) (2006) 913-30.
[215] V.A. Lorenz-Fonfria, J. Heberle, Proton transfer and protein conformation dynamics in photosensitive proteins by time-resolved step-scan Fourier-transform infrared spectroscopy, J Vis Exp (88) (2014) e51622.
[216] D. Kaur, U. Khaniya, Y. Zhang, M.R. Gunner, Protein Motifs for Proton Transfers That Build the Transmembrane Proton Gradient, Front Chem 9 (2021) 660954.
[217] D. Pines, E.T.J. Nibbering, E. Pines, Monitoring the Microscopic Molecular Mechanisms of Proton Transfer in Acid-base Reactions in Aqueous Solutions, Israel Journal of Chemistry 55(11-12) (2015) 1240-1251.
[218] V. Borshchevskiy, K. Kovalev, E. Round, R. Efremov, R. Astashkin, G. Bourenkov, D. Bratanov, T. Balandin, I. Chizhov, C. Baeken, I. Gushchin, A. Kuzmin, A. Alekseev, A. Rogachev, D. Willbold, M. Engelhard, E. Bamberg, G. Buldt, V. Gordeliy, True-atomic-resolution insights into the structure and functional role of linear chains and low-barrier hydrogen bonds in proteins, Nat Struct Mol Biol 29(5) (2022) 440-450.
[219] L.S. Brown, Light-driven proton transfers and proton transport by microbial rhodopsins - A biophysical perspective, Biochim Biophys Acta Biomembr 1864(5) (2022) 183867.
[220] C.J.T. de Grotthuss, Mémoire sur la décomposition de l'eau et des corps qu'elle tient en dissolution à l'aide de l'électricité galvanique, Rome, 1805.
[221] D. Marx, Proton transfer 200 years after von Grotthuss: insights from ab initio simulations, Chemphyschem 7(9) (2006) 1848-70.

[222] M. Ceriotti, J. Cuny, M. Parrinello, D.E. Manolopoulos, Nuclear quantum effects and hydrogen bond fluctuations in water, Proc Natl Acad Sci USA 110(39) (2013) 15591-6.
[223] D. Kaur, Y. Zhang, K.M. Reiss, M. Mandal, G.W. Brudvig, V.S. Batista, M.R. Gunner, Proton exit pathways surrounding the oxygen evolving complex of photosystem II, Biochim Biophys Acta Bioenerg 1862(8) (2021) 148446.
[224] C. Nadolny, G. Zundel, Fourier transform infrared spectroscopic studies of proton transfer processes and the dissociation of Zn2+-bound water in alcohol dehydrogenases, Eur J Biochem 247(3) (1997) 914-9.
[225] H.L. Axelrod, E.C. Abresch, M.L. Paddock, M.Y. Okamura, G. Feher, Determination of the binding sites of the proton transfer inhibitors Cd2+ and Zn2+ in bacterial reaction centers, Proc Natl Acad Sci U S A 97(4) (2000) 1542-7.
[226] M.H. Stowell, T.M. McPhillips, D.C. Rees, S.M. Soltis, E. Abresch, G. Feher, Light-induced structural changes in photosynthetic reaction center: implications for mechanism of electron-proton transfer, Science 276(5313) (1997) 812-6.
[227] P. Mitchell, Epilogue: from energetic abstraction to biochemical mechanism, Symp. Soc. Gen. Microbiol, 1977, pp. 383-423.
[228] M.L. Paddock, S.H. Rongey, G. Feher, M.Y. Okamura, Pathway of proton transfer in bacterial reaction centers: replacement of glutamic acid 212 in the L subunit by glutamine inhibits quinone (secondary acceptor) turnover, Proc Natl Acad Sci U S A 86(17) (1989) 6602-6.
[229] L. Drachev, M. Mamedov, A.Y. Mulkidjanian, A.Y. Semenov, V. Shinkarev, M. Verkhovsky, Electrogenesis associated with proton transfer in the reaction center protein of the purple bacterium Rhodobacter sphaeroides, FEBS Lett 259(2) (1990) 324-326.
[230] R. Hienerwadel, S. Grzybek, C. Fogel, W. Kreutz, M.Y. Okamura, M.L. Paddock, J. Breton, E. Nabedryk, W. Mantele, Protonation of Glu L212 following QB- formation in the photosynthetic reaction center of Rhodobacter sphaeroides: evidence from time-resolved infrared spectroscopy, Biochemistry 34(9) (1995) 2832-43.
[231] E. Nabedryk, J. Breton, R. Hienerwadel, C. Fogel, W. Mantele, M.L. Paddock, M.Y. Okamura, Fourier transforms infrared difference spectroscopy of secondary quinone acceptor photoreduction in proton transfer mutants of Rhodobacter sphaeroides, Biochemistry 34(45) (1995) 14722-32.
[232] A.Y. Mulkidjanian, Conformationally controlled pK-switching in membrane proteins: one more mechanism specific to the enzyme catalysis?, FEBS Lett 463(3) (1999) 199-204.
[233] M.L. Paddock, P.H. McPherson, G. Feher, M.Y. Okamura, Pathway of proton transfer in bacterial reaction centers: replacement of serine-L223 by alanine inhibits electron and proton transfers associated with reduction of quinone to dihydroquinone, Proc Natl Acad Sci U S A 87(17) (1990) 6803-7.
[234] M.L. Paddock, S.H. Rongey, P.H. McPherson, A. Juth, G. Feher, M.Y. Okamura, Pathway of proton transfer in bacterial reaction centers: role of aspartate-L213 in proton transfers associated with reduction of quinoneto dihydroquinone, Biochemistry 33(3) (1994) 734-45.
[235] M.L. Paddock, G. Feher, M.Y. Okamura, Proton transfer pathways and mechanism in bacterial reaction centers, FEBS Lett 555(1) (2003) 45-50.
[236] D.A. Cherepanov, S.I. Bibikov, M.V. Bibikova, D.A. Bloch, L.A. Drachev, O.A. Gopta, D. Oesterhelt, A.Y. Semenov, A.Y. Mulkidjanian, Reduction and protonation of the secondary quinone acceptor of Rhodobacter sphaeroides photosynthetic reaction center: kinetic model based on a comparison of wild-type chromatophores with mutants carrying Arg-->Ile substitution at sites 207 and 217 in the L-subunit, Biochim Biophys Acta 1459(1) (2000) 10-34.

[237] A.Y. Mulkidjanian, M.A. Kozlova, D.A. Cherepanov, Ubiquinone reduction in the photosynthetic reaction centre of Rhodobacter sphaeroides: interplay between electron transfer, proton binding and flips of the quinone ring, Biochem Soc Trans 33(Pt 4) (2005) 845-50.
[238] J.P. Klare, E. Bordignon, M. Engelhard, H.J. Steinhoff, Sensory rhodopsin II and bacteriorhodopsin: light activated helix F movement, Photochem Photobiol Sci 3(6) (2004) 543-7.
[239] J.K. Lanyi, Proton transfers in the bacteriorhodopsin photocycle, Biochimica et Biophysica Acta (BBA)-Bioenergetics 1757(8) (2006) 1012-1018.
[240] P. Nogly, T. Weinert, D. James, S. Carbajo, D. Ozerov, A. Furrer, D. Gashi, V. Borin, P. Skopintsev, K. Jaeger, K. Nass, P. Bath, R. Bosman, J. Koglin, M. Seaberg, T. Lane, D. Kekilli, S. Brunle, T. Tanaka, W. Wu, C. Milne, T. White, A. Barty, U. Weierstall, V. Panneels, E. Nango, S. Iwata, M. Hunter, I. Schapiro, G. Schertler, R. Neutze, J. Standfuss, Retinal isomerization in bacteriorhodopsin captured by a femtosecond x-ray laser, Science 361(6398) (2018).
[241] B. Schobert, L.S. Brown, J.K. Lanyi, Crystallographic structures of the M and N intermediates of bacteriorhodopsin: assembly of a hydrogen-bonded chain of water molecules between Asp-96 and the retinal Schiff base, J Mol Biol 330(3) (2003) 553-70.
[242] T. Marti, H. Otto, T. Mogi, S.J. Rosselet, M.P. Heyn, H.G. Khorana, Bacteriorhodopsin mutants containing single substitutions of serine or threonine residues are all active in proton translocation, J Biol Chem 266(11) (1991) 6919-27.
[243] H.J. Steinhoff, R. Mollaaghababa, C. Altenbach, K. Hideg, M. Krebs, H.G. Khorana, W.L. Hubbell, Time-resolved detection of structural changes during the photocycle of spin-labeled bacteriorhodopsin, Science 266(5182) (1994) 105-7.
[244] H. Luecke, B. Schobert, J.P. Cartailler, H.T. Richter, A. Rosengarth, R. Needleman, J.K. Lanyi, Coupling photoisomerization of retinal to directional transport in bacteriorhodopsin, J Mol Biol 300(5) (2000) 1237-55.
[245] T. Rink, M. Pfeiffer, D. Oesterhelt, K. Gerwert, H.J. Steinhoff, Unraveling photoexcited conformational changes of bacteriorhodopsin by time resolved electron paramagnetic resonance spectroscopy, Biophys J 78(3) (2000) 1519-30.
[246] J. Heberle, J. Fitter, H.J. Sass, G. Buldt, Bacteriorhodopsin: the functional details of a molecular machine are being resolved, Biophys Chem 85(2-3) (2000) 229-48.
[247] M. Lazaratos, M. Siemers, L.S. Brown, A.N. Bondar, Conserved hydrogen-bond motifs of membrane transporters and receptors, Biochim Biophys Acta Biomembr 1864(6) (2022) 183896.
[248] C. Zscherp, R. Schlesinger, J. Tittor, D. Oesterhelt, J. Heberle, In situ determination of transient pKa changes of internal amino acids of bacteriorhodopsin by using time-resolved attenuated total reflection Fourier-transform infrared spectroscopy, Proceedings of the National Academy of Sciences 96(10) (1999) 5498-5503.
[249] Y. Cao, G. Varo, A.L. Klinger, D.M. Czajkowsky, M.S. Braiman, R. Needleman, J.K. Lanyi, Proton transfer from Asp-96 to the bacteriorhodopsin Schiff base is caused by a decrease of the pKa of Asp-96 which follows a protein backbone conformational change, Biochemistry 32(8) (1993) 1981-1990.
[250] L.A. Drachev, A.D. Kaulen, L.V. Khitrina, V.P. Skulachev, Fast stages of photoelectric processes in biological membranes. I. Bacteriorhodopsin, Eur J Biochem 117(3) (1981) 461-70.
[251] L. Drachev, A. Kaulen, V. Skulachev, Correlation of photochemical cycle, H+ release and uptake, and electric events in bacteriorhodopsin, FEBS Lett 178(2) (1984) 331-335.
[252] P. Brzezinski, M.L. Paddock, M.Y. Okamura, G. Feher, Light-induced electrogenic events associated with proton uptake upon forming QB- in bacterial wild-type and mutant reaction centers, Biochim Biophys Acta 1321(2) (1997) 149-56.

[253] L. Drachev, B. Kaurov, M. Mamedov, A.Y. Mulkidjanian, A.Y. Semenov, V. Shinkarev, V. Skulachev, M. Verkhovsky, Flash-induced electrogenic events in the photosynthetic reaction center and bc1 complexes of Rhodobacter sphaeroides chromatophores, Biochimica et Biophysica Acta (BBA)-Bioenergetics 973(2) (1989) 189-197.
[254] M.A. Kozlova, H.D. Juhnke, D.A. Cherepanov, C.R. Lancaster, A.Y. Mulkidjanian, Proton transfer in the photosynthetic reaction center of Blastochloris viridis, FEBS Lett 582(2) (2008) 238-42.
[255] M. Engelhard, K. Gerwert, B. Hess, W. Kreutz, F. Siebert, Light-driven protonation changes of internal aspartic acids of bacteriorhodopsin: an investigation by static and time-resolved infrared difference spectroscopy using [4-13C]aspartic acid labeled purple membrane, Biochemistry 24(2) (1985) 400-7.
[256] O.A. Gopta, D.A. Cherepanov, W. Junge, A.Y. Mulkidjanian, Proton transfer from the bulk to the bound ubiquinone Q(B) of the reaction center in chromatophores of Rhodobacter sphaeroides: retarded conveyance by neutral water, Proc Natl Acad Sci U S A 96(23) (1999) 13159-64.
[257] A.A. Wegener, I. Chizhov, M. Engelhard, H.J. Steinhoff, Time-resolved detection of transient movement of helix F in spin-labelled pharaonis sensory rhodopsin II, J Mol Biol 301(4) (2000) 881-91.
[258] A. Warshel, S.T. Russell, Calculations of electrostatic interactions in biological systems and in solutions, Q Rev Biophys 17(3) (1984) 283-422.
[259] M.E. Bozdaganyan, A.V. Lokhmatikov, N. Voskoboynikova, D.A. Cherepanov, H.J. Steinhoff, K.V. Shaitan, A.Y. Mulkidjanian, Proton leakage across lipid bilayers: Oxygen atoms of phospholipid ester linkers align water molecules into transmembrane water wires, Biochim Biophys Acta Bioenerg 1860(6) (2019) 439-451.
[260] T.K. Harris, G.J. Turner, Structural basis of perturbed pKa values of catalytic groups in enzyme active sites, IUBMB Life 53(2) (2002) 85-98.
[261] D. Herschlag, M.M. Pinney, Hydrogen Bonds: Simple after All?, Biochemistry 57(24) (2018) 3338-3352.
[262] P.A. Sigala, E.A. Ruben, C.W. Liu, P.M. Piccoli, E.G. Hohenstein, T.J. Martinez, A.J. Schultz, D. Herschlag, Determination of Hydrogen Bond Structure in Water versus Aprotic Environments To Test the Relationship Between Length and Stability, J Am Chem Soc 137(17) (2015) 5730-40.
[263] B. Koeppe, P.M. Tolstoy, H.H. Limbach, Reaction pathways of proton transfer in hydrogen-bonded phenol-carboxylate complexes explored by combined UV-vis and NMR spectroscopy, J Am Chem Soc 133(20) (2011) 7897-908.
[264] B. Koeppe, J. Guo, P.M. Tolstoy, G.S. Denisov, H.H. Limbach, Solvent and H/D isotope effects on the proton transfer pathways in heteroconjugated hydrogen-bonded phenol-carboxylic acid anions observed by combined UV-vis and NMR spectroscopy, J Am Chem Soc 135(20) (2013) 7553-66.
[265] S. Pylaeva, C. Allolio, B. Koeppe, G.S. Denisov, H.H. Limbach, D. Sebastiani, P.M. Tolstoy, Proton transfer in a short hydrogen bond caused by solvation shell fluctuations: an ab initio MD and NMR/UV study of an (OHO)(-) bonded system, Phys Chem Chem Phys 17(6) (2015) 4634-44.
[266] A. Fersht, Enzyme structure and mechanism, 1985.
[267] V.N. Uversky, The intrinsic disorder alphabet. III. Dual personality of serine, Intrinsically Disord Proteins 3(1) (2015) e1027032.
[268] A.E. Senior, M.K. al-Shawi, Further examination of seventeen mutations in Escherichia coli F1-ATPase beta-subunit, J Biol Chem 267(30) (1992) 21471-8.

[269] J.P. van der Wolk, M. Klose, J.G. de Wit, T. den Blaauwen, R. Freudl, A.J. Driessen, Identification of the magnesium-binding domain of the high-affinity ATP-binding site of the Bacillus subtilis and Escherichia coli SecA protein, J Biol Chem 270(32) (1995) 18975-82.
[270] S. Lobau, J. Weber, S. Wilke-Mounts, A.E. Senior, F1-ATPase, roles of three catalytic site residues, J Biol Chem 272(6) (1997) 3648-56.
[271] A. Frelet, M. Klein, Insight in eukaryotic ABC transporter function by mutation analysis, FEBS Lett 580(4) (2006) 1064-84.
[272] J. John, H. Rensland, I. Schlichting, I. Vetter, G.D. Borasio, R.S. Goody, A. Wittinghofer, Kinetic and structural analysis of the Mg(2+)-binding site of the guanine nucleotide-binding protein p21H-ras, J Biol Chem 268(2) (1993) 923-9.
[273] D.N. Frick, S. Banik, R.S. Rypma, Role of divalent metal cations in ATP hydrolysis catalyzed by the hepatitis C virus NS3 helicase: magnesium provides a bridge for ATP to fuel unwinding, J Mol Biol 365(4) (2007) 1017-32.
[274] T. Yamashita, H. Unno, Y. Mori, H. Tani, K. Moriishi, A. Takamizawa, M. Agoh, T. Tsukihara, Y. Matsuura, Crystal structure of the catalytic domain of Japanese encephalitis virus NS3 helicase/nucleoside triphosphatase at a resolution of 1.8 A, Virology 373(2) (2008) 426-36.
[275] R. Yang, R. Scavetta, X.B. Chang, Interaction between the bound Mg.ATP and the Walker A serine residue in NBD2 of multidrug resistance-associated protein MRP1 plays a crucial role for the ATP-dependent leukotriene C4 transport, Biochemistry 47(32) (2008) 8456-64.
[276] S. Dehghani-Tafti, V. Levdikov, A.A. Antson, B. Bax, C.M. Sanders, Structural and functional analysis of the nucleotide and DNA binding activities of the human PIF1 helicase, Nucleic Acids Res 47(6) (2019) 3208-3222.
[277] Y.X. Dai, W.F. Chen, N.N. Liu, F.Y. Teng, H.L. Guo, X.M. Hou, S.X. Dou, S. Rety, X.G. Xi, Structural and functional studies of SF1B Pif1 from Thermus oshimai reveal dimerization-induced helicase inhibition, Nucleic Acids Res 49(7) (2021) 4129-4143.
[278] P.D. Coureux, H.L. Sweeney, A. Houdusse, Three myosin V structures delineate essential features of chemo-mechanical transduction, EMBO J 23(23) (2004) 4527-37.
[279] Y. Lin, S. Lu, J. Zhang, Y. Zheng, Structure of an inactive conformation of GTP-bound RhoA GTPase, Structure 29(6) (2021) 553-563 e5.
[280] A. Kumawat, S. Chakrabarty, K. Kulkarni, Nucleotide Dependent Switching in Rho GTPase: Conformational Heterogeneity and Competing Molecular Interactions, Sci Rep 7 (2017) 45829.
[281] S. Pasqualato, J. Cherfils, Crystallographic evidence for substrate-assisted GTP hydrolysis by a small GTP binding protein, Structure 13(4) (2005) 533-40.
[282] C. Kotting, K. Gerwert, Proteins in action monitored by time-resolved FTIR spectroscopy, Chemphyschem 6(5) (2005) 881-8.
[283] A. Barth, C. Zscherp, What vibrations tell us about proteins, Q Rev Biophys 35(4) (2002) 369-430.
[284] C.L. Parke, E.J. Wojcik, S. Kim, D.K. Worthylake, ATP hydrolysis in Eg5 kinesin involves a catalytic two-water mechanism, J Biol Chem 285(8) (2010) 5859-67.
[285] E.J. Wojcik, N.A. Dalrymple, S.R. Alford, R.A. Walker, S. Kim, Disparity in allosteric interactions of monastrol with Eg5 in the presence of ADP and ATP: a difference FT-IR investigation, Biochemistry 43(31) (2004) 9939-49.
[286] Y. Yan, V. Sardana, B. Xu, C. Homnick, W. Halczenko, C.A. Buser, M. Schaber, G.D. Hartman, H.E. Huber, L.C. Kuo, Inhibition of a mitotic motor protein: where, how, and conformational consequences, J Mol Biol 335(2) (2004) 547-54.
[287] J.C. Cochran, J.E. Gatial, 3rd, T.M. Kapoor, S.P. Gilbert, Monastrol inhibition of the mitotic kinesin Eg5, J Biol Chem 280(13) (2005) 12658-67.

[288] B. Jun, S. Kim, Real-time structural transitions are coupled to chemical steps in ATP hydrolysis by Eg5 kinesin, J Biol Chem 285(15) (2010) 11073-7.
[289] R. Xu, Y. Yang, X. Zheng, Unique structural features of the adenylate kinase hCINAP/AK6 and its multifaceted functions in carcinogenesis and tumor progression, FEBS Lett 595(16) (2021) 2071-2084.
[290] C.E. Drakou, A. Malekkou, J.M. Hayes, C.W. Lederer, D.D. Leonidas, N.G. Oikonomakos, A.I. Lamond, N. Santama, S.E. Zographos, hCINAP is an atypical mammalian nuclear adenylate kinase with an ATPase motif: structural and functional studies, Proteins 80(1) (2012) 206-20.
[291] R. Knihtila, G. Holzapfel, K. Weiss, F. Meilleur, C. Mattos, Neutron Crystal Structure of RAS GTPase Puts in Question the Protonation State of the GTP gamma-Phosphate, J Biol Chem 290(52) (2015) 31025-36.
[292] D.D. Leipe, E.V. Koonin, L. Aravind, STAND, a class of P-loop NTPases including animal and plant regulators of programmed cell death: multiple, complex domain architectures, unusual phyletic patterns, and evolution by horizontal gene transfer, J. Mol. Biol. 343(1) (2004) 1-28.
[293] I. Rayment, H.M. Holden, The three-dimensional structure of a molecular motor, Trends Biochem Sci 19(3) (1994) 129-34.
[294] C.A. Smith, I. Rayment, X-ray structure of the magnesium(II)-pyrophosphate complex of the truncated head of Dictyostelium discoideum myosin to 2.7 A resolution, Biochemistry 34(28) (1995) 8973-81.
[295] I. Rayment, C. Smith, R.G. Yount, The active site of myosin, Annu Rev Physiol 58 (1996) 671-702.
[296] A.M. Gulick, C.B. Bauer, J.B. Thoden, I. Rayment, X-ray structures of the MgADP, MgATPgammaS, and MgAMPPNP complexes of the Dictyostelium discoideum myosin motor domain, Biochemistry 36(39) (1997) 11619-28.
[297] R. Fedorov, M. Bohl, G. Tsiavaliaris, F.K. Hartmann, M.H. Taft, P. Baruch, B. Brenner, R. Martin, H.J. Knolker, H.O. Gutzeit, D.J. Manstein, The mechanism of pentabromopseudilin inhibition of myosin motor activity, Nat Struct Mol Biol 16(1) (2009) 80-8.
[298] W.W. Cleland, Low-barrier hydrogen bonds and low fractionation factor bases in enzymatic reactions, Biochemistry 31(2) (1992) 317-9.
[299] P.A. Frey, S.A. Whitt, J.B. Tobin, A low-barrier hydrogen bond in the catalytic triad of serine proteases, Science 264(5167) (1994) 1927-30.
[300] C.L. Perrin, J.B. Nielson, "Strong" hydrogen bonds in chemistry and biology, Annu Rev Phys Chem 48 (1997) 511-44.
[301] C.L. Perrin, Are short, low-barrier hydrogen bonds unusually strong?, Acc Chem Res 43(12) (2010) 1550-7.
[302] W.Y. Wahlgren, G. Pal, J. Kardos, P. Porrogi, B. Szenthe, A. Patthy, L. Graf, G. Katona, The catalytic aspartate is protonated in the Michaelis complex formed between trypsin and an in vitro evolved substrate-like inhibitor: a refined mechanism of serine protease action, J Biol Chem 286(5) (2011) 3587-96.
[303] P. Kumar, P.K. Agarwal, M.B. Waddell, T. Mittag, E.H. Serpersu, M.J. Cuneo, Low-Barrier and Canonical Hydrogen Bonds Modulate Activity and Specificity of a Catalytic Triad, Angew Chem Int Ed Engl 58(45) (2019) 16260-16266.
[304] P. Kumar, P.K. Agarwal, M.J. Cuneo, On the Case of the Misplaced Hydrogens, Chembiochem 22(2) (2021) 288-297.
[305] G.N. Nagy, R. Suardiaz, A. Lopata, O. Ozohanics, K. Vekey, B.R. Brooks, I. Leveles, J. Toth, B.G. Vertessy, E. Rosta, Structural Characterization of Arginine Fingers: Identification of an Arginine Finger for the Pyrophosphatase dUTPases, J Am Chem Soc 138(45) (2016) 15035-15045.

[306] B. Grigorenko, I. Polyakov, A. Nemukhin, Mechanisms of ATP to cAMP Conversion Catalyzed by the Mammalian Adenylyl Cyclase: A Role of Magnesium Coordination Shells and Proton Wires, J Phys Chem B 124(3) (2020) 451-460.
[307] A. Lopata, P.G. Jambrina, P.K. Sharma, B.R. Brooks, J. Toth, B.G. Vertessy, E. Rosta, Mutations decouple proton transfer from phosphate cleavage in the dutpase catalytic reaction, Acs Catalysis 5(6) (2015) 3225-3237.
[308] W.W. Cleland, P.A. Frey, J.A. Gerlt, The low barrier hydrogen bond in enzymatic catalysis, J Biol Chem 273(40) (1998) 25529-32.
[309] P.D. Ngo, S.O. Mansoorabadi, P.A. Frey, Serine Protease Catalysis: A Computational Study of Tetrahedral Intermediates and Inhibitory Adducts, J Phys Chem B 120(30) (2016) 7353-9.
[310] B.A. Reikhardt, P.D. Shabanov, Catalytic Subunit of PKA as a Prototype of the Eukaryotic Protein Kinase Family, Biochemistry. Biokhimiia 85(4) (2020) 409-424.
[311] J.A. Endicott, M.E. Noble, L.N. Johnson, The structural basis for control of eukaryotic protein kinases, Annu Rev Biochem 81 (2012) 587-613.
[312] T. Kottke, V.A. Lorenz-Fonfria, J. Heberle, The Grateful Infrared: Sequential Protein Structural Changes Resolved by Infrared Difference Spectroscopy, J Phys Chem B 121(2) (2017) 335-350.
[313] D. Sehnal, S. Bittrich, M. Deshpande, R. Svobodova, K. Berka, V. Bazgier, S. Velankar, S.K. Burley, J. Koca, A.S. Rose, Mol* Viewer: modern web app for 3D visualization and analysis of large biomolecular structures, Nucleic Acids Res 49(W1) (2021) W431-W437.
[314] W.L. DeLano, The PyMOL Molecular Graphics System, Version 1.7.2.1, Schrödinger, LLC., 2010.

Table 1. Structural traits of representative P-loop NTPases of different classes

P-loop class, activation mechanism	Representative protein structure	Site ID in Table S1	Figure in the text	PDB entry ID	NTP or NTP analog	Walker A motif (K-3 and K+1 residues)		Walker B Asp/Glu	Stimulatory moieties	Coordination of W_{cat}[a]
Kinase-GTPase Division										
TRAFAC Interaction with the activating partner or dimerization in the presence of the activating partner leads to the stabilization of the Switch I loop and insertion of diverse stimulatory moieties into the catalytic site	RhoA	3508	1C,E	1OW3	GDP-MgF_3^-	Ala15	Thr19	Asp59	Arg85†-NH2 (AG)	Gln63^{D+4}-OE1, Thr37^{SwI}-CO
	MnmE	236	2A	2GJ8	GDP-AlF_4^-	Asn226	Ser230	Asp270	K^+ ion (AG)	Thr251^{SwI}-CO, Gly249^{T-2}-HN, Thr250^{T-1}-HN, Gly273^{D+3}-HN, Gly273^{D+3}-CO*
	Dynamin	3550	3A	2X2E	GDP-AlF_4^-	Ser41	Ser45	Asp136	K^+ or Na^+ ion (G)	Thr65^{SwI}-CO, Gly139^{D+3}-HN, Gly139^{D+3}-CO*, Gln40^{K-4}-OE1*
	Atlastin	3661	3B	6B9F	GDP-AlF_4^-	Arg77	Ser81	Asp146	Arg77^{K-3}-NH2 (AG)	Gly149^{D+3}-HN, Thr120^{SwI}-CO, Gly149^{D+3}-CO*, Asp152^{D+6}-OD2*
	$G\alpha_3$	3545	3C	2ODE	GDP-AlF_4^-	Glu43	Ser47	Asp200	Arg178^{T-3}-NH1 (AG)	Thr181^{SwI}-CO, Gln204^{D+4}-OE1, Gly203^{D+3}-HN
	Myosin II	42	3D	1VOM	ADP-VO_4^-	Gly182	Thr186	Asp454	Asn233^{S-4}-ND2 (AG)	Ser237^{SwI}-CO, Ser236^{S-1}-OG, Gly457^{D+3}-HN, Gly457^{D+3}-CO, Arg238^{S+1}*-NH1, Glu459^{D+5}*-OE1
SIMIBI Monomeric domains dimerize and provide activating Lys or Arg fingers for each other in response to the interaction with the activating partner	GET3	64	4A	2YNM	ADP-AlF_4^-	Gly39	Ser43	Asp151	Lys37†-NZ (AG)	Asp66^{WB+1}-OD2, Asp155†-OD1, Lys68^{WB+1}-NZ, Gly154^{D+3}-HN, Lys37†-HN*
	Signal recognition particle	3522	4B	2CNW	GDP-AlF_4^-	Gly108	Thr112	Asp187	Arg138-NH1 (AG)	Gly190^{D+3}-HN, Asp135^{WB+1}-OD2, GTP†-O3'*, Gly190^{D+3}-CO*, Glu284†-OE1*
Kinases Rearrangement of the lid domain upon binding of the second substrate leads to the insertion of Arg/Lys fingers into the catalytic site	Thymidylate kinase	1207	4C	1NN5	ANP	Arg16	Ser20	Asp96	Arg16^{K-3}-NH1 (AG?), Arg97^{D+1}-NH2 (G)	The second substrate is coordinated by Arg45^{WB+1}-NH2, Arg-97^{D+1}-NE, Glu149^{Lid}-OE1, Pro43-CO*
	Adenosine 5'-phosphosulfate kinase	1490	4D	4BZX	ANP	Gly453	Ser457	Asp478	Lys562^{Lid}-NZ (G)	The second substrate is coordinated by Asp41^{D+2}-OD1, Lys562^{Lid}-NZ, Arg483^{D+5}-NH2, Arg497-NH1
	Adenylate kinase	xxx0	S8B	3SR0	ADP-AlF_4^-	Gly10	Gly14	Asp81	Arg124^{Lid}-NH1 (AG) Arg124^{Lid}-NH2 (G) Arg150^{Lid}-NH1 (G) Arg161^{Lid}-NH1(G)	The second substrate (phosphate acceptor) is coordinated by Arg150^{Lid}-NH2, Arg85^{D+4}-NH1, Arg85^{D+4}-NH2, Arg36^{WB+1}-NH1, Arg36^{WB+1}-NH2

P-loop class, activation mechanism	Representative protein structure	Site ID in Table S1	Figure in the text	PDB entry ID	NTP or NTP analog	Walker A motif (K-3 and and K+1 residues)		Walker B motif Asp/Glu	Stimulatory moieties	Coordination of W_{cat}[a]
ASCE Division										
AAA+ / SF3 ATPases In a hexamer, the binding /hydrolysis of ATP in one subunit causes conformational changes activating the adjacent subunit; the activation involves class-specific helical domain	N-ethylmaleimide sensitive factor	359	5A	1NSF	ATP	His546	Thr550	Asp603	Lys708‡-NZ (AG) Lys631†-NZ (G)	Asp604^{D+1}-OD2, Lys631†-NZ, Ser647^{WB-1}-OG
	SV40 large T antigen helicase (SF3)	372	5B	1SVM	ATP	Asp429	Thr433	Glu473	Lys418†-NZ (AG), Arg540†-NH2 (G)	Asp474^{E+1}-OD1, Asn529^{WB-1}-OD1, Arg498†-NH1, Arg540†-NH2
Helicases SF1/2: Rearrangement of the C-terminal domain upon DNA or RNA binding leads to the insertion of an Arg finger into the nucleotide-binding domain	Chikungunya virus nsP2 helicase (SF1)	N/A	1D, 1F	6JIM	ADP-AlF$_4^-$	Gly189	Ser193	Asp252	Arg312‡-NH2 (AG), Arg416‡-NH1 (G), Arg416‡-NH2 (G),	Glu253^{D+1}-OE2, Gln283^{D+1}-OE2, Gly384‡-HN
	HCV NS3 helicase (SF2)	136	5C	3KQL	ADP-AlF$_4^-$	Gly207	Ser211	Asp290	Arg467‡-NH2 (AG), Arg467‡ -NH1 (G), Arg467‡ -NH2 (G), Arg464‡ -NH1 (G), Arg464‡ -NH2 (G),	Glu291^{D+1}-OE1, Gln460‡-OE1, Arg464‡-NH2, Gly417‡-NH, Ala323-NH^{WB+1}*
	Multifunctional helicase Pif1p (SF1)	233	12B	5O6B [192]	ADP-AlF$_4^-$	Gly261	Ser265	Asp-341	Arg417‡-NH2 (AG)	Glu342^{D+1}-OE1, Gln381^{WB-1}-OE1, Arg734‡-NH1, Gly709‡-HN
ABC ATPases: Monomeric domains dimerize and provide activating LSGGQ motifs for each other in response to the substrate binding	Maltose transporter	154	5D	3PUW	ADP-AlF$_4^-$	Gly39	Ser43	Asp158	Ser135†-OG (G), Gly137†-HN (G)	Gln82^{WB+1}-NE2, Glu159^{D+1}-OE1, Glu159^{D+1}-OE2, Asn163†-CO, His192 $^{WB-1}$-NE2
F_1/RecA-like: In an oligomer, ATP binding/hydrolysis in one subunit causes conformational changes that activate the adjacent subunit by inserting Arg/Lys fingers	F_1-ATPase	18	6A	1H8E	ADP-AlF$_4^-$	Gly159	Thr163	Asp256	Arg373†-NH1 (AG), Arg189^{WB-1}-NH1 (G), Arg189^{WB-1}-NH2 (G),	Glu188^{WB-1}-OE1, Arg260^{D+4}-NH2, Ser344†-CO
	Replicative helicase DnaB	N/A	6B	6T66	GDP-AlF$_4^-$	Ser231	Thr235	Asp340	Arg439†-NE (G), Lys437†-NZ (G)	Glu259^{WB+1}**, Tyr341^{D+1}** Gln381^{WB-1}** Arg439†
	Circadian clock protein KaiC	683	6C	4TL7	ATP	Gly49	Thr53	Asp145	Lys224†-NZ (G) Arg226†-NH2 (G)	Glu183^{WB-1}-OE1**, Ser146^{D+1}**, Phe199†-CO
	Recombinase RadA	1376	6D	3EW9	ANP	Gly108	Thr112	Asp211	K^+-503 (G), K^+-504 (G)	Glu151^{WB+1}**, Ser212^{D+1}** Gln257^{WB-1}**,
	RecA	100	N/A	3CMX [129]	ADP-AlF$_4^-$	Ser69	Thr73	Asp144	Lys248†-NZ (G) Lys250†-NZ (G)	Glu96^{D+1}**, Phe216**†-CO, Gln194**$^{D-1}$,

Residue numbers are as in the listed PDB structures;
[a] – polar atoms, located within 3.6Å from the catalytic water molecule;
AG – the stimulatory residue inserts between α-phosphate and γ-phosphate (or its mimic)
G – the stimulatory residue is only coordinating γ-phosphate or its mimic
† – residue from a polypeptide chain other than the P-loop containing one;
‡ – residues from a domain other than the described P-loop domain;
* – residue coordinates the attacking water molecule via another water molecule (e.g. Fig. 4B);
** – catalytic water molecule not resolved, coordinating residue(s) were inferred from structure superposition and literature data;

7. Supplementary Materials

Supplementary Figures

Supplementary File 1. Consideration of tentative activation mechanisms in STAND, KAP, VirD/PilT and FtsK-HerA classes of P-loop ATPases

Supplementary Table 1. Results of the computational analysis of all available structures of the P-loop proteins in complex with NTPs and NTP-like molecules. The Microsoft Excel table contains the list with characteristics of all analyzed structures, together with key functional residues of the Walker A and Walker B motifs, Arg, Lys, and Asn fingers, as well as distances from (1) the respective atoms of NTPs/their analogs to the K-3 residues and Arg/Lys fingers, as well as (2) from $[Asp/Glu]^{WB}$ to $[Ser/Thr]^{K+1}$. Each row contains the data for one catalytic site in one structure. Catalytic sites containing "properly bound" NDP:AlF_4^- complexes that we deemed to be reliable TS-analogs (see Table S3 in the accompanying paper [41] for detailed description of AlF_4^- and Mg^{2+} binding in such structures) are marked with "y" or "*" in column "site rel"; they are colored green. The sites with "unproperly bound" NDP:AlF_4^- complexes are colored pink. All columns present in the Sheet A of the Table S1 (data) are described in the Sheet B.

Supplementary Table 2. Analysis of the bonding pattern within the catalytic sites of the RhoA GTPase and F_1-ATPase as a function of the TS analog bound.

Supplementary Figures to the manuscript "Common mechanism of activated catalysis in P-loop fold nucleoside triphosphatases - "united in diversity" by Maria I. Kozlova, Daria N. Shalaeva, Daria V. Dibrova, Armen Y Mulkidjanian

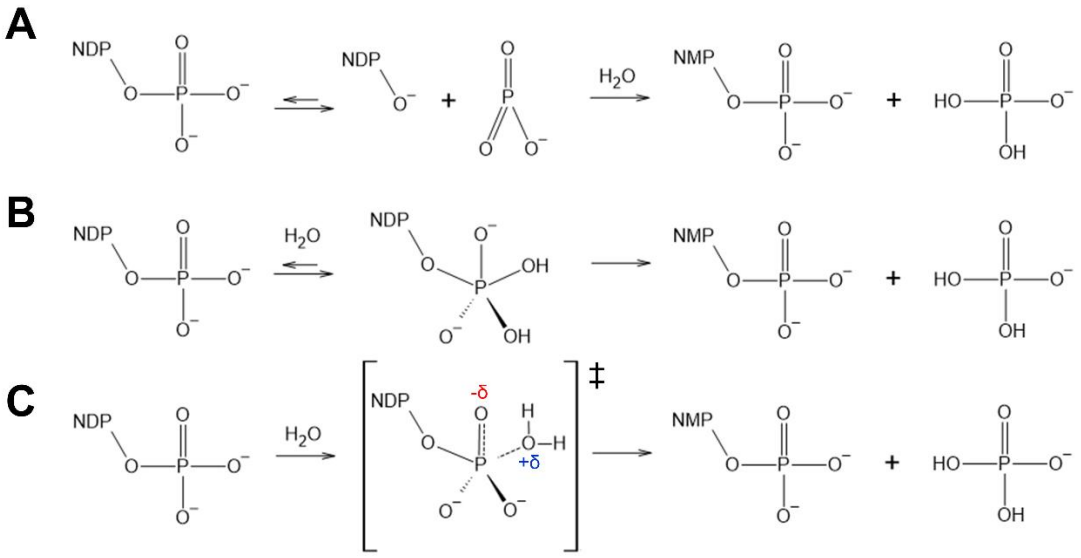

Figure S1. Tentative mechanisms of NTP hydrolysis. Dissociative (**A**), associative (**B**), and concerted pathways (**C**). See the main text for further details and references.

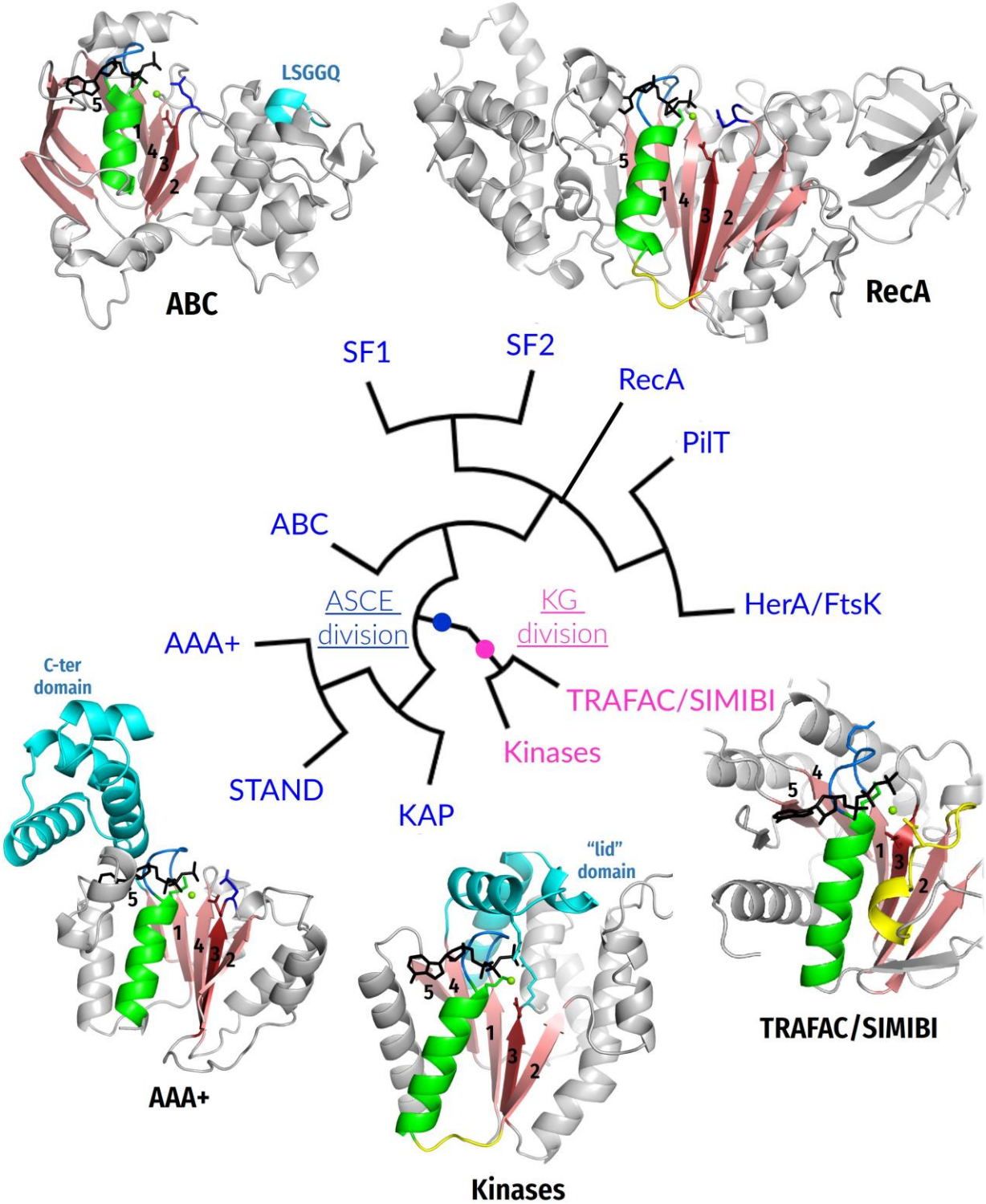

Figure S2. Cladogram of higher-order relationships between major divisions/classes of P-loop NTPases with depicted typical structures.

The cladogram (as modified from [1]) shows the two major divisions: the kinase-GTPase (KG) division and the ASCE (additional strand, catalytic E) division. The β-strands forming the cores

of P-loop domains are numbered in a traditional way [1, 2]. These β-strands are colored pink, the P-loop is shown in blue, the following α_1-helix is shown in green, the K-loop/Switch I in TRAFAC class NTPases as well as the corresponding loops in other NTPases are colored in yellow, NTP analogs are shown as black sticks, Mg^{2+} ions are shown as green spheres, the rest of proteins is shown as gray cartoons. The reference residues of Walker A and Walker B motifs (lysine (K) and aspartate (D), respectively), as well as the catalytic glutamate (E) in ASCE NTPases are shown as sticks. The following reference crystal structures are depicted: ABC – antibacterial peptide ABC transporter McjD of *Escherichia coli*, PDB ID 5EG1 [3]; RecA/F_1 –F_1-ATPase of *Caldalaklibacillus thermarum*, PDB ID 5HKK [4]; AAA+ –clamp loader γ-subunit *E. coli*, PDB ID 1NJG [5]; Kinases –thymidylate kinase of *E. coli*, PDB ID 4TMK [6]; TRAFAC/SIMIBI – nitrogenase ATPase subunit of *Azotobacter vinelandii*, PDB ID 4WZB [7].

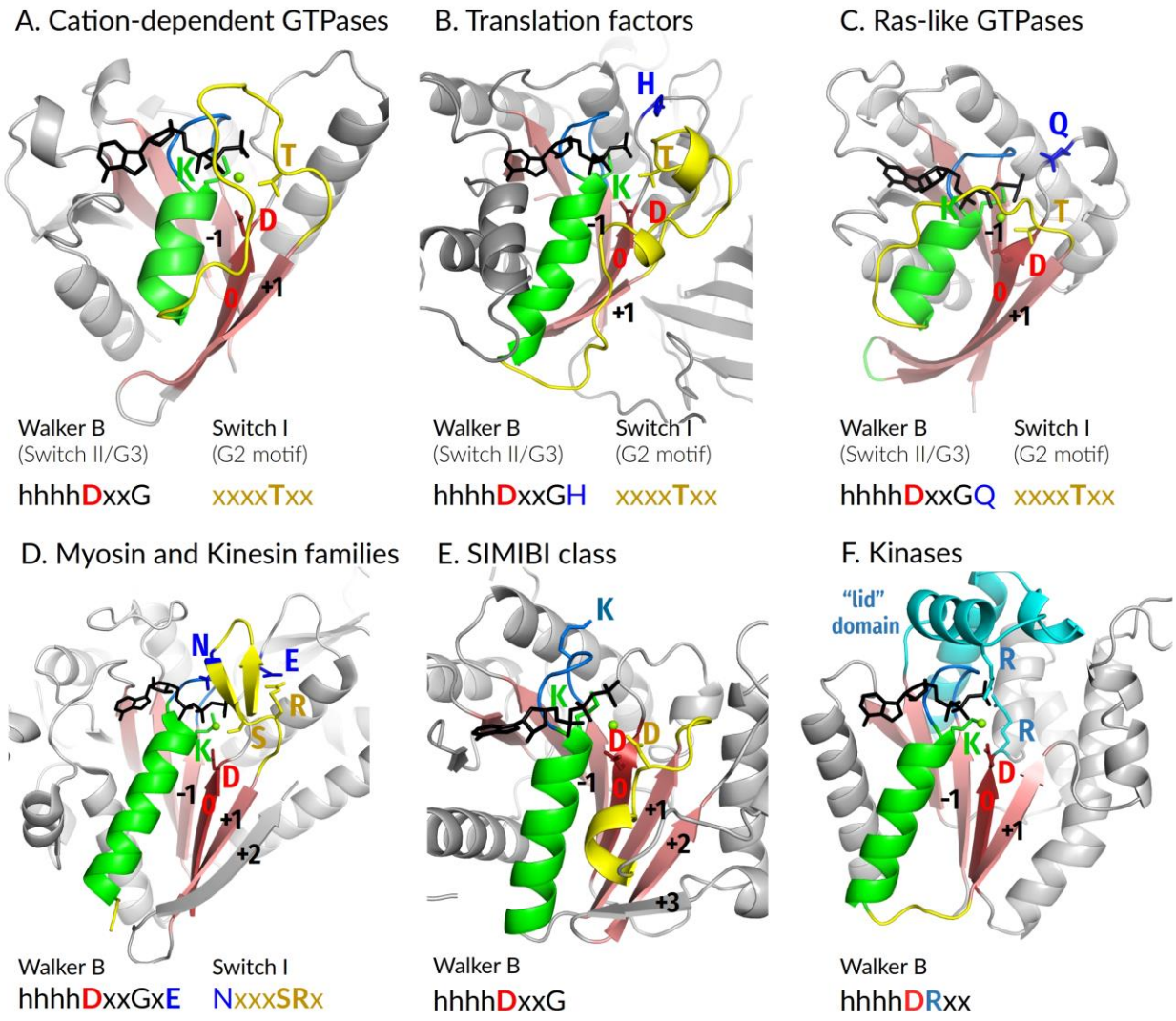

Figure S3. P-loop domain organization and conserved motifs in P-loop NTPases of the Kinase-GTPase division.

The β-strands forming the cores of P-loop domains are numbered relative to the Walker B motif-containing WB-strand as suggested in the main text. Color code as in Fig. S2. The following crystal structures are depicted: A, MnmE GTPase of *E. coli*, PDB ID 2GJ8 [8]; B, Elongation factor EF-Tu of *Thermus thermophilus* HB8, PDB ID 4V5L [9]; C, Human Ras-GTPase, PDB ID 1WQ1, [10]; D, Myosin II of *Dictyostelium discoideum*, PDB ID 1W9L; E, nitrogenase ATPase subunit of *Azotobacter vinelandii*, PDB ID 4WZB [7]; F, thymidylate kinase of *E. coli*, PDB ID 4TMK [6].

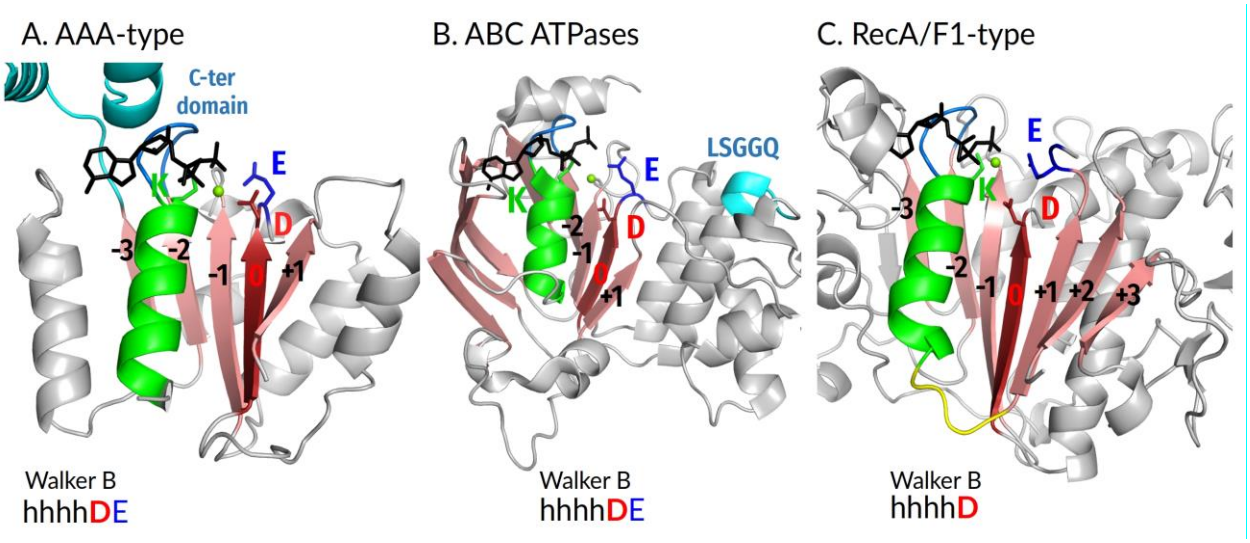

Figure S4. P-loop domain organization and conserved motifs in P-loop NTPases of the ASCE division.

The β-strands forming the cores of P-loop domains are numbered relative to the Walker B motif-containing WB-strand as suggested in the main text. Color code as in Fig. S2. The following crystal structures are depicted: A, AAA+ Clamp Loader Gamma Subunit of *E. coli*, PDB ID 1NJG [5]; B, antibacterial peptide ABC transporter McjD of *E.coli*, PDB ID 5EG1 [3]; C, F_1-ATPase of *Caldalaklibacillus thermarum***,** PDB ID 5HKK [4].

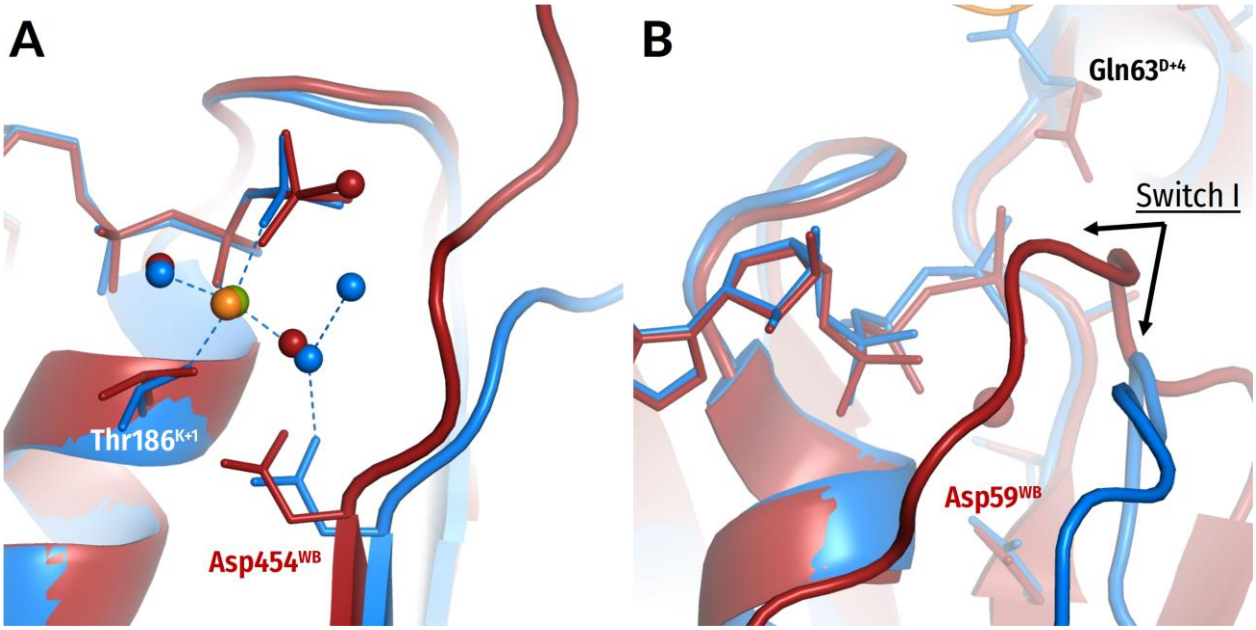

Figure S5. Structures of same P-loop NTPases with transition state analogs and substrate/substrate analogs bound, respectively.

The structures with bound substrate or substrate analogs are shown in blue with their Mg^{2+} ions in green; the structures with transition state analogs bound are shown in dark red with their Mg^{2+} ions in orange. Cations and water molecules are shown as spheres. The following crystal structures are depicted**: A,** Myosin II from *Dictyostelium discoideum* in complex with a bound ATP molecule (blue, PDB ID 1FMW [11]) and with a transition state analog ADP:VO_4^- bound (dark red, PDB ID 1VOM [12]); **B,** Ras-like GTPase RhoA with a bound non-hydrolyzable substrate analog GNP (blue, PDB 6V6M, [13]) and a complex of Rho with RhoGAP and a transition state analog GDP:MgF_3^- (dark red, ODB 1OW3, [14]).

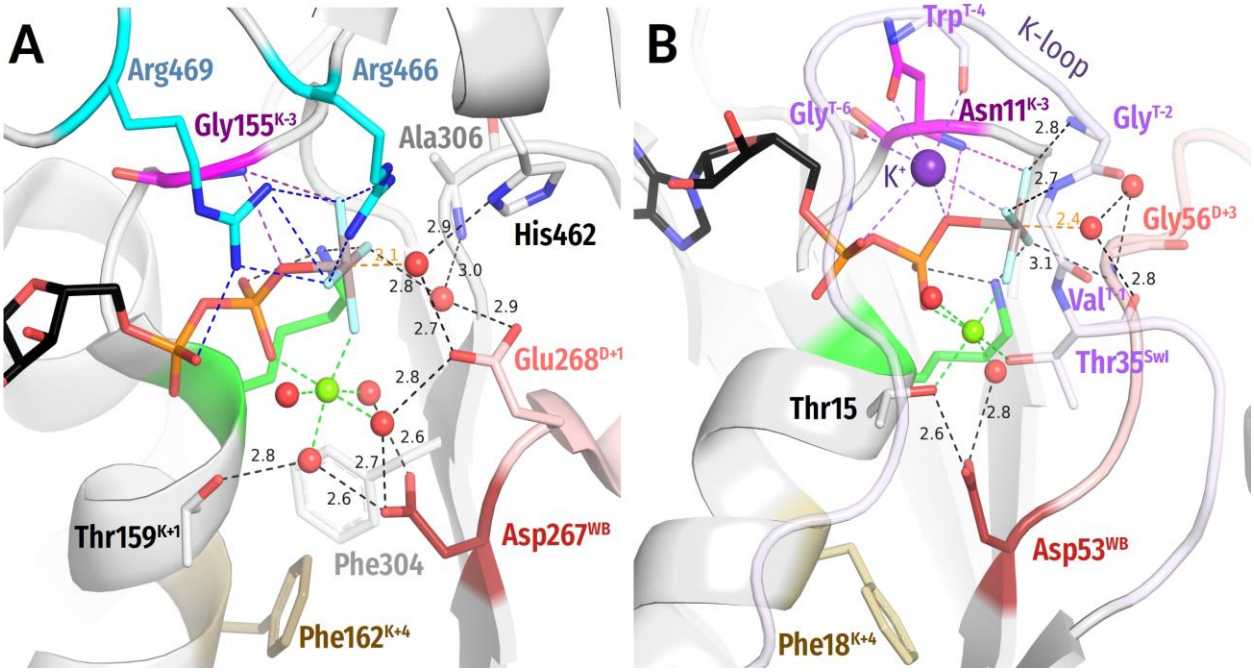

Fig. S6. Interference of Phe^{K+4} with the Asp^{WB} — [Ser/Thr]$^{K+1}$ bonding.

A. The only detected structure with properly bound AlF_4^- and, still, long distance between Asp^{WB} and [Ser/Thr]$^{K+1}$ is the mitochondrial yeast DEAD box protein Mss116p where this distance is about 4 Å, see Panel A and (PDB 3I62 [15]). The structure analysis has shown that the formation of the H-bond between Asp^{WB} and [Ser/Thr]$^{K+1}$ is prevented by the Phe162^{K+4} residue. It interacts with Phe304 of the WB-1 strand so that these two residues intercalate between Walker A and Walker B motifs and prevent the formation of the H-bond (Panel A). Remarkably, the Thr^{K+1} is not directly coordinating Mg^{2+}, pointing to a possibility of a crystallization artefact or an inactive configuration of the binding site with the Phe^{K+4} acting as a regulatory switch.

B. A phenylalanine residue is not unique in K+4 position, it is also found in the well-studied K^+-stimulated GTPase FeoB. In its GDP:AlF_4^--containing structure (PDB ID 7BWV), the homologous Phe18^{K+1} is, however, in a different rotameric position and do not interfere with the Asp^{WB} – [Ser/Thr]$^{K+1}$ bond (Panel B). Notably, in this structure the residue is not involved in a π-π interaction with another phenylalanine residue that would orient it towards the Asp^{WB} —Thr^{K+1} bond (cf Panel A).

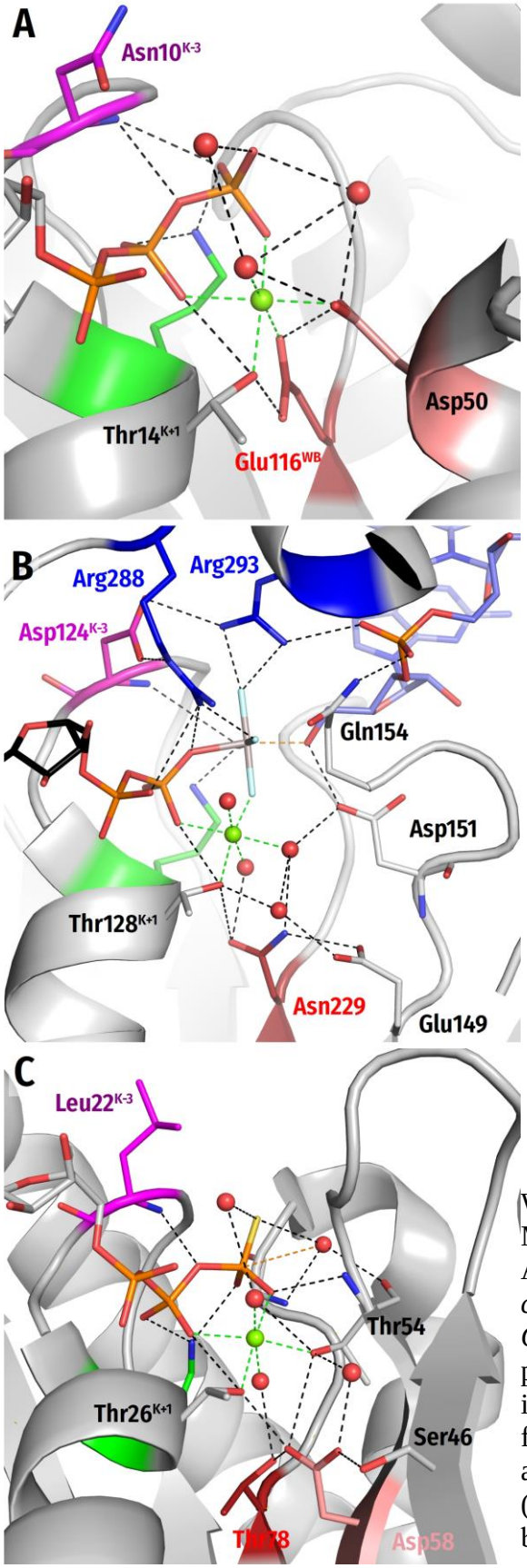

Figure S7. Deviations from a typical Walker B motif. Color code as in Fig. 1E,F.

A. In a few cases, which are considered in detail in [16], the long side chain of Glu^{WB} reaches Mg^{2+} and directly coordinates it, forming also a H-bond with $[Ser/Thr]^{K+1}$, as shown in Panel A for the Dethiobiotin synthetase (BioD) from *Helicobacter pylori* complexed with GTP (PDB 3QXJ [17]). In this enzyme, the γ-phosphate group is transferred on the carboxy group of 7,8-diaminononanoate, which is likely to be deprotonated at neutral pH, so that no proton trapping is needed. In a few more conventional cases, the Glu^{WB} residue, similarly to Asp^{WB}, does not reach Mg^{2+}, interacts with Mg^{2+}-coordinating water and makes an H-bond with $[Ser/Thr]^{K+1}$, see [16].

B. An Asn229 residue links W3, W6 and $Thr131^{K+1}$ in the wild-type polynucleotide kinase of *Caenorhabditis elegans*, see Panel B for its structure with bound ssRNA dinucleotide GC and ADP:AlF_4^- (PDB ID 4OI1 and [16, 18]). In this case, however, the adjacent WB+1 strand has a $^{149}ELD^{151}$ triad at its C-cap. In the TS-like AlF_4^--containing structure, the Glu149 residue is connected via a bridging water molecule to $Thr131^{K+1}$ and to W3, whereas Asp151 makes a short H-bond (2.48 Å) with the hydroxyl of the RNA ribose. Deprotonation of this hydroxyl yields the nucleophile that attacks the γ-phosphate. We believe that the functions of Asp^{WB} are divided between Asn229 and Glu149 in this polynucleotide kinase. The $Asn229^{WB}$ residue serves as a structural linker to the Walker A motif, whereas Glu149 serves as a trap for the proton that is taken by Asp151 from W_{cat}.

While the same Asn-Glu-Asp triad is found in other Metazoa enzymes, Asp substitutes for Asn229 and Asn substitutes for Glu149 in *Saccharomyces cerevisiae*, *Schizosaccharomyces pombe*, and *Candida albicans*. Hence, in evolutionarily primary primitive microorganisms, a single Asp^{WB} appears to interact with W6 and Thr^{K+1} and to obtain a proton from the catalytic Asp residue at the C-cap of the adjacent WB+1 strand; in the *C. elegans* structure (PDB ID 4OI1 [18]), Asn229 and Asp 151 are linked by W6. The "primordial" dyad of aspartates is

functionally similar but structurally distinct from the $Asp^{WB}L^{D+1}Asp^{D+2}$ aspartate dyads found in some other kinase families, see Fig. 4D and [19]. Generally, the overall diversity of proton routes within kinases [19] might reflect the diversity of second substrates in these enzymes, see Section 2.2.

C. A natural mutation in an otherwise typical small TRAFAC class GTPase MglA changed Asp^{WB} to Thr. The structure of MglA GTPase of *Myxococcus xanthus* with a bound non-hydrolizable analog of GTP is shown (PDB ID: 6IZW and [20]). The enzyme retained its function owing to the appearance of an Asp residue at the N-terminus of the adjacent antiparallel WB+1 strand [16]. The resulting topology of the catalytic site is typical for P-loop NTPases.

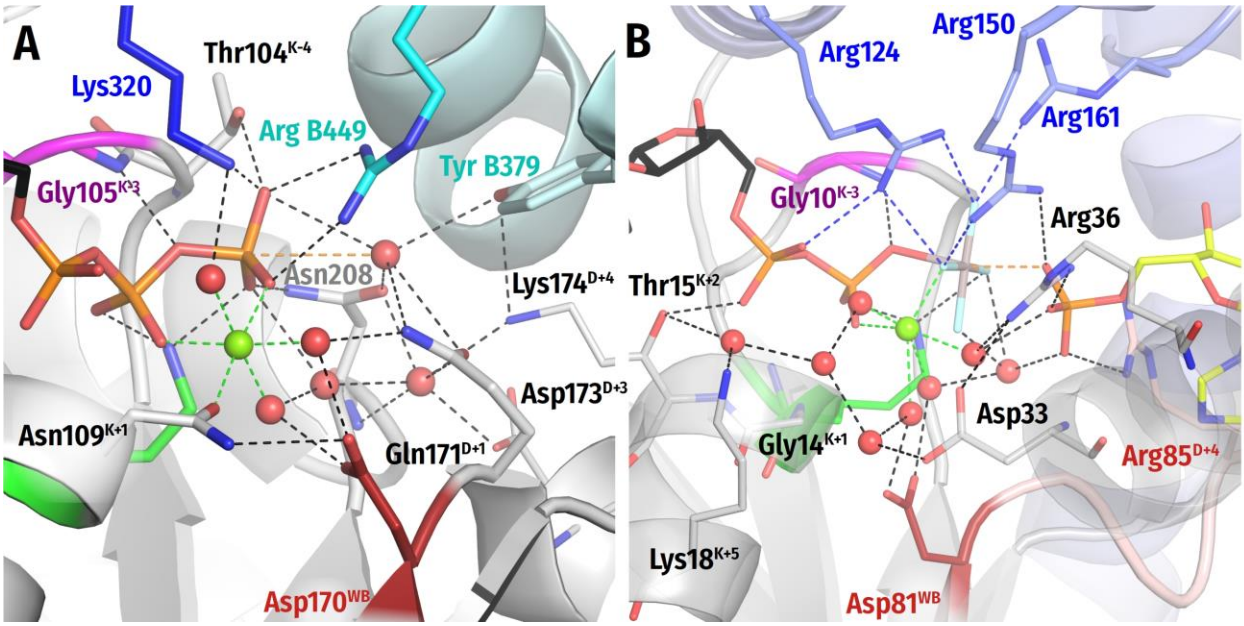

Fig. S8. Residues other than [Ser/Thr] in the K+1 position of the Walker A motif. Colors as in Fig. 3-6 in the main text. Lys^{WA} shown in green, Asp^{WB} in dark red, adjacent monomer and its residues in cyan, Arg and Lys finger from the same polypeptide chain in blue.

A, an asparagine residue replaces $[Ser/Thr]^{K+1}$ in such distantly related AAA+ ATPases as torsinA of metazoa and DnaC helicase loader of some enterobacteria including *E. coli* [16, 21, 22]. In addition, the potentially W_{cat}-stabilizing "catalytic" $[Glu/Asp]^{D+1}$ – ubiquitous in AAA+ ATPases [23] – is replaced by Asn^{D+1} in torsinA (but not in DnaC). The ATPase activity of both these proteins are very low, so it is not yet clear if they are true ATPases or simply work as switches that change their conformation depending on whether ATP or ADP is bound in the catalytic site [21, 22, 24, 25]. Shown is the high-resolution ATP-containing structure of human torsinA in complex with its activator LULL1 (PDB ID 5J1S [26]). It can be seen that $Asn109^{K+1}$ makes the canonic H-bond with $Asp170^{WB}$ which could increase the proton affinity of the latter. While $Asn171^{D+1}$ cannot transfer a proton from W_{cat}, a water chain – similar to one observed in TRAFAC class NTPases (Fig. 7B, 12D-F) – connects W_{23} with $Asp170^{WB}$ via the Mg^{2+}-coordinating W6 molecule. In AAA+ NTPases, a Lys/Arg residue always interacts with γ-phosphate and, supposedly, W_{cat} (see section 2.2.2.2, Fig. 5A,B, and [27, 28]). In torsinA, this is the Arg449 residue of LULL1. In the absence of negatively charged Asp/Glu^{D+1}, the interaction of a positively charged Arg449 with W_{cat}, by dramatically decreasing its proton affinity, may trigger proton transfer from W_{cat}, via W6, to $Asp170^{WD}$. Subsequently, the proton can move to β-phosphate via W6. Hence, the structure is compatible with involvement of $Asp170^{WB}$ as a proton trap in torsinA and could explain its, albeit slow, ATPase activity.

B, Adenylate kinase of *Aquifex aeolicus* ([PDB 3SR0] [29]), see the main text.

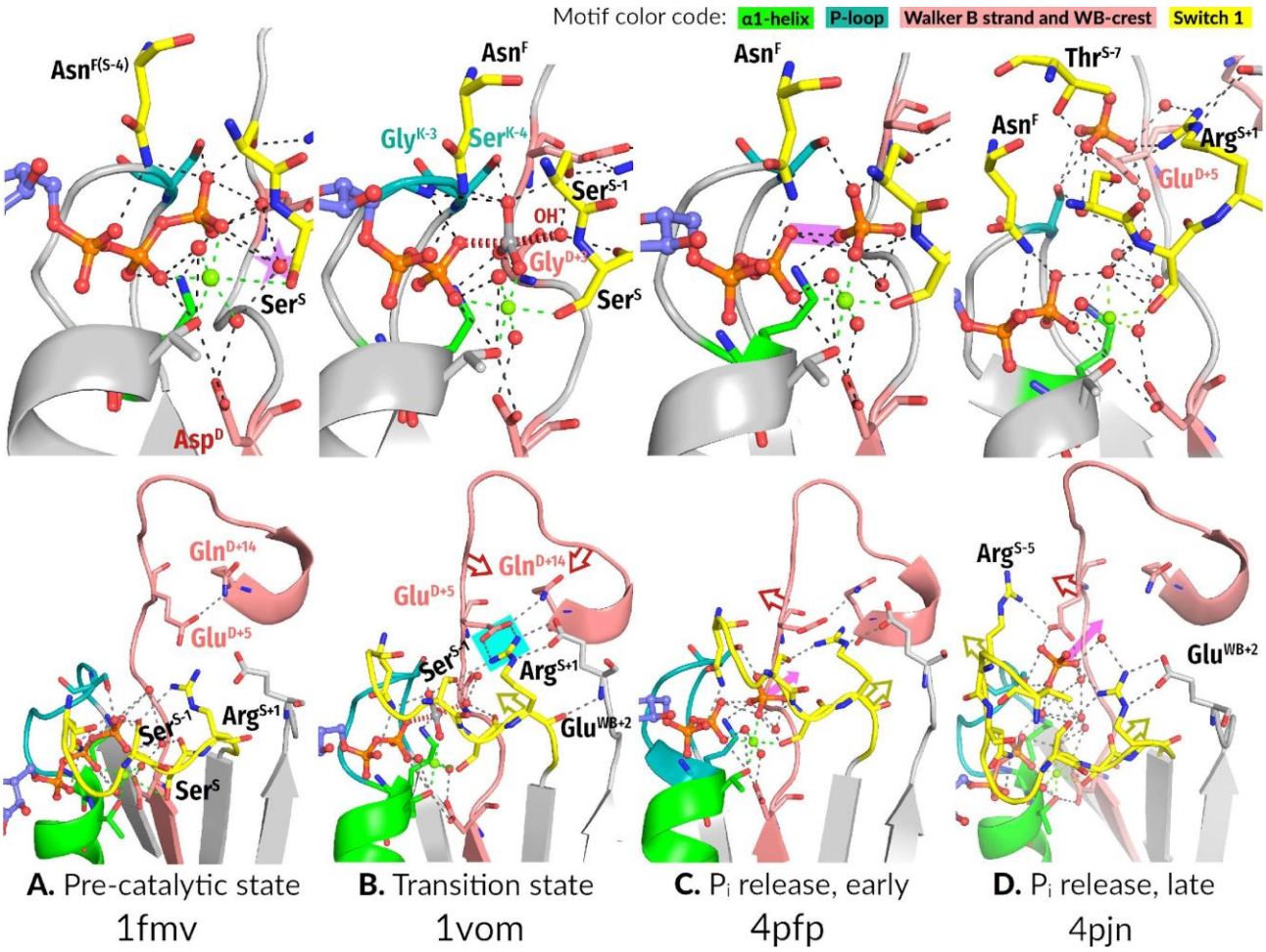

Figure S9. Catalytic cycle of myosin as inferred from the available set of crystal structures. The top and bottom rows show similar structures differently zoomed.

Given that myosin is one of the few P-loop NTPases with a set of high-quality crystal structures including those mimicking the pre-transition, transition, and several post-transition states (see also Supplementary Table 1), we tentatively reconstruct the catalytic cycle of myosin as follows:

A) (top) In the substrate-bound state (ATP-soaked myosin crystals, PDB ID 1FMW [11]), the catalytic pocket is not constricted, and the proton pathway from the would-to-be W_{cat} in the W_{12} position (highlighted with a star) to Asp^{WB} (via W6) is clearly seen.

(bottom) In this state, Glu^{D+5} of WB-crest and Arg^{S+1} of Switch I motif are remote from each other, and each residue is only interacting with its neighbors in the polypeptide chain. Glu^{D+5} is forming an H-bond with Gln^{D+14}, while Arg^{S+1} is in contact with Ser^{S-1} (bottom).

B) (top) In the ADP:VO_4^--containing structure, which mimics the transition state (PDB 1VOM [12]), the site is constricted, and W_{12}, after giving its proton via W6 to Asp^{WB}, is pushed upwards into the attack position of **OH$^-_{cat}$**, here mimicked by the oxygen atom of VO_4^- . In this position, **OH$^-_{cat}$** is stabilized by the side chain of Ser^{S-1}, **CO** of Ser^{S}, and **HN** of Gly^{D+3}. Also in this state, the Asn finger comes closer to the phosphate chain and interacts with α-phosphate and one of the

oxygen atoms of VO_4^-, another oxygen atom of VO_4^- interacts with Gly^{K-3} and with the side chain of Ser^{K-4}. The WB-crest is brought closer to the catalytic site: an oxygen atom of VO_4^- is coordinated by Gly^{D+3}. Here, the distance between $\mathbf{OH^-_{cat}}$ and W6 is 4.8 Å, which, supposedly, precludes the proton at Asp^{WB} from returning to W_{cat}. The proton, however, can pass to β-phosphate; all the tentative proton transfer steps on the way to β-phosphate are of 2.9 Å.

(bottom) An extensive salt bridge network is formed between WB-crest, Switch I and the adjoining domain. Arg^{S+1} interacts with Ser^{S-1} and Glu^{D+5} (bonds highlighted in bright cyan), whereas subsequent residues of the WB-crest are contacting the adjoining protein domain.

C and D) In the two subsequent post-transition states (mimicked by differently P_i-soaked ADP-containing myosin structures with PDB IDs 4PFP and 4PJN [30]), catalytic site opens up: the release of $H_2PO_4^{2-}$ is coupled with breaking of salt bridges between WB-crest and Switch I. Hence the exergonic release of P_i drives the opening of the catalytic pocket, which, in turn, is coupled to the mechanical movement. The Asn finger no longer interacts with the outgoing $H_2PO_4^{2-}$ moiety. In the early post-transition state the proton is already engaged in the H-bond between O^{3B} and O^{3G} (C, top, the H-bond is highlighted in purple), while in the late post-transition state (D), hydrogen-bonded networks are further rearranged: the outgoing $H_2PO_4^{2-}$ no longer contacts residues involved in P_γ coordination during the previous steps (D, bottom); $H_2PO_4^{2-}$ gets directly engages with Glu^{D+5} and Arg^{S+1} pulling apart the WB-crest and Switch I (D, bottom).

References

[1] A. Krishnan, A.M. Burroughs, L.M. Iyer, L. Aravind, Comprehensive classification of ABC ATPases and their functional radiation in nucleoprotein dynamics and biological conflict systems, Nucleic Acids Res 48(18) (2020) 10045-10075.

[2] D.D. Leipe, Y.I. Wolf, E.V. Koonin, L. Aravind, Classification and evolution of P-loop GTPases and related ATPases, J Mol Biol 317(1) (2002) 41-72.

[3] S. Mehmood, V. Corradi, H.G. Choudhury, R. Hussain, P. Becker, D. Axford, S. Zirah, S. Rebuffat, D.P. Tieleman, C.V. Robinson, K. Beis, Structural and Functional Basis for Lipid Synergy on the Activity of the Antibacterial Peptide ABC Transporter McjD, J Biol Chem 291(41) (2016) 21656-21668.

[4] S.A. Ferguson, G.M. Cook, M.G. Montgomery, A.G. Leslie, J.E. Walker, Regulation of the thermoalkaliphilic F1-ATPase from Caldalkalibacillus thermarum, Proc Natl Acad Sci U S A 113(39) (2016) 10860-5.

[5] M. Podobnik, T.F. Weitze, M. O'Donnell, J. Kuriyan, Nucleotide-induced conformational changes in an isolated Escherichia coli DNA polymerase III clamp loader subunit, Structure 11(3) (2003) 253-63.

[6] A. Lavie, N. Ostermann, R. Brundiers, R.S. Goody, J. Reinstein, M. Konrad, I. Schlichting, Structural basis for efficient phosphorylation of 3'-azidothymidine monophosphate by Escherichia coli thymidylate kinase, Proc Natl Acad Sci U S A 95(24) (1998) 14045-50.

[7] F.A. Tezcan, J.T. Kaiser, D. Mustafi, M.Y. Walton, J.B. Howard, D.C. Rees, Nitrogenase complexes: multiple docking sites for a nucleotide switch protein, Science 309(5739) (2005) 1377-80.

[8] A. Scrima, A. Wittinghofer, Dimerisation-dependent GTPase reaction of MnmE: how potassium acts as GTPase-activating element, EMBO J 25(12) (2006) 2940-51.
[9] R.M. Voorhees, T.M. Schmeing, A.C. Kelley, V. Ramakrishnan, The mechanism for activation of GTP hydrolysis on the ribosome, Science 330(6005) (2010) 835-838.
[10] K. Scheffzek, M.R. Ahmadian, W. Kabsch, L. Wiesmuller, A. Lautwein, F. Schmitz, A. Wittinghofer, The Ras-RasGAP complex: structural basis for GTPase activation and its loss in oncogenic Ras mutants, Science 277(5324) (1997) 333-8.
[11] C.B. Bauer, H.M. Holden, J.B. Thoden, R. Smith, I. Rayment, X-ray structures of the apo and MgATP-bound states of Dictyostelium discoideum myosin motor domain, J Biol Chem 275(49) (2000) 38494-9.
[12] C.A. Smith, I. Rayment, X-ray structure of the magnesium(II).ADP.vanadate complex of the Dictyostelium discoideum myosin motor domain to 1.9 A resolution, Biochemistry 35(17) (1996) 5404-17.
[13] Y. Lin, S. Lu, J. Zhang, Y. Zheng, Structure of an inactive conformation of GTP-bound RhoA GTPase, Structure 29(6) (2021) 553-563 e5.
[14] D.L. Graham, P.N. Lowe, G.W. Grime, M. Marsh, K. Rittinger, S.J. Smerdon, S.J. Gamblin, J.F. Eccleston, MgF(3)(-) as a transition state analog of phosphoryl transfer, Chem Biol 9(3) (2002) 375-81.
[15] M. Del Campo, A.M. Lambowitz, Structure of the Yeast DEAD box protein Mss116p reveals two wedges that crimp RNA, Mol Cell 35(5) (2009) 598-609.
[16] M. Kanade, S. Chakraborty, S.S. Shelke, P. Gayathri, A Distinct Motif in a Prokaryotic Small Ras-Like GTPase Highlights Unifying Features of Walker B Motifs in P-Loop NTPases, J Mol Biol 432(20) (2020) 5544-5564.
[17] P.J. Porebski, M. Klimecka, M. Chruszcz, R.A. Nicholls, K. Murzyn, M.E. Cuff, X. Xu, M. Cymborowski, G.N. Murshudov, A. Savchenko, A. Edwards, W. Minor, Structural characterization of Helicobacter pylori dethiobiotin synthetase reveals differences between family members, Febs J 279(6) (2012) 1093-105.
[18] A. Dikfidan, B. Loll, C. Zeymer, I. Magler, T. Clausen, A. Meinhart, RNA specificity and regulation of catalysis in the eukaryotic polynucleotide kinase Clp1, Mol Cell 54(6) (2014) 975-86.
[19] D.D. Leipe, E.V. Koonin, L. Aravind, Evolution and classification of P-loop kinases and related proteins, J Mol Biol 333(4) (2003) 781-815.
[20] J. Baranwal, S. Lhospice, M. Kanade, S. Chakraborty, P.R. Gade, S. Harne, J. Herrou, T. Mignot, P. Gayathri, Allosteric regulation of a prokaryotic small Ras-like GTPase contributes to cell polarity oscillations in bacterial motility, PLoS Biol 17(9) (2019) e3000459.
[21] M. Nagy, H.C. Wu, Z. Liu, S. Kedzierska-Mieszkowska, M. Zolkiewski, Walker-A threonine couples nucleotide occupancy with the chaperone activity of the AAA+ ATPase ClpB, Protein Sci 18(2) (2009) 287-93.
[22] A. Matte, L.T.J. Delbaere, ATP-binding Motifs, Encyclopedia of Life Sciences (ELS), John Wiley & Sons, Ltd, Chichester, 2010.
[23] L.M. Iyer, D.D. Leipe, E.V. Koonin, L. Aravind, Evolutionary history and higher order classification of AAA+ ATPases, J. Struct. Biol. 146(1-2) (2004) 11-31.
[24] A.E. Rose, R.S. Brown, C. Schlieker, Torsins: not your typical AAA+ ATPases, Crit Rev Biochem Mol Biol 50(6) (2015) 532-49.
[25] C. Zhao, R.S. Brown, A.R. Chase, M.R. Eisele, C. Schlieker, Regulation of Torsin ATPases by LAP1 and LULL1, Proc Natl Acad Sci U S A 110(17) (2013) E1545-54.

[26] F.E. Demircioglu, B.A. Sosa, J. Ingram, H.L. Ploegh, T.U. Schwartz, Structures of TorsinA and its disease-mutant complexed with an activator reveal the molecular basis for primary dystonia, Elife 5 (2016).
[27] T. Ogura, S.W. Whiteheart, A.J. Wilkinson, Conserved arginine residues implicated in ATP hydrolysis, nucleotide-sensing, and inter-subunit interactions in AAA and AAA+ ATPases, J. Structural Biology 146(1-2) (2004) 106-12.
[28] P. Wendler, S. Ciniawsky, M. Kock, S. Kube, Structure and function of the AAA+ nucleotide binding pocket, Biochim. Biophys. Acta 1823(1) (2012) 2-14.
[29] S.J. Kerns, R.V. Agafonov, Y.J. Cho, F. Pontiggia, R. Otten, D.V. Pachov, S. Kutter, L.A. Phung, P.N. Murphy, V. Thai, T. Alber, M.F. Hagan, D. Kern, The energy landscape of adenylate kinase during catalysis, Nat Struct Mol Biol 22(2) (2015) 124-31.
[30] P. Llinas, T. Isabet, L. Song, V. Ropars, B. Zong, H. Benisty, S. Sirigu, C. Morris, C. Kikuti, D. Safer, H.L. Sweeney, A. Houdusse, How actin initiates the motor activity of Myosin, Dev Cell 33(4) (2015) 401-12.

Supplementary File 1 to the manuscript "Common mechanism of activated catalysis in P-loop fold nucleoside triphosphatases – united in diversity" by Maria I. Kozlova, Daria N. Shalaeva, Daria V. Dibrova, Armen Y Mulkidjanian

Classes of P-loop NTPases with ambiguous mechanisms of stimulation and W_{cat} stabilization.

For several large families and even classes of P-loop NTPases, there are no structures with full-fledged catalytic sites containing TS-analogs. Only assumptions can be made on their stimulatory moieties and environments of W_{cat}.

.

Kinase-GTPase Division:

***Septins and septin-like proteins* of the TRAFAC class** appear to be stimulated by His residues, which are reciprocally inserted into the catalytic sites upon dimerization of the NTPase domains; the dimerization, supposedly, is induced by the interaction with the activating partner(s) [1, 2]. In septins, the NE2 group of the stimulatory His residue appears to enter the AG site and to link the O^{2A} and O^{3G} atoms [2]. For septins, no TS-like structures are available. Still, in the GNP-containing structure of human septin 12 (PDB ID 6MQ9 [3]) the water molecules next to γ-phosphate interact with NH^{D+3} and residues of the Switch I motif.

ASCE Division:

STAND (*signal transduction ATPases with numerous domains)* ATPases unite apoptotic ATPases (animal apoptosis regulators CED4/Apaf-1, plant disease resistance proteins, and bacterial AfsR-like transcription regulators) and the ATPases of the NACHT superfamily, which consists of the animal disease response ATPases such as CARD4, the NAIP proteins and other ATPases [4]. The Walker B motif of these ATPases contains two consecutive acidic residues [4]. In addition to the P-loop domain, most proteins of the STAND class carry a unique

HETHS domain - the third helical domain, which is present only in this class of proteins [4]. Since some proteins of the STAND class have a conserved Arg residue within the P-loop domain, analogous to the Arg finger of AAA+ ATPases, it was suggested that their activation mechanism is similar to that of AAA+ ATPases [4]. However, available structures of Apaf-1 (Apoptotic protease activating factor 1) suggest a direct involvement of the HETHS domain in the ATP hydrolysis. Structures of Apaf-1 are available for the two states of the protein: the ADP-bound (no Mg^{2+}), "inactive" state (PDB ID 3SFZ [5]), and the "active" state, with Mg-ATP and cytochrome *c* bound (PDB ID 3JBT [6]). It is important to note, that Apaf-1 does not have ATPase activity, so that "active" and "inactive" states differ in the ability of the protein to oligomerize into an apoptosome. In the ATP-bound state, a Tyr residue forms an H-bond with the γ-phosphate (Fig. SF1_1B). In the ADP-bound state, a His residue from the HETHS domain attains a position next to α and β-phosphates and from the same side as Arg/Lys fingers in other P-loop NTPases (Fig. SF1_1B). This His residue is conserved in the majority of STAND proteins [4]. Specifically, a His residue is seen in the similar position in the ADP-containing STAND protein with a tetratricopeptide repeat sensor PH0952 from *Pyrococcus horikoshii* (see Fig. SF1_1C, PDB ID 6MFV [7]). STAND proteins appear to be special; unlike other P-loop NTPases, they convert from a closed form occluding an ADP molecule to an ATP-bound open form prone to multimerize [7]. Hence, Apaf-1 and its homologs cannot serve as a reliable representative for the whole class, especially considering the diversity of domain architectures and the presence of a conserved Arg residue in the P-loop domains of some families. Still, it is tempting to speculate, that the His residue, which is conserved within the STAND class, may be the activating moiety in those enzymes that are capable of hydrolyzing ATP, similarly to aforementioned septins. Structures of STAND ATPases with TS analogs bound are needed for clarification of the activation mechanism and the positioning of $\mathbf{W_{cat}}$.

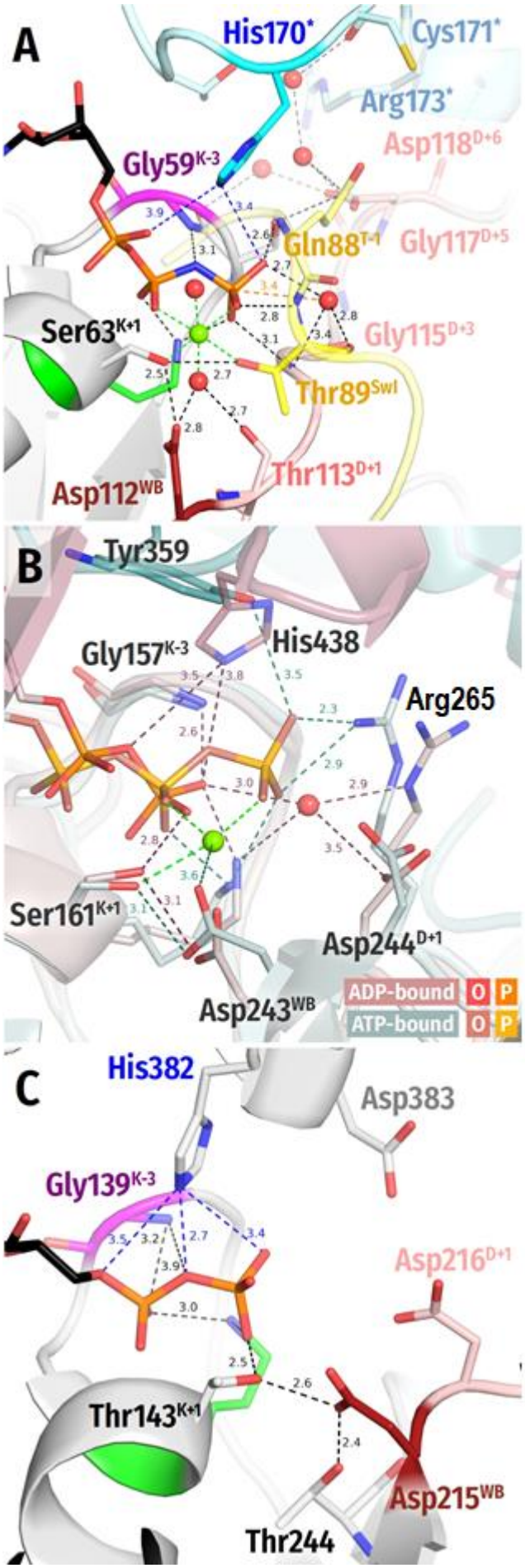

Figure SF1_1. Tentative His fingers in septins and STAND ATPases.

A. Structure of human septin 12 (PDB ID 6MQ9 [3]) complexed with GNP. Protein surrounding NTP-binding site is shown as a cartoon, functionally relevant residues are shown as sticks, water molecules are shown as red spheres, Mg^{2+} as a green sphere. P-loop lysine is shown in green, K-3 residue is shown in magenta. Asp^{WB} is shown in dark red and following residues in light red. Switch 1 residues are shown in yellow, residues belonging to adjacent monomer are highlighted in cyan and marked with an asterisk. All distances are given in ångströms.

B. Superimposed structures of murine apoptotic peptidase activating factor 1 (Apaf-1):

<u>In shades of pink:</u> ADP-bound form (PDB 3SFZ [5]). Water molecule is shown as a red sphere. HETHS domain is shown in a darker shade of pink. The distances are highlighted in dark pink.

<u>In shades of teal:</u> dATP-bound form (PDB ID 3JBT [6]). Mg ion is shown as a green sphere. HETHS domain is shown in a darker shade of teal. The distances are highlighted in dark teal.

C. Structure of the STAND protein with a tetratricopeptide repeat sensor PH0952 from *Pyrococcus horikoshii* (PDB ID 6MFV [7]). Colors as in panel A.

VirB/PilT-like class unites ATPases of the type IVa pili, GspE proteins of the type II secretion system, FlaI proteins of the archaeal flagellar system, and VirB11 proteins of the type IV secretion system [8-13]. In addition to the C-terminal nucleotide-binding P-loop domain, PilT-like ATPases have an N-terminal two-layer α/β sandwich domain, similar to the well-known ligand-binding PAS domain [14]. In the hexameric enzymes, the PAS-like domain provides the Arg finger to the AG site of the bound NTP molecule of the same subunit; an additional Arg finger can interact with γ-phosphate, see the structure in Fig. SF1_2A. In this structure, Ser^{K+1} forms a H-bond with Glu^{E+4} (highlighted in yellow), which, as shown on the panel, is connected to Glu^{WB} by a complex system of water bridges (highlighted in cyan). They resemble those in the PRC (see Fig. 10A in the main text), so that Glu^{WB} is likely to serve as a proton trap in PilT-like NTPases. The Asp^{E+1} residue on the C-cap is far from γ-phosphate. In the absence of TS-like structures, it cannot be fully excluded that Asp^{E+1} comes closer to the ATP molecule upon activation so that Asp^{E+1} interacts with W_{cat}. Alternatively, Glu^{E+4} of the WB-crest can well perform this function and transmit a proton to the buried Glu^{WB}.

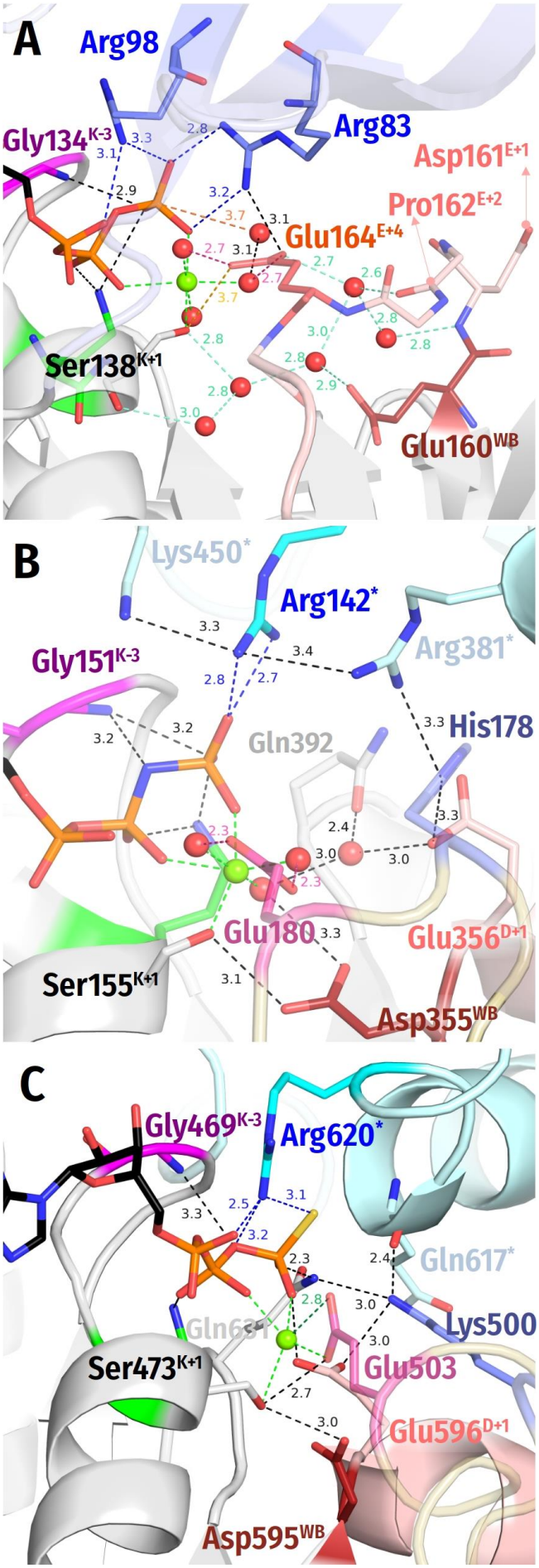

Fig. SF1_2. **Nucleotide-binding sites of P-loop NTPases of VirB/PilT and FtsK-HerA classes.**

A. Structure of the twitching motility pilus retraction ATPase PilT4 from *Geobacter metallireducens*, PDB ID 6OJX [13]). Protein surrounding the NTP-binding site is shown as a cartoon, functionally relevant residues are shown as sticks, water molecules are shown as red spheres, Mg^{2+} as a green sphere. The P-loop lysine is shown in green, the K-3 residue is shown in magenta. Glu^{WB} is shown in dark red and the following residues in pale red. The PAS domain is shown in pale blue and its Arg fingers are shown in blue. All distances are indicated in Å.

B. Crystal structure of the HerA hexameric DNA translocase from *Sulfolobus solfataricus* (PDB 4D2I[15]). Residues belonging to adjacent monomer are highlighted in cyan and marked with an asterisk. The additional Glu residue is shown in pink and the loop harboring it is shown in beige. Other colors as in panel A.

C. Cryo-EM structure of FtsK from *Pseudomonas aeruginosa* PAO1 with resolution of 3.7 Å [16].

Colors as in panel B.

FtsK-HerA pumping ATPases are related to, but not monophyletic with the PilT-like ATPases. The ***HerA ATPases*** are present in all archaea and some bacteria [17] and participate in the repair of double strand DNA breaks [15]. The structure of HerA hexamer from *Sufolobus solfataricus*, in complex with AMP-PNP, a non-hydrolysable analogue of ATP, shows two Arg and one Lys residue pointing towards the triphosphate chain. The Glu355^{WB} residue interacts with Ser155^{K+1} and W6, whereas Glu356^{D+1} points towards the anticipated position of $\mathbf{W_{cat}}$ [15], see Fig. SF1_2B. An additional class-specific Glu residue (Glu180 in the HerA hexamer from *Sufolobus solfataricus*, colored pink), similarly to Glu^{E+4} in PilT4 coordinates W3and W5, Mg^{2+} ligands #3 and #5.

The titular ***FtsK ATPases*** are motor protein that translocate double-stranded DNA during chromosome segregation. A recently reported cryo-EM structure of FtsK of *Pseudomonas aeruginosa* PAO1 with resolution of 3.7 Å indicates that an Arg residue analogous to the arginine finger of the AAA+ superfamily interacts with the NTP-binding site of the adjacent subunit Fig. SF1_2C [16]. The additional Glu residue is also present, but, contrary to HerA, it interacts with Ser^{K+1}, similarly to Glu^{D+4} in PilT-like class ATPases, cf Fig. SF1_2A. The Asp^{WB} is also close, at only 3 Å away of Ser^{K+1}. It is followed by Glu^{D+1} that points towards γ-phosphate and may stabilize W_{cat} in the TS.

Unless TS-like structures of FtsK, HerA, and VirB/PilT-like ATPases with their constricted catalytic sites are obtained, the functions and interactions of their additional Glu residues will remain obscure. Hence, the TS-like, constricted site in any of these ATPases may resemble either that of HerA and FtsK ATPases (where [Asp/Glu]^{WB} interacts with Ser^{K+1}, and the additional Glu interacts with ligands of Mg^{2+}) or that of PilT-like ATPases (where the additional Glu makes a H-bond with Ser^{K+1}). It cannot be fully excluded that two carboxylic groups reach the [Ser/Thr]$^{K+1}$ residue in the TS in the case of these NTPases.

KAP ATPases named after Kidins220/ARMS (mammalian neuronal membrane proteins) and PifA (F-plasmid protein involved in phage T7 exclusion)**,** supposedly, use a AAA-type activation mechanism [18]. The KAP family proteins lack the Arg finger within the P-loop domain proper but carry a conserved arginine in the C-terminal helical segment, which could potentially function as an activating moiety, similar to Sensor 2 of the AAA+ ATPases [18]. Still, in the absence of structures of KAP proteins, both the activation mechanism and the $\mathbf{W_{cat}}$ positioning in enzymes of this class remain unclear.

References

[1] M. Sirajuddin, M. Farkasovsky, E. Zent, A. Wittinghofer, GTP-induced conformational changes in septins and implications for function, Proc. Natl. Acad. Sci. USA 106(39) (2009) 16592-7.

[2] H.V.D. Rosa, D.A. Leonardo, G. Brognara, J. Brandao-Neto, H. D'Muniz Pereira, A.P.U. Araujo, R.C. Garratt, Molecular Recognition at Septin Interfaces: The Switches Hold the Key, J Mol Biol 432(21) (2020) 5784-5801.

[3] D. Castro, S.M.O. da Silva, H.D. Pereira, J.N.A. Macedo, D.A. Leonardo, N.F. Valadares, P.S. Kumagai, J. Brandao-Neto, A.P.U. Araujo, R.C. Garratt, A complete compendium of crystal structures for the human SEPT3 subgroup reveals functional plasticity at a specific septin interface, IUCrJ 7(Pt 3) (2020) 462-479.

[4] D.D. Leipe, E.V. Koonin, L. Aravind, STAND, a class of P-loop NTPases including animal and plant regulators of programmed cell death: multiple, complex domain architectures, unusual phyletic patterns, and evolution by horizontal gene transfer, J. Mol. Biol. 343(1) (2004) 1-28.

[5] T.F. Reubold, S. Wohlgemuth, S. Eschenburg, Crystal structure of full-length Apaf-1: how the death signal is relayed in the mitochondrial pathway of apoptosis, Structure 19(8) (2011) 1074-83.

[6] M. Zhou, Y. Li, Q. Hu, X.C. Bai, W. Huang, C. Yan, S.H. Scheres, Y. Shi, Atomic structure of the apoptosome: mechanism of cytochrome c- and dATP-mediated activation of Apaf-1, Genes Dev 29(22) (2015) 2349-61.

[7] M.N. Lisa, V. Cvirkaite-Krupovic, E. Richet, G. Andre-Leroux, P.M. Alzari, A. Haouz, O. Danot, Double autoinhibition mechanism of signal transduction ATPases with numerous domains (STAND) with a tetratricopeptide repeat sensor, Nucleic Acids Res 47(7) (2019) 3795-3810.

[8] P.J. Planet, S.C. Kachlany, R. DeSalle, D.H. Figurski, Phylogeny of genes for secretion NTPases: identification of the widespread tadA subfamily and development of a diagnostic key for gene classification, Proc Natl Acad Sci U S A 98(5) (2001) 2503-8.

[9] K.G. Aukema, E.M. Kron, T.J. Herdendorf, K.T. Forest, Functional dissection of a conserved motif within the pilus retraction protein PilT, J Bacteriol 187(2) (2005) 611-8.

[10] S.N. Savvides, H.J. Yeo, M.R. Beck, F. Blaesing, R. Lurz, E. Lanka, R. Buhrdorf, W. Fischer, R. Haas, G. Waksman, VirB11 ATPases are dynamic hexameric assemblies: new insights into bacterial type IV secretion, EMBO J 22(9) (2003) 1969-80.

[11] K.A. Satyshur, G.A. Worzalla, L.S. Meyer, E.K. Heiniger, K.G. Aukema, A.M. Misic, K.T. Forest, Crystal structures of the pilus retraction motor PilT suggest large domain movements and subunit cooperation drive motility, Structure 15(3) (2007) 363-376.
[12] J.M. Mancl, W.P. Black, H. Robinson, Z. Yang, F.D. Schubot, Crystal Structure of a Type IV Pilus Assembly ATPase: Insights into the Molecular Mechanism of PilB from Thermus thermophilus, Structure 24(11) (2016) 1886-1897.
[13] M. McCallum, S. Benlekbir, S. Nguyen, S. Tammam, J.L. Rubinstein, L.L. Burrows, P.L. Howell, Multiple conformations facilitate PilT function in the type IV pilus, Nat Commun 10(1) (2019) 5198.
[14] C.P. Ponting, L. Aravind, PAS: a multifunctional domain family comes to light, Curr Biol 7(11) (1997) R674-7.
[15] N.J. Rzechorzek, J.K. Blackwood, S.M. Bray, J.D. Maman, L. Pellegrini, N.P. Robinson, Structure of the hexameric HerA ATPase reveals a mechanism of translocation-coupled DNA-end processing in archaea, Nat Commun 5 (2014) 5506.
[16] N.L. Jean, T.J. Rutherford, J. Lowe, FtsK in motion reveals its mechanism for double-stranded DNA translocation, Proc Natl Acad Sci U S A 117(25) (2020) 14202-14208.
[17] L.M. Iyer, K.S. Makarova, E.V. Koonin, L. Aravind, Comparative genomics of the FtsK-HerA superfamily of pumping ATPases: implications for the origins of chromosome segregation, cell division and viral capsid packaging, Nucleic Acids Res 32(17) (2004) 5260-79.
[18] L. Aravind, L.M. Iyer, D.D. Leipe, E.V. Koonin, A novel family of P-loop NTPases with an unusual phyletic distribution and transmembrane segments inserted within the NTPase domain, Genome Biol. 5(5) (2004) R30.